MECHANISTIC STUDIES ON RADICAL S-ADENOSYL-L-METHIONINE ENZYMES INVOLVED IN MENAQUINONE, THIAMIN AND COBALAMIN BIOSYNTHESIS

A Dissertation

by

SUMEDH VARAD JOSHI

Submitted to the Office of Graduate and Professional Studies of
Texas A&M University
in partial fulfillment of the requirements for the degree of

DOCTOR OF PHILOSOPHY

Chair of Committee,	Tadhg P. Begley
Committee Members,	Frank M. Raushel
	Wenshe Liu
	Thomas Meek
Head of Department,	Simon W. North

December 2019

Major Subject: Chemistry

ABSTRACT

Menaquinone (Vitamin K) is an electron transfer cofactor that is an essential component for all the domains of life. Recently discovered, futalosine-dependent menaquinone biosynthetic pathway uses radical chemistry to assemble the aromatic core of menaquinone. Aminofutalosine synthase (MqnE)- a radical S-Adenosylmethionine (SAM) enzyme, catalyzes the key C-C bond formation reaction in this pathway converting 3-((1-carboxyvinyl)oxy)benzoic acid to Aminofutalosine. We have proposed a novel reaction mechanism for the MqnE catalyzed radical rearrangement involving a radical addition to the stable benzene ring. In support of this mechanism, we have successfully trapped the captodative and aryl radical anion intermediates using intramolecular, fast and radical triggered carbon-halogen bond fragmentation reactions (β-scission and $S_{RN}1$ fragmentation).

We have utilized exogenous radical trapping agents such as 5,5-dimethyl-1-pyrroline-N- oxide (DMPO), and sodium dithionite to trap radical intermediates in MqnE catalyzed reaction as a DMPO-spin adduct and sulfinate adduct respectively. We also have developed a chemical derivatization strategy for these sulfinate adducts to facilitate their chromatographic detection under aerobic conditions. These radical trapping strategies are generally useful in the study of other transient enzymatic radicals.

Using a mechanism-guided approach, we have identified potent inhibitors of MqnE and have demonstrated their inhibitory activity against important human pathogens - *Helicobacter pylori and Campylobacter jejuni.* The best inhibitor exhibits tight-binding

inhibition kinetics and has comparable antibacterial to currently approved antibiotics in the treatment of *H. pylori* infections.

Thiamin Pyrimidine Synthase (ThiC) and its paralog- hydroxybenzimidazole Synthase (BzaF) play a pivotal role in the biosynthesis of thiamin (Vitamin B_1) and cobalamin (Vitamin B_{12}) by converting 5-aminoimidazole ribonucleotide (AIR) to hydroxymethyl pyrimidine phosphate (HMP-P) and 5- hydroxybenzimidazole (5-HBI) respectively. ThiC catalyzes the most complex unresolved radical rearrangement in primary metabolism. We have used rationally designed substrate analogs to study early steps of the ThiC and BzaF catalyzed reactions and have trapped a ribose based radical intermediate in the form of a sulfinate adduct using sodium dithionite as a trapping agent. These studies have demonstrated that ThiC and BzaF reactions follow a fragmentation-recombination mechanism and have enabled us to propose credible mechanistic hypotheses for these unprecedented transformations.

DEDICATION

To all my teachers who taught me to think……

ACKNOWLEDGEMENTS

I want to take the opportunity to thank all the people who have played a role in my journey towards doctoral studies in Chemistry.

First and foremost, I thank my research advisor, Prof. Tadhg Begley, for giving me the opportunity to work on the most exciting and challenging projects in his lab and providing all the resources and intellectual inputs. Tadhg always gave me the freedom to think independently and showed faith in my systematic approach to problem-solving. Tadhg was also instrumental in initiating collaborations, which enabled me to learn about new techniques beyond my core expertise. Equally important were the opportunities Tadhg provided me to participate in research paper & grant proposal writing, host eminent scientists, and to attend prestigious conferences. Putting everything together, I could not have asked for better training as a graduate student!

I express my gratitude to my committee members - Prof. Frank Raushel, Prof. Wenshe Liu and Prof. Thomas Meek. Their insightful feedback during my student seminar, journal club presentations and prelim was very important.

Special thanks to Dr. Dhananjay Bhandari for being my friend, philosopher & guide throughout my Ph. D. tenure. Apart from being a lab-mate, Dhananjay was also my roommate and helped me to get settled in the new country very smoothly. I was highly impressed with his unbiased, rigorous and uncompromising approach while working on some of the most complex projects in the lab.

Dr. Dmytro Fedoseyenko, I can't thank you enough. Dmytro and I worked together as a team throughout my Ph. D. tenure on exciting projects like MqnE, ThiC & BzaF. Dmytro is one of the finest synthetic chemists and has a great ability to think out of the box. Dmytro's excitement towards solving complex scientific problems is very impressive and served as a great source of motivation for me. Our countless scientific discussions on a daily basis were the key to getting an early breakthrough on ThiC. I will cherish these exciting times throughout my life.

I would like to thank Derek Gagnon from Prof. R. David Britt's lab at UC Davis. Derek, thanks for being a great collaborator for the EPR studies on MqnE and bearing with all my silly questions about EPR. I also enjoyed working with Mark Nesbit, Richard Sayler and Lizhi Tao from the Britt lab. Thanks to Rodrigo Ducati and Mu Feng from Prof. Vern Schramm's lab for helping with the *in vivo* inhibition studies. Thanks, Jian for constructing MqnE mutants for me under strict deadline pressure. I am thankful to Prof. Steven Almo and Tyler Grove for generously sharing their crystal structure of MqnE with us. Thanks to Lisa Perez and Carla Saunders for assisting in the computational studies. All the AIR isotopologues were synthesized by Dr. Sameh Abdelwahed enabled me to propose the structure of Compound X in ThiC. I am sincerely thankful to Sameh.

I am thankful to Angad and Nilkamal for being my mentors in the early days of graduate school. Thanks to Isita for being a good friend and a curious scientist. Brainstorming on her project was a very effective way to learn about flavoenzymes. I had a great opportunity to mentor young graduate students Hannah and Vishav. This was a

very productive and enriching experience for me. I am also thankful to past and present Begley lab members for their enthusiasm towards science.

I am deeply thankful to my teachers at Institute of Chemical Technology (ICT), Mumbai, India. Prof. S. D. Samant introduced me to the magical and logical world of organic chemistry. Prof. K. G. Akamanchi taught us a course on 'Natural product Chemistry' which is the major reason I decided to pursue my doctoral studies in enzymology. I am also thankful to Prof. M. S. Degani, who played an important role in my training on computational chemistry. My ICT years while pursuing my B. Tech. in Pharmaceutical Technology helped me develop an aptitude to think systematically & logically and express my thoughts coherently and confidently. This ensured a smooth transition from Pharmacy to Biological chemistry in my graduate studies.

Shirin, you have been an amazing friend and one of the brightest people I have ever met. Learning organic chemistry from you and Abhishek was an enlightening experience. Emotional support and motivation from both of you were very important to sail through the turbulent times. Mihir, I always enjoyed long discussions on CADD and Indian classical music with you.

I would like to thank Rachit for being a great roommate in Cherry 201. I have some fond memories with you while cooking delicious food and watching Marvel movies together. Tejas, I found a very good friend in you who shared the same cultural values and the love for Indian classical music. All the music concerts we attended together in Houston were the most enjoyable. Aishwarya, Trupthi and Prakruthi thanks a lot for being enthusiastic and supportive friends and making my stay in College Station enjoyable.

I would like to thank my parents for their unconditional love and the role they have played in shaping my core values. I inherited the love for Indian classical music from my parents. Love and blessings from my grandparents are also very important in my life. My cousins- Viraj, Kedar and Ketan and my dear friend Abhishek, you all have always motivated me and have made me proud. My entire family from Shrirang Niwas also has played an important role in my journey throughout.

This dissertation would not have been possible without the foundations laid by everyone mentioned above. Thanks to all my friends, colleagues, faculty and staff for making my time at Texas A&M University a great experience.

CONTRIBUTORS AND FUNDING SOURCES

Contributors

This work was supervised by a dissertation committee consisting of Professor Tadhg P. Begley (chair), Professor Frank M. Raushel and Professor Wenshe Liu from the Department of Chemistry and Professor Thomas Meek from the Department of Biochemistry and Biophysics.

The substrate analogs **28, 35, 38, 48, 66, 91, 114, 115, 116** mentioned in Chapter 2, 3, 4 were synthesized by Dr. Dmytro Fedoseyenko from Prof. Tadhg Begley's research group. Isotopologues of AIR in chapter 4 were synthesized by Dr. Sameh Abdelwahed. *In vivo* inhibition experiments against *H. pylori* and *C. jejuni* in chapter 3 were performed by Dr. Rodrigo Ducati and Mu Feng from Prof. Vern Schramm's lab at Albert Einstein College of Medicine, NY.

All other work conducted for the thesis (or) dissertation was completed by the student independently.

Funding Sources

Graduate study was supported by a fellowship from Texas A&M University. This work was also made possible in part by the National Science Foundation under Grant Number [1507191] and Robert A. Welch Foundation (A0034).

NOMENCLATURE

5’dA	5’-deoxyadenosine
AIR	Aminoimidazole Ribonucleotide
ATP	Adenosine triphosphate
CIP	Calf intestinal phosphatase
EIC	Extracted Ion Chromatogram
EPR	Electron Paramagnetic Resonance
HPLC	High Performance Liquid Chromatography
HMP-P	4-amino-5-hydroxymethyl-2-methylpyrimidine phosphate
IRN	Imidazole Ribonucleotide
kda	kilodalton
KPi	Potassium phosphate
LC-MS	Liquid Chromatography-Mass Spectrometry
MTA	Methylthioadenosine
NMR	Nuclear Magnetic Resonance
PDB	Protein Data Bank
SAM	S-Adenosyl-L-methionine
Tris	Tris(hydroxymethyl)aminomethane

TABLE OF CONTENTS

Page

LIST OF FIGURES

Page

1. INTRODUCTION*

Menaquinone **12** is a lipid-soluble cofactor that transfers electrons between membrane-bound redox enzymes in the electron transport chain of the respiratory and photosynthetic systems in microorganisms and plants.[3] In humans and other mammals, menaquinone is an essential vitamin (vitamin K) required for the remarkable γ-carboxylation of glutamic acid residues in proteins involved in blood clotting and bone formation (Figure 1.1).[4-6] Humans do not biosynthesize vitamin K and acquire it from food (vegetables and vegetable oils) and from its biosynthesis in the gut microbiome.[7] Vitamin K deficiency in humans leads to the synthesis of abnormal forms of coagulation factors resulting in prolonged clotting time and hemorrhaging.[7]

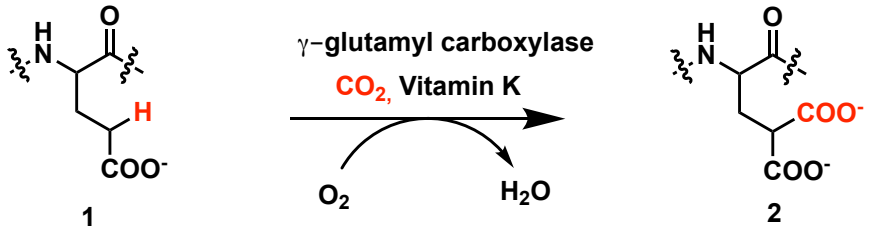

Figure 1.1 Vitamin K mediated carboxylation of glutamate residues

*Figures 1.1-1.3 and the text are adapted and reprinted in parts with permission from "Novel enzymology in futalosine dependent menaquinone biosynthesis" by Joshi S., Fedoseyenko D. , Mahanta N. ,Manion H., Naseem S., Dairi T., Begley T. Cur. Opin. Chem. Biol. 2018, 47, 134 -141. Copyright 2018 Elsevier.

1.1. Biosynthesis of menaquinone

In prokaryotes, there are two different pathways for the biosynthesis of the naphthoquinol core of menaquinone. The majority of bacteria produce menaquinone by the well-studied o-succinylbenzoate (OSB) pathway (the classical pathway, Figure 1.2).[8-9] An alternative pathway (the futalosine pathway, Figure 1.3), was recently discovered in *Streptomyces coelicolor.*[10-12] This pathway is distributed only in prokaryotes and no microorganism has yet been found that uses both pathways.[10] Analogous convergent biosynthetic strategies have been observed in the biosynthesis of other cofactors such as thiamin, nicotinamide, and pyridoxal phosphate.[13-14]

Both the classical and the futalosine pathway diverge at chorismate and re-converge after naphthoquinol formation.[12, 15] The chemistry used for naphthoquinol assembly is fundamentally different for the two pathways. The classical pathway utilizes well-understood thiamin-dependent decarboxylative carbo-ligation and Claisen condensation reactions for C-C bond formation (Figure 1.2), while the futalosine pathway employs radical chemistry (Figure 1.3). At this time, we do not understand why microorganisms utilize one pathway over the other: both pathways proceed from readily available precursors and both can proceed under aerobic and anaerobic conditions.

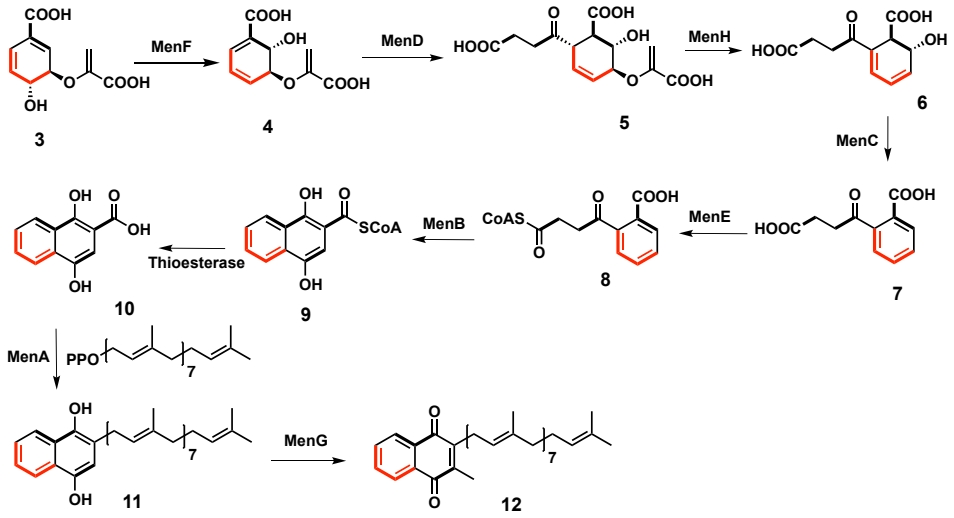

Figure 1.2 Classical menaquinone biosynthesis

1.2. The classical menaquinone biosynthetic pathway

In the classical pathway (Figure 1.2), chorismate **3**, is initially converted into isochorismate **4**, by MenF.[16] In the next step, **5** is formed from **4** and 2-ketoglutarate in a thiamin pyrophosphate-dependent reaction catalyzed by MenD.[17] Then, MenH catalyzes the conversion of **5** into **6** in a 1,4-elimination reaction.[18] MenC catalyzed dehydration of **6** gives o-succinylbenzoate (OSB) **7** - the first aromatic compound on the pathway.[19-20] MenE catalyzes the formation of o-succinylbenzoyl-CoA **8**,[21] which undergoes a MenB catalyzed cyclization to give **9**.[22] It is notable that this reaction does not require initial activation of the carboxylate by phosphorylation or thioester formation. Thioester hydrolysis[23] gives **10** which then undergoes a MenA catalyzed ipso substitution reaction with isoprenoid pyrophosphates, of varying lengths, to give **11**. A final MenG catalyzed SAM-dependent methylation completes the biosynthesis of menaquinone **12**. Mechanistic

and structural studies on all of the enzymes on this pathway are at an advanced stage.[8, 17-25]

1.3. The futalosine-dependent menaquinone biosynthesis pathway

The futalosine-dependent pathway to menaquinone was first discovered and validated in *Streptomyces coelicolor* using precursor labeling studies, genetic studies, genome sequence comparisons, and the isolation of intermediates from mutant strains.[10] Sequence analysis suggests that this pathway is the primordial pathway for menaquinone biosynthesis.[26] The current state of our understanding of the biosynthetic chemistry is outlined in Figure 3.[10-11, 27] MqnA catalyzes the dehydration of chorismate to give **13**. Aminofutalosine synthase (MqnE), a radical SAM enzyme, then converts **13** to **14**.[27] Aminofutalosine **14** undergoes glycosidic bond hydrolysis to form **16** either directly using MTAN or via futalosine **15**, using MqnF and MqnB.[27-29] Compound **16** is then converted into **17** by MqnC, also a radical SAM enzyme.[10, 30] MqnD, an aldolase, converts **17** to **18**.[10] Sequence analysis of the *S. coelicolor* A3(2) genome suggests that MqnP (SCO4491, prenylation), MqnL and MqnM (SCO4490 and SCO4492, decarboxylation), and MenG (SCO4556, methylation) are likely to be involved in the later steps of menaquinone biosynthesis.[10, 31-33]

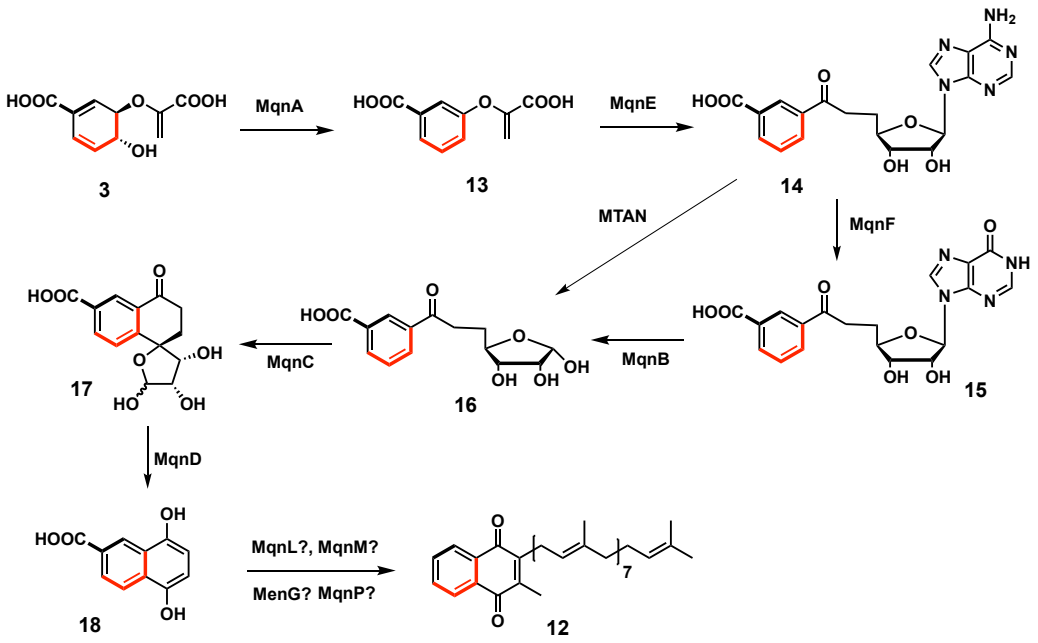

Figure 1.3 Futalosine dependent menaquinone biosynthesis pathway

1.4. Introduction to radical SAM enzymes

Radical SAM enzymes, first classified as a superfamily in 2001[34], utilize a [4Fe−4S] cluster and S-adenosylmethionine (SAM, **19**) to initiate a diverse set of radical reactions that are otherwise difficult or impossible to catalyze by polar mechanisms [35]. Currently, there are >300,000 sequences annotated in this superfamily [36-37]. These enzymes harbor a redox-active [4Fe-4S] cluster, which is typically ligated by 3 conserved cysteine residues constituting a CX_3CX_2C motif [38] (Figure 1.4). Radical SAM enzymes catalyze the reductive homolytic cleavage of the C-S bond of SAM **19** to generate the highly reactive 5'-deoxyadenosyl radical **20** (Figure 1.5). This radical typically abstracts a hydrogen atom from the substrate directly or via a protein residue based radical. The resulting substrate radical usually undergoes a rearrangement or fragmentation reaction to give the product

radical which is typically quenched by an electron transfer or H atom abstraction[39]. Detailed mechanistic investigations on these enzymes have been limited by poorly understood enzyme inactivation reactions and by the absence of generally applicable strategies for trapping transient radical intermediates[40-41]. Radical SAM enzymes are especially prevalent in cofactor biosynthesis and have been shown to catalyze complex radical rearrangement reactions[42]. The recently discovered futalosine-dependent menaquinone biosynthetic pathway also features two radical SAM enzymes (MqnE and MqnC) which play a central role in the formation of the naphthoquinone core of menaquinone [10, 27].

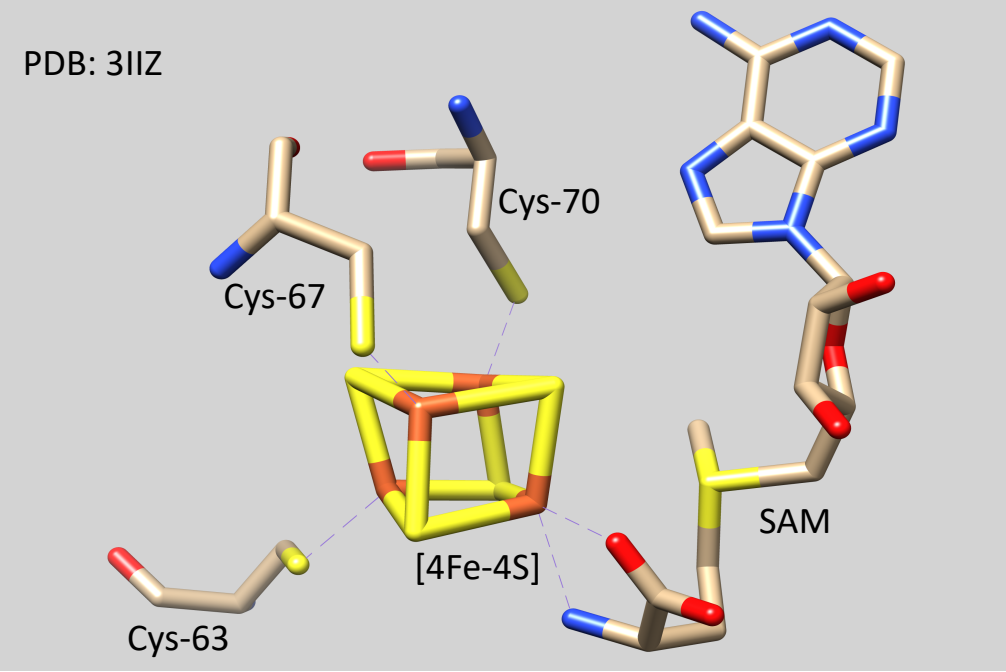

Figure 1.4 Typical active site architecture of radical SAM enzymes

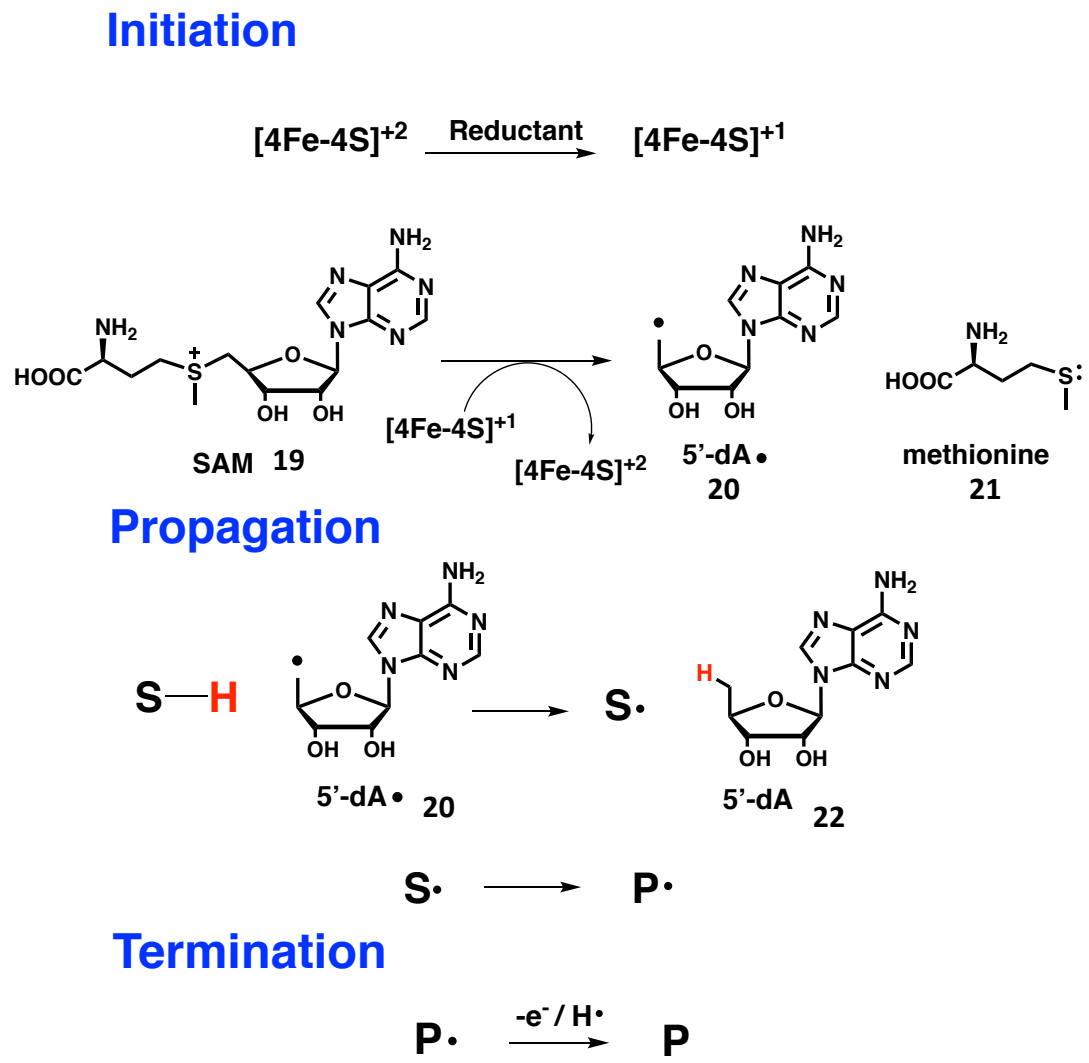

Figure 1.5 Radical generation, propagation and termination steps catalyzed by radical SAM enzymes

2. MECHANISTIC STUDIES ON AMINOFUTALOSINE SYNTHASE (MQNE)†

2.1. MqnE catalyzed reaction

Aminofutalosine synthase (MqnE)- a radical S-Adenosylmethionine (SAM) enzyme, catalyzes the key C-C bond formation reaction in this pathway converting 3-((1-carboxyvinyl)oxy)benzoic acid **13** to Aminofutalosine **14** (Figure 2.1). The utilization of the adenosyl radical for C-C bond formation, rather than hydrogen atom abstraction, is a new catalytic motif in radical SAM enzymology[35, 42]. The second example of this versatile transformation has been experimentally demonstrated in the hopanoid biosynthetic pathway[43-44] and this chemistry may also be used in the biosynthesis of griseolic acid.[27]

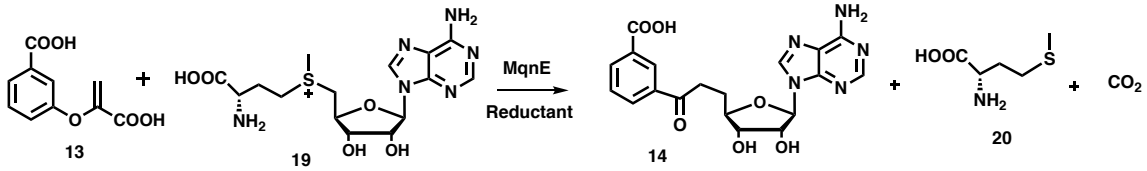

Figure 2.1 MqnE catalyzed reaction

2.2. Mechanistic proposal for the MqnE catalyzed reaction

Our current mechanistic proposal for aminofutalosine synthase (MqnE) is outlined in Figure 2.2. In this proposal, the 5'-deoxyadenosyl radical **20** adds to 3-[(1-carboxyvinyl) oxy]-benzoic acid **13** to form the captodative radical 2**3**. Rearrangement of 2**3**, via the spiroepoxide **24**, generates **25**. Analogous O-neophyl rearrangements have been

† Figures 2.2-2.47 and the text are adapted and reprinted in parts with permission from "Aminofutalosine Synthase: Evidence for Captodative and Aryl Radical Intermediates Using β-Scission and SRN1 Trapping Reactions" by Joshi S., Mahanta N., Fedoseyenko D., Williams H., Begley T. J. Am. Chem. Soc. 2017, 139, 10952-10955. Copyright 2017 American Chemical Society.

previously reported in the synthetic chemistry literature.[45,46,47] Decarboxylation followed by deprotonation to form the aryl radical anion **27** and an electron transfer to the [4Fe-4S]$^{+2}$ cluster completes the reaction. These type of radical additions to benzene rings, while relatively frequent, are still poorly understood reactions in biosynthesis.[48]

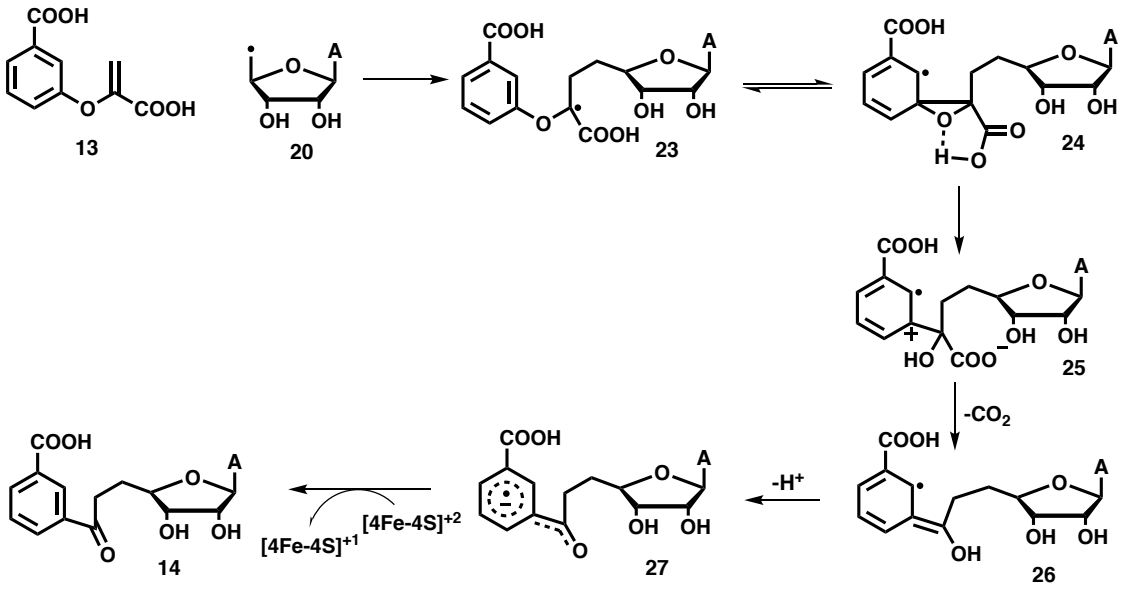

Figure 2.2 Mechanistic proposal for the aminofutalosine synthase-catalyzed conversion of 3-[(1-carboxyvinyl) oxy]-benzoic acid 13 to aminofutalosine 14.

2.3. Michaelis Menten kinetics of MqnE catalyzed reaction

Expression of the His-tagged *Thermus thermophilus mqnE* in *Escherichia coli* gave catalytically active (~25 turnovers) enzyme. The Michaelis-Menten constants for the reaction at 25^{0}C, determined using a discontinuous HPLC assay, were: k_{cat} = 0.22 ± 0.08 min^{-1}, $K_{m(\mathbf{1})}$ = 335 ± 98 μM and $K_{m(SAM)}$ = 13.3 ± 0.9 μM. (Figure 2.3) The slow k_{cat} is consistent with most other radical SAM enzymes.[35]

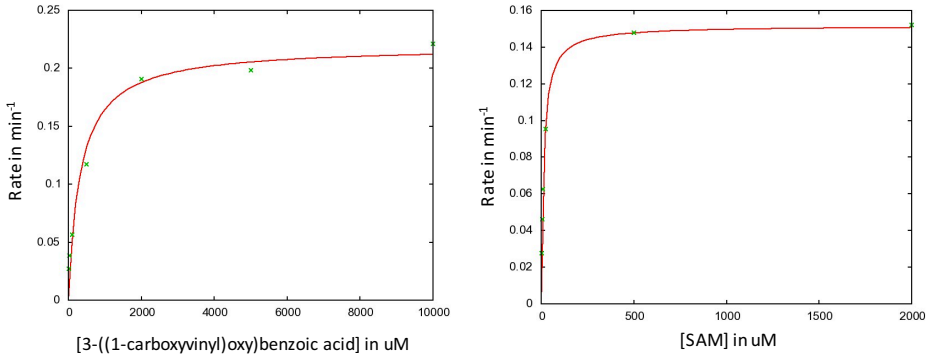

Figure 2.3 Steady-state Plot of Rate versus [S] determined by an HPLC assay

2.4. Captodative intermediate trapping

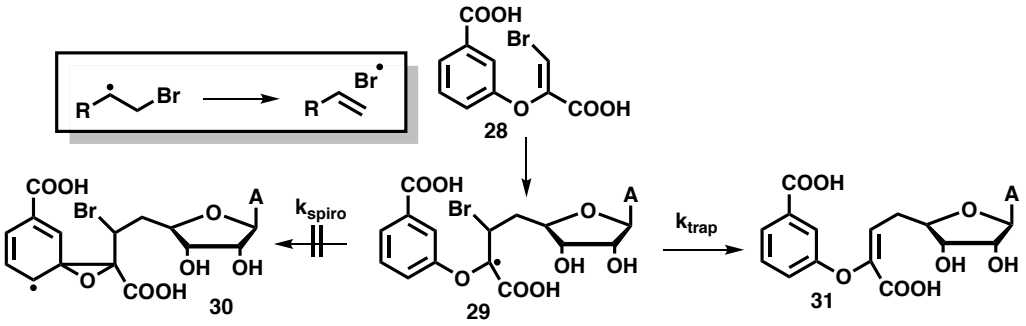

Figure 2.4 Strategy for trapping the captodative radical using the facile fragmentation of a C-Br bond beta to a radical center.

Our first strategy for trapping the captodative radical **23** was based on the rapid homolysis of a C-Br bond beta to a radical center ($k_{C\text{-}Br}$ = 3x10^8 s^{-1}).[49] When the brominated substrate analog **28**, synthesized as shown in Figure 2.39-2.41, was incubated with MqnE, SAM and dithionite, HPLC analysis of the resulting reaction mixture showed the formation of a new compound eluting at 15.5 min. (Figure 2.5). This compound was identified as **31** by NMR and MS analysis (Figures 2.5 – 2.11). MS-MS fragmentation

analysis of the minor reaction products also demonstrated the formation of a small quantity of the isomeric adenosyl radical addition product **32** eluting at 15.75 min. (Figure 2.5, 2.12, 2.13) Analogous isomeric addition products have been reported for NosL.[40] Rearranged products resulting from the spirocyclization reaction were not observed. This suggests that $k_{spiro} < 1.5x10^7\ s^{-1}$ (5% detection limit for the rearranged product).

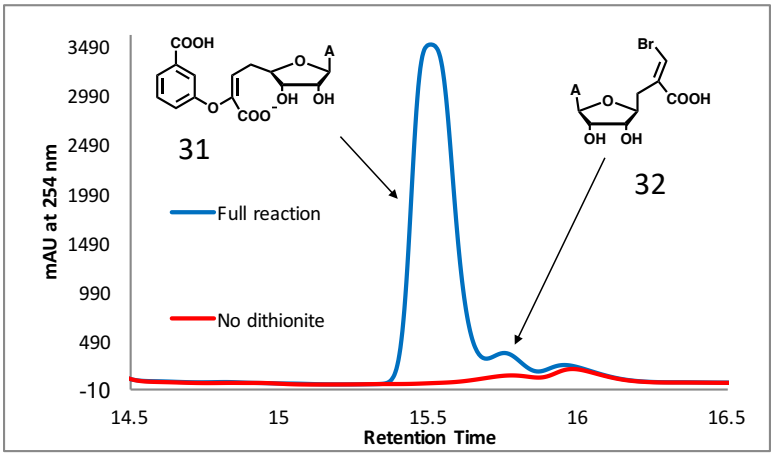

Figure 2.5 HPLC chromatogram of the MqnE-catalyzed reaction with **28**.

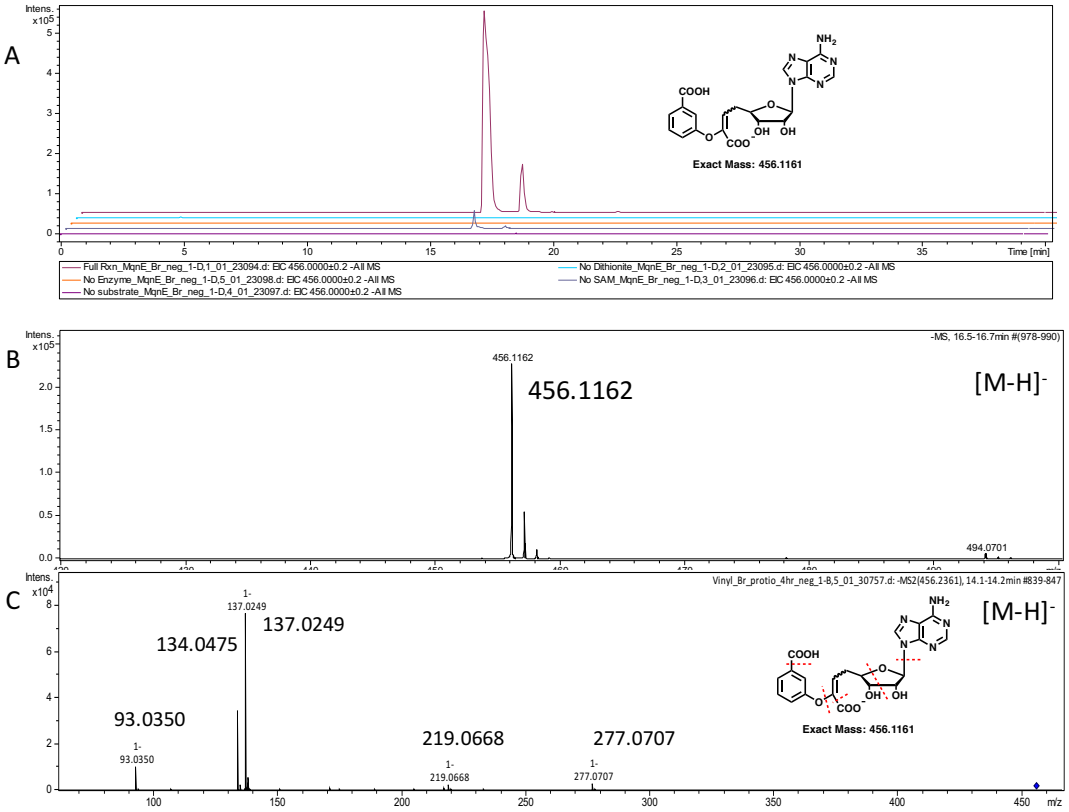

Figure 2.6 LCMS analysis of **31** formed in the MqnE-catalyzed reaction with **28**. A) LC-MS analysis showing EIC [M-H]- = 456.1 Da suggesting that this compound is **31**. B) MS of **31** C) MS-MS fragmentation analysis of **31.**

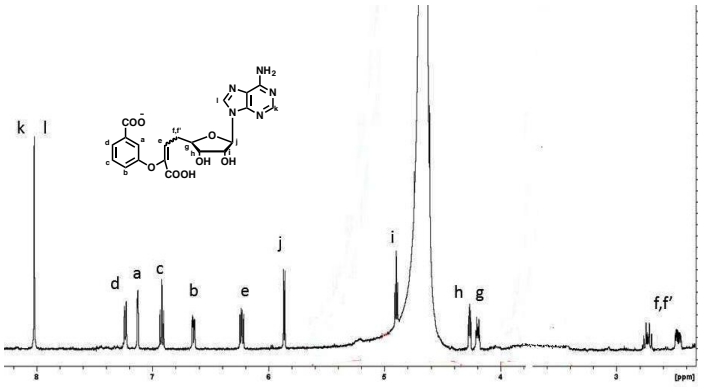

Figure 2.7 ^{1}H NMR (500 MHz, D_2O) spectrum of compound **31**

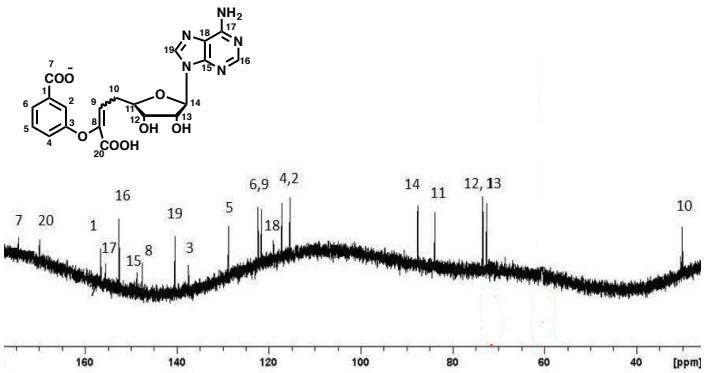

Figure 2.8 ^{13}C NMR (125 MHz, D_2O) spectrum of compound **31**.

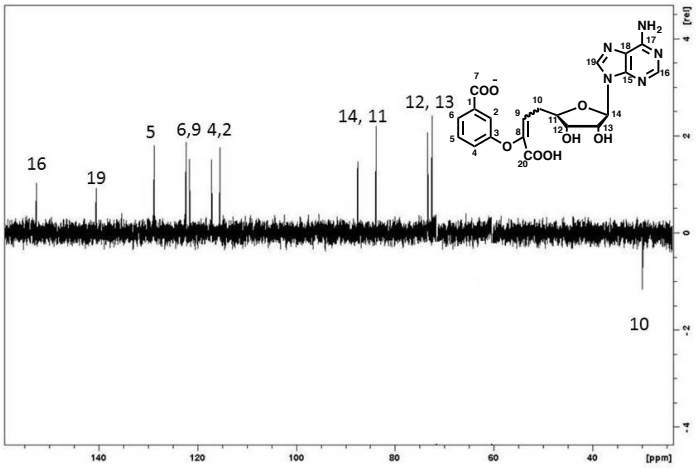

Figure 2.9 ^{13}C DEPT -135 NMR (125 MHz, D_2O) spectrum of compound **31**.

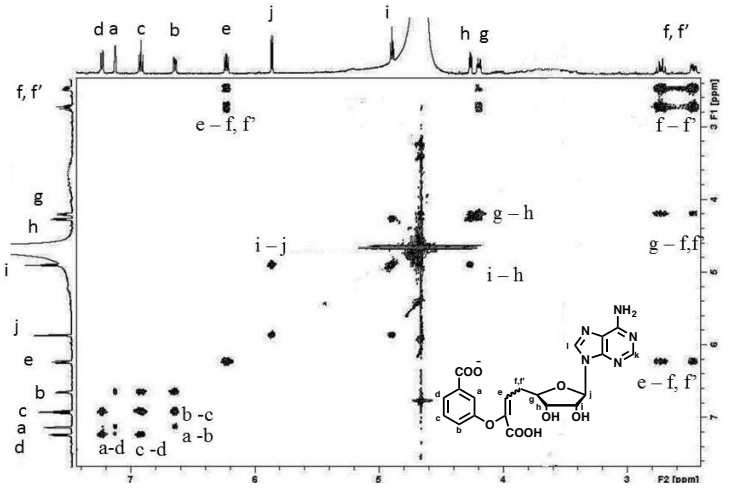

Figure 2.10 ^{1}H COSY spectrum of compound **31**.

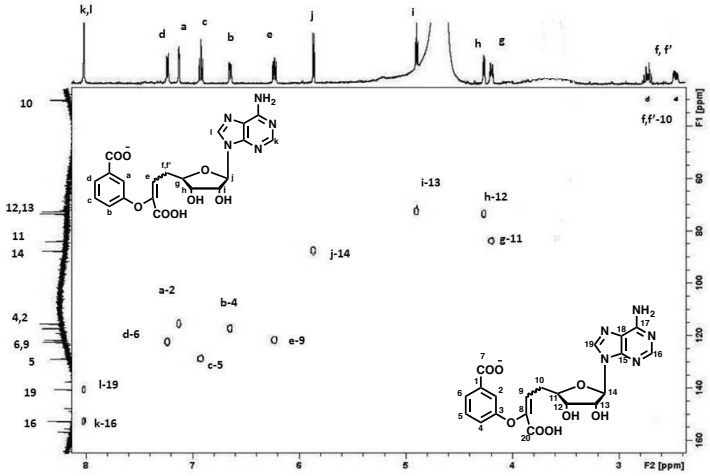

Figure 2.11 HSQC spectrum of compound **31**.

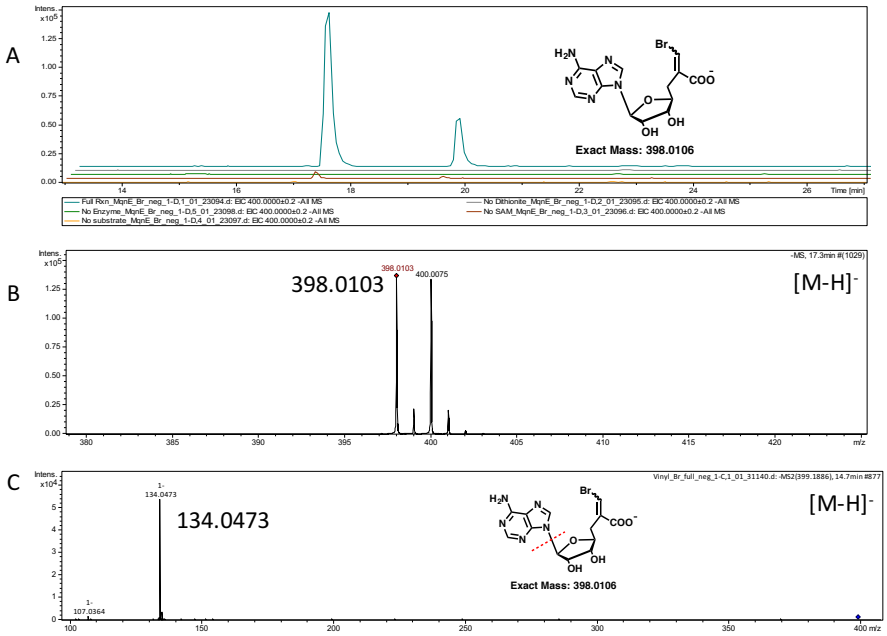

Figure 2.12 LCMS analysis of **32** formed in the MqnE-catalyzed reaction with **28**. A) LC-MS analysis showing EIC [M-H]- = 398.0 Da suggesting that this compound is **32**. B) MS of **32**. C) MS-MS fragmentation analysis of **32**

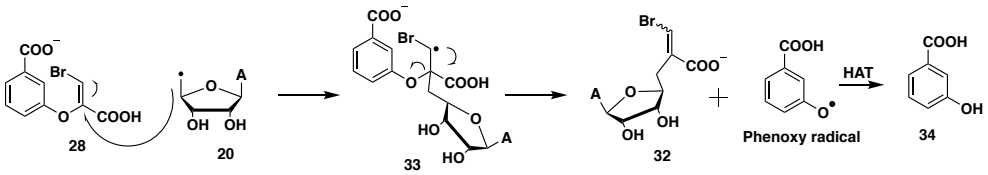

Figure 2.13 Mechanistic proposal for the formation of **32** in the MqnE-catalyzed

To obtain a better estimate of k_{spiro}, we also tested the analogous chloro-substituted substrate (Figure 2.42- 2.43), which is less prone to the beta scission reaction ($k_{C\text{-}Cl} = 4x10^6$ s^{-1}).[49] HPLC and LCMS analysis of the resulting reaction mixture revealed **31** as the major product. No rearranged products were detected. A small amount of the isomeric radical addition product was also observed with the chloro-substituted substrate analog (Figure 2.14-2.16). From this experiment, we can estimate that $k_{spiro} < 2x10^5$ s^{-1} (5% detection

limit). This is an upper limit because the C-Cl fragmentation rate has not been corrected for captodative stabilization or for conformational effects at the active site that might create a stereoelectronic barrier to the beta scission reaction. We anticipate that the spirocyclization rate will be relatively slow because it involves dearomatization of the benzene ring and formation of a strained intermediate. It is also likely that formation of the spirocyclic intermediate is energetically unfavorable and that the reaction is driven by the facile decarboxylation of **25**.

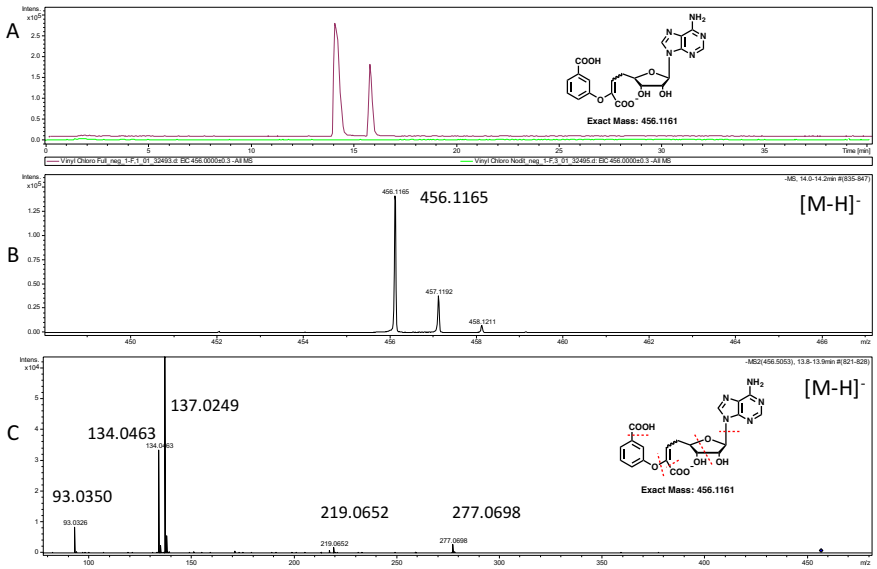

Figure 2.14 LCMS analysis of the formation of **31** in the MqnE-catalyzed reaction with **35**. A) LC-MS analysis showing EIC [M-H]- = 456.1 Da suggesting that this product is **31**. B) Mass Spectra of **31** C) MS-MS fragmentation analysis of **31**

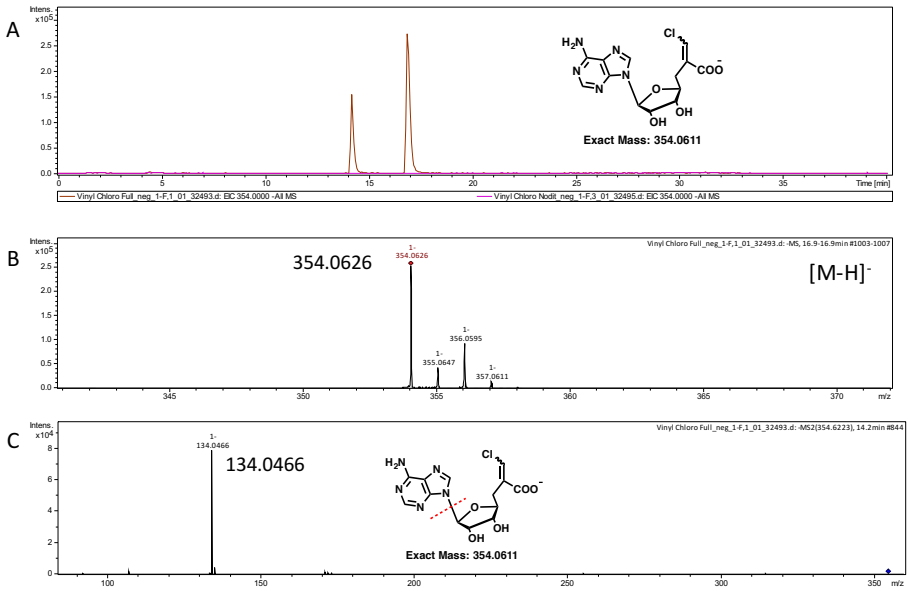

Figure 2.15 LCMS Analysis of the formation of **37** in the MqnE-catalyzed reaction with **35**. A) LC-MS analysis showing EIC [M-H]- = 354.0 Da suggesting that this compound is **37**. B) MS of **37** C) MS-MS fragmentation analysis of **37**.

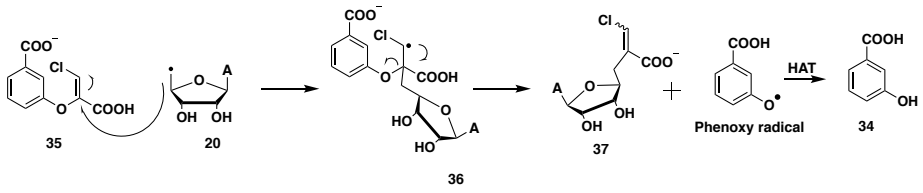

Figure 2.16 Mechanistic proposal for the formation of **37**

Our mechanistic proposal suggests that the substrate vinylic carboxylic acid may function as the acid catalyst for the ring opening of the spiroepoxide **24**. This suggests that replacing the vinylic carboxylic acid of **13** with the corresponding amide might block the conversion of **24** to **25** and result in intermediate trapping.

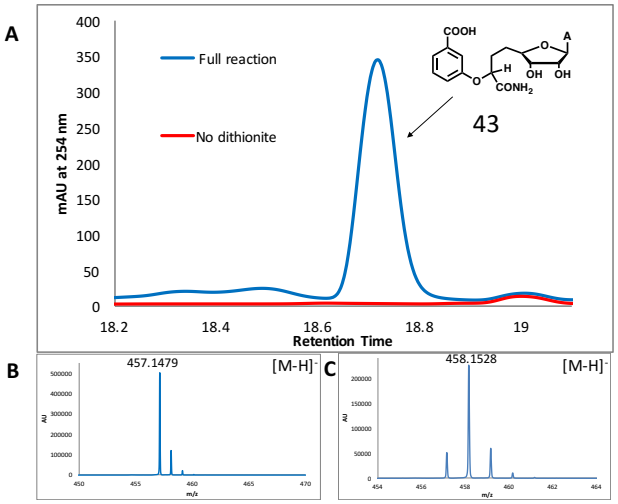

Figure 2.17 The MqnE-catalyzed reaction of the substrate amide analog **38**. A) HPLC chromatogram of the reaction mixture. B) MS of the major reaction product eluting at 18.75 minutes. C) MS of the product for the reaction run in 95% D2O containing buffer.

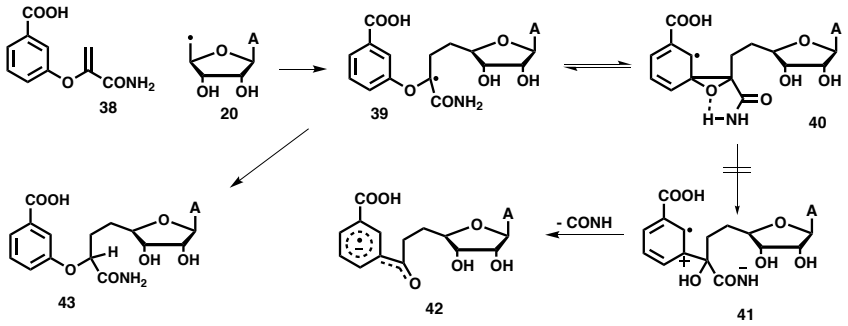

Figure 2.18 Mechanistic proposal for the MqnE catalyzed reaction of the amide analog **38**.

Amide analog **38** was synthesized as shown in Figure 2.44- 2.45 and treated with MqnE under standard reaction conditions. HPLC and LCMS analysis of the resulting reaction mixture indicated the formation of a single major product (Figure 2.17) with m/z: 457.1479, consistent with the trapping of the captodative radical, **39**. This was confirmed by the complete NMR characterization of **43** (Figure 2.19- 2.24). Running the reaction in

95% D_2O containing buffer demonstrated that the hydrogen atom is derived from an exchangeable position on MqnE (Figure 2.17, B&C).

A mechanistic proposal for the formation of **43** is outlined in Figure 2.18. We propose that **39** undergoes reversible spirocyclization to **40**. However, because the amide is much less acidic than the carboxylic acid in the native substrate **13**, ring opening of the spiroepoxide **40** is retarded sufficiently to allow off path trapping of the captodative radical by hydrogen atom transfer.

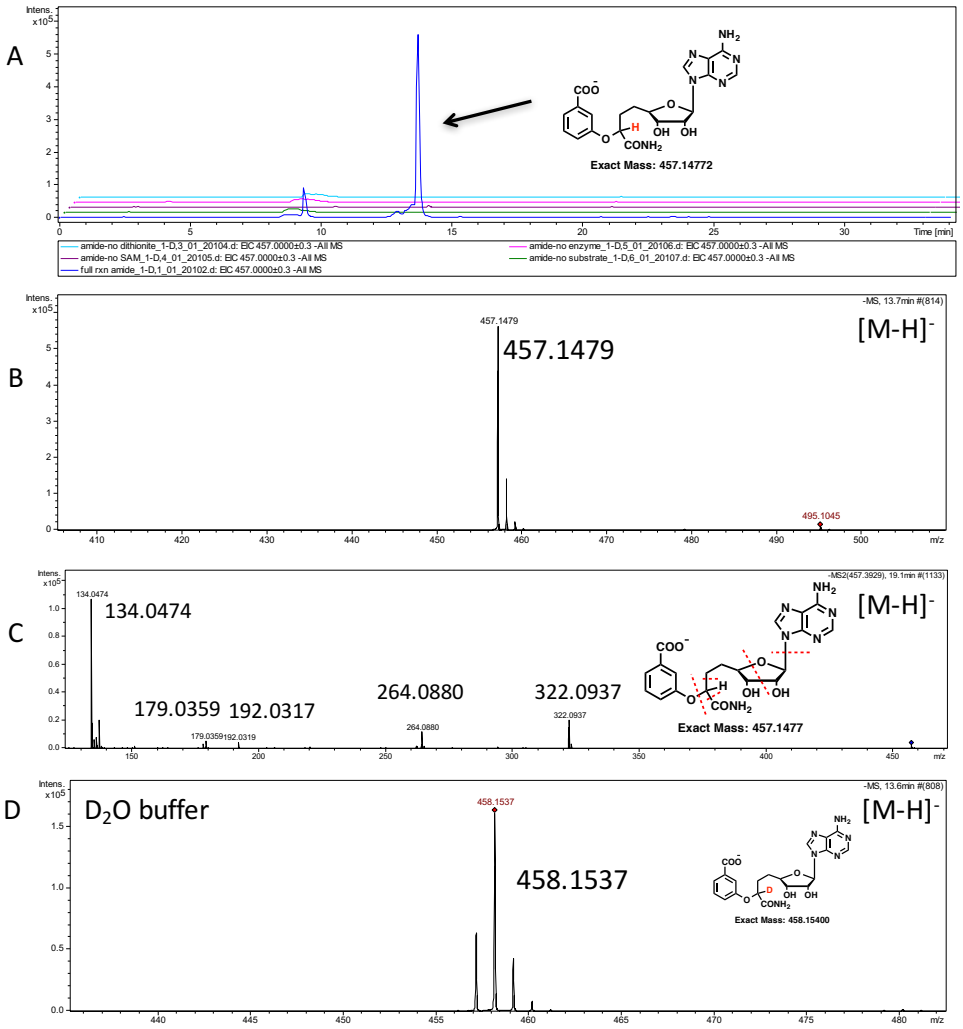

Figure 2.19 LCMS Analysis of the formation of **43** in the MqnE-catalyzed reaction with **38**. A) LC-MS analysis showing EIC [M-H]- = 457.1 Da suggesting that this compound is **43**. B) MS of **43** C) MS-MS fragmentation analysis of 4**3** D) LC-MS analysis showing EIC [M-H]- = 458.1 Da suggesting deuterium incorporation in compound **43** when reaction is run in 95% D_2O containing buffer.

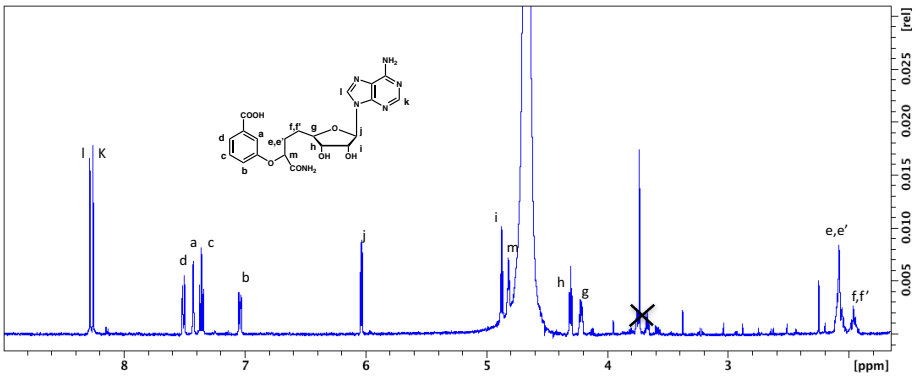

Figure 2.19 ^{1}H NMR (500 MHz, D_2O) spectrum of compound **43**.

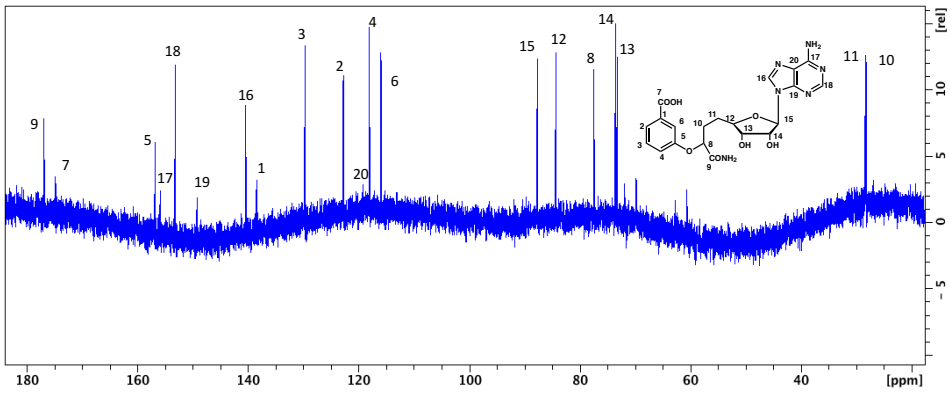

Figure 2.20 ^{13}C NMR (125 MHz, D_2O) spectrum of compound **43**.

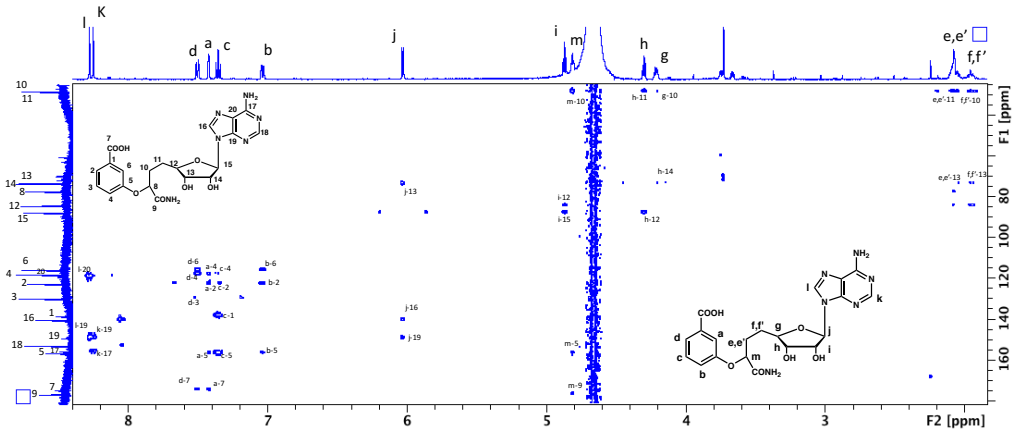

Figure 2.21 HMBC spectrum of compound **43**.

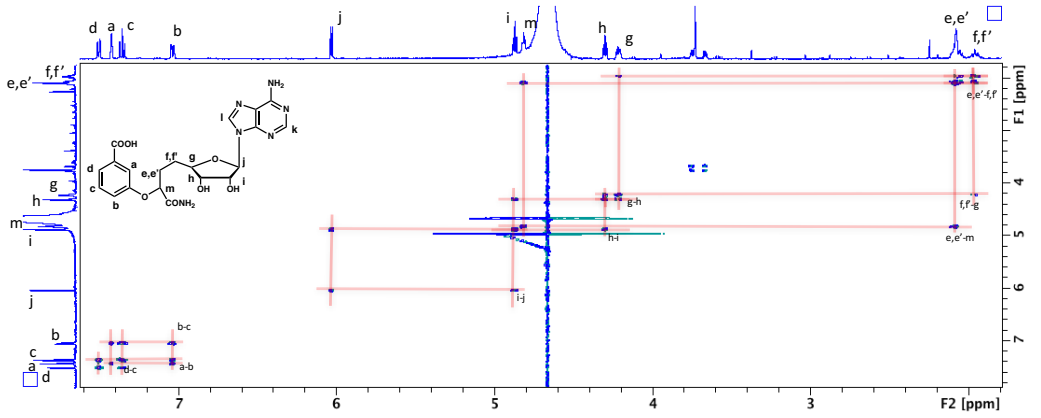

Figure 2.22 ^{1}H COSY spectrum of compound **43**.

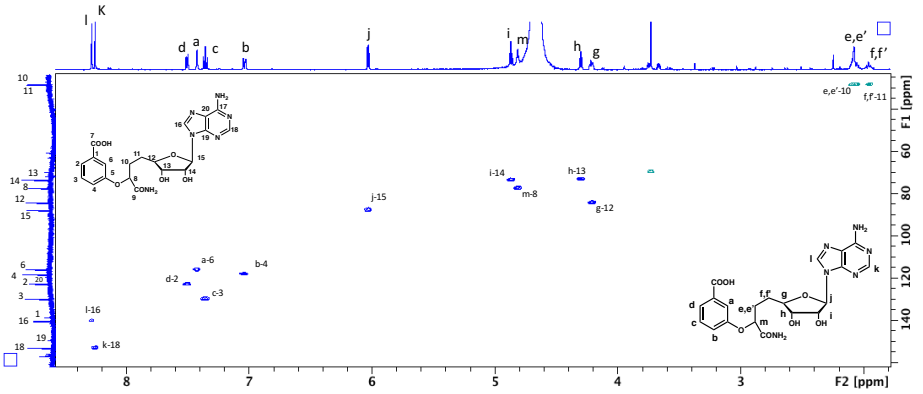

Figure 2.23 HSQC spectrum of compound **43**.

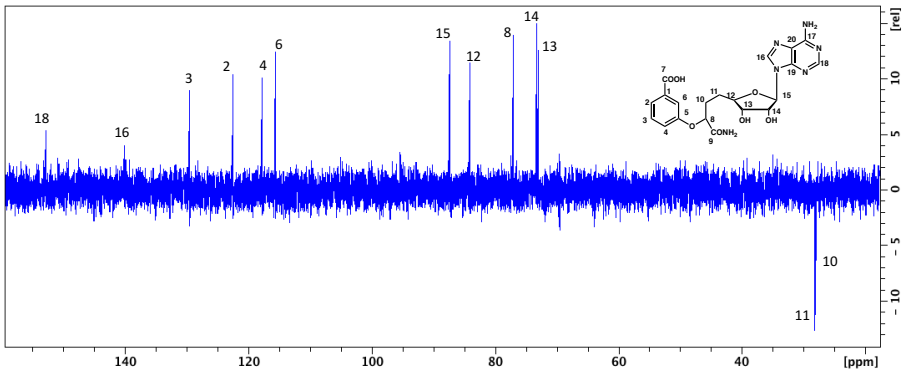

Figure 2.24 DEPT 135 spectrum of **43**.

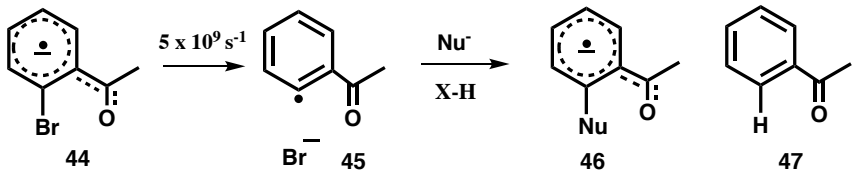

Figure 2.25 The radical substitution mechanism of aryl halide radical anions ($S_{RN}1$).

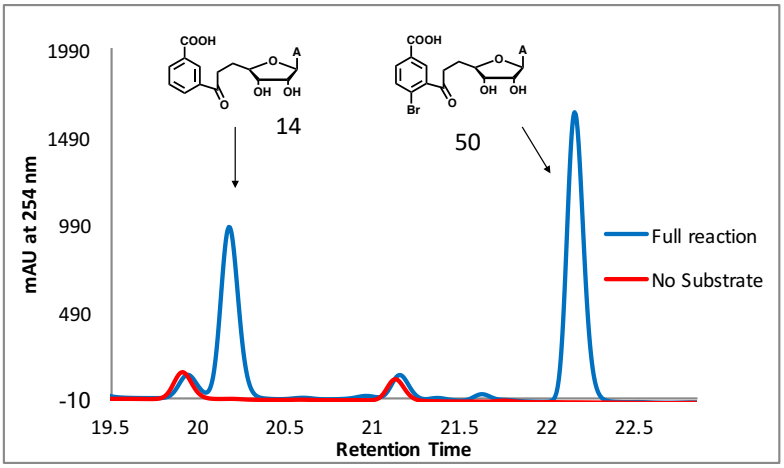

Figure 2.26 HPLC analysis of the MqnE-catalyzed reaction with **48**

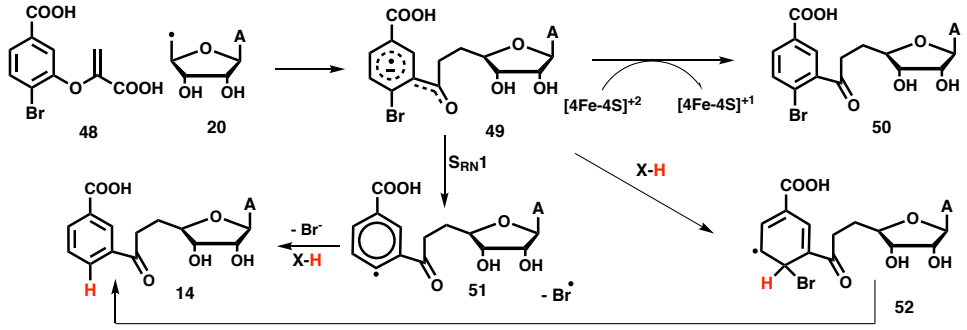

Figure 2.27 Mechanistic proposal for the MqnE-catalyzed rearrangement of the brominated substrate analog **48**

2.5. Aryl radical anion trapping

The next set of experiments were targeted towards detection of the aryl radical anion **27** using the propensity of halogenated aryl radical anions to undergo substitution/hydrogen atom abstraction reactions. An example of such a reaction from the organic chemistry literature, for a closely related compound, is shown in Figure 2.25. Electron transfer from the SOMO of the aryl ring to the C-Br σ* orbital weakens the C-

Br bond resulting in rapid loss of bromide to give the aryl radical **45** which can then react with a nucleophile to give **46** (reverse of the fragmentation reaction) or undergo hydrogen atom transfer from a suitable donor to form **47**.[50-51] Based on this chemistry, we hypothesized that bromo analog **48** should enable us to probe for the aryl radical anion **27** proposed in Figure 2.2. Compound **48** was synthesized as shown in Figure 2.46- 2.47 and treated with MqnE under standard reaction conditions. HPLC and LCMS analysis of the resulting reaction mixture indicated the formation of two major products (Figure 2.26, S42) with masses that were consistent with those expected for aminofutalosine **14** and bromo-aminofutalosine **50** (Figure 2.28- 2.30). This was confirmed by the complete NMR characterization of **50** (Figure 2.31-2.36) and the co-elution of the signal at 20.1 minutes with authentic aminofutalosine **14** generated in the MqnE reaction with the native substrate **13** (Figure 2.37). These results are consistent with the formation of an aryl radical anion intermediate **49** (Figure 2.27). An alternative mechanism involving protonation of the aryl radical anion (**49** to **52** in Figure 2.27) was excluded by running the reaction in 95% deuterated buffer. Under these conditions, 65% of the aminofutalosine **8** was non-deuterated (Figure 2.28) consistent with the formation of **50** by hydrogen atom transfer from a non-acidic center rather than proton transfer from an exchangeable acidic center.

Our mechanistic proposal indicates that the MqnE reaction is completed by the oxidation of the aryl radical anion **27** by the $[4Fe\text{-}4S]^{2+}$ cluster. This implies that there is no net consumption of reducing equivalents during the reaction. This was verified by the observation of multiple enzyme turnovers in the presence of stoichiometric amounts of sodium dithionite (Figure 2.38).[52]

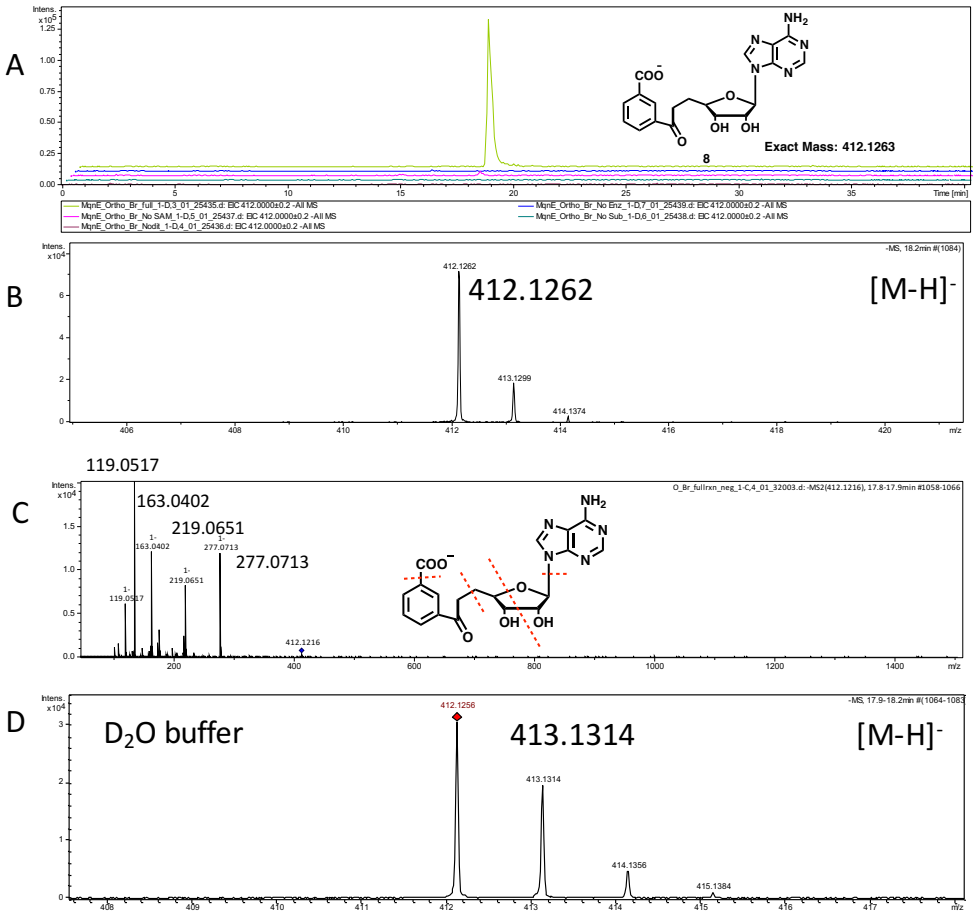

Figure 2.28 LCMS Analysis of the formation of **14** in the MqnE catalyzed reaction with **48**. A) LC-MS analysis showing EIC [M-H]- = 412.0 Da suggesting that this compound is **14**. B) MS of **14**. C) MS-MS fragmentation analysis of **14**. D) LC-MS analysis showing EIC [M-H]- = 413.

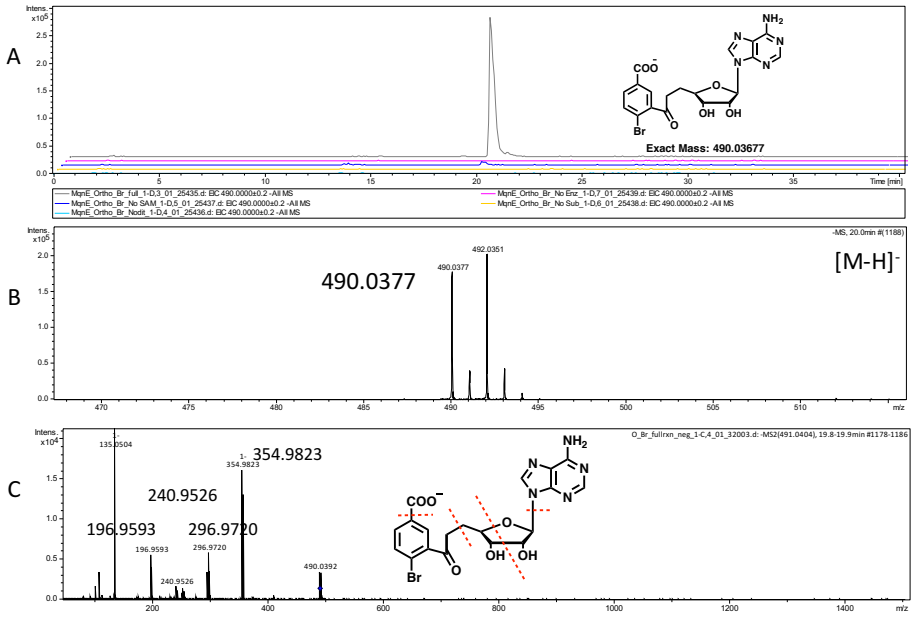

Figure 2.29 LCMS Analysis of the formation of **50** in the MqnE catalyzed reaction with **48**. A) LC-MS analysis showing EIC [M-H]- = 490.0 Da suggesting that this compound is **50**. B) MS of **50**. C) MS-MS fragmentation analysis of **50**.

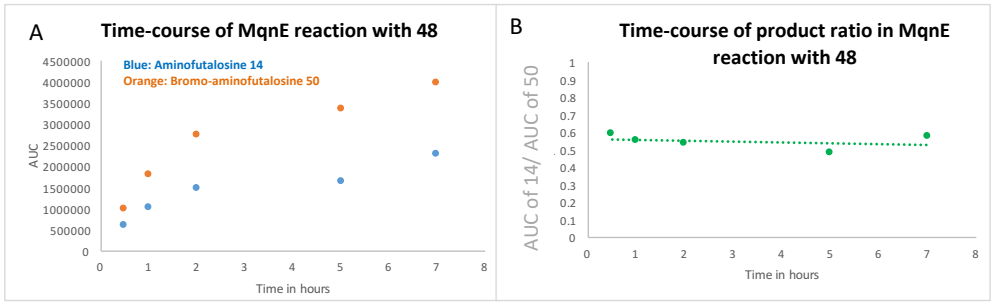

Figure 2.30 A) Time course of formation of **14** and **50**. B) The relative product ratio of **14** and **50** remains constant over time period of the reaction.

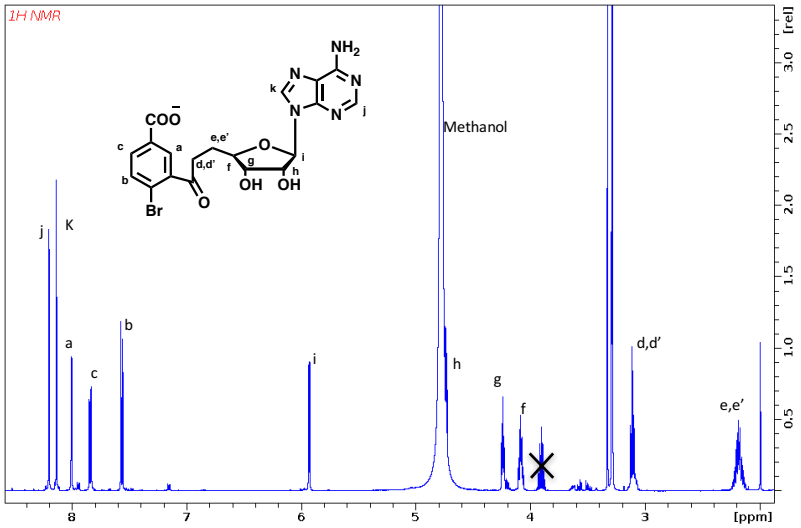

Figure 2.31 ^{1}H NMR spectrum of compound **50**.

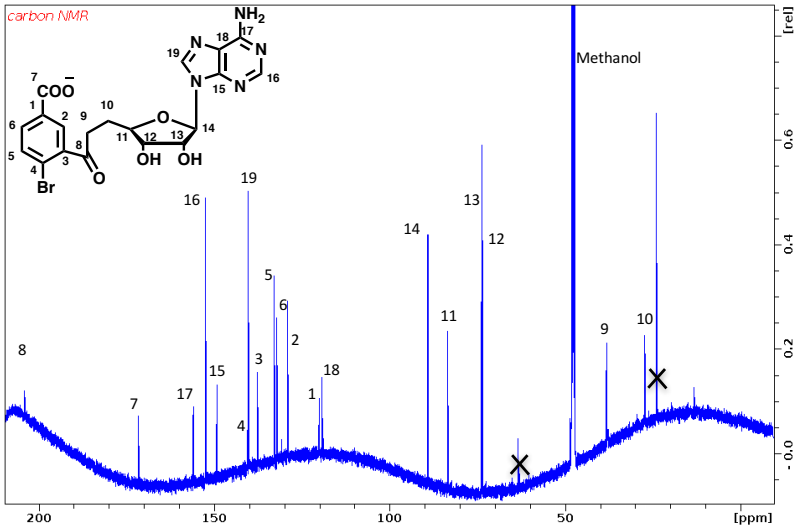

Figure 2.32 ^{13}C NMR spectrum of compound **50**

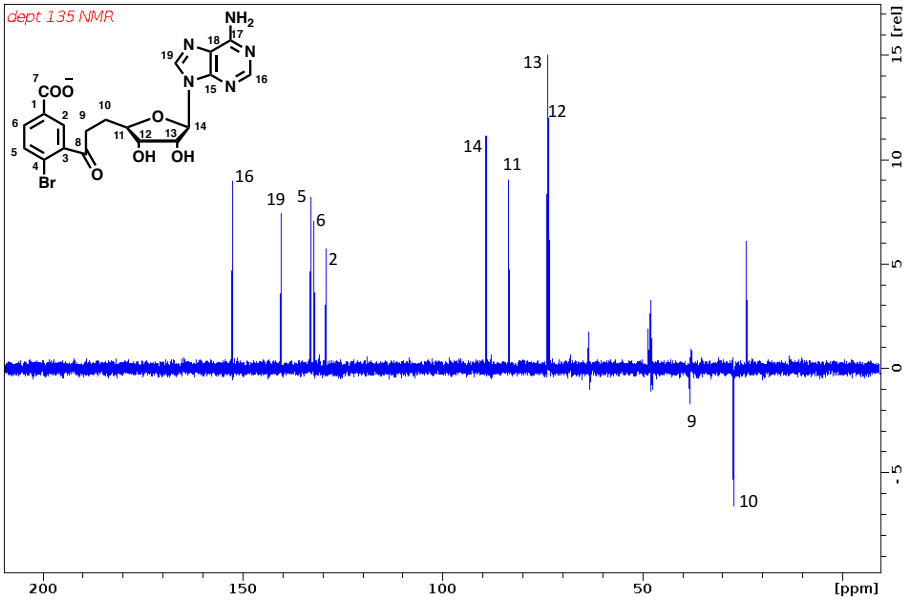

Figure 2.33 DEPT-135 NMR spectrum of compound **50**

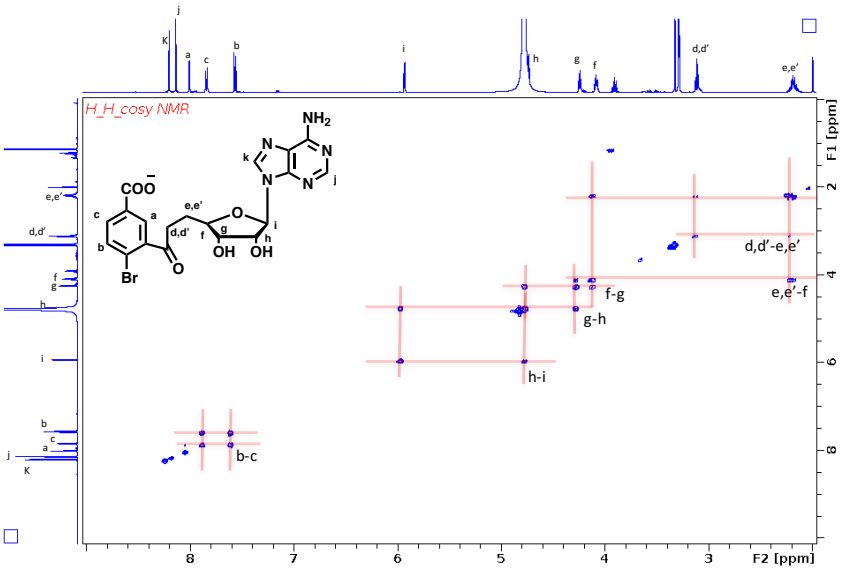

Figure 2.34 ^{1}H-^{1}H COSY NMR spectrum of compound **50**.

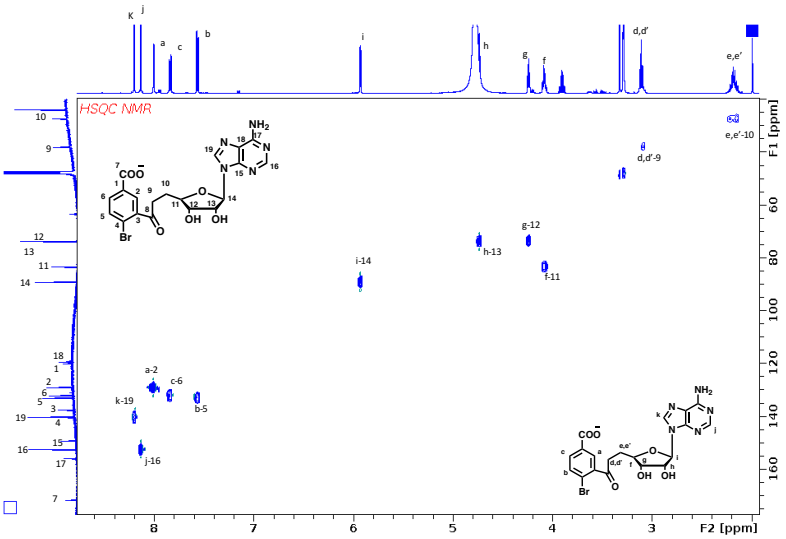

Figure 2.35 HSQC NMR spectrum of compound **50**.

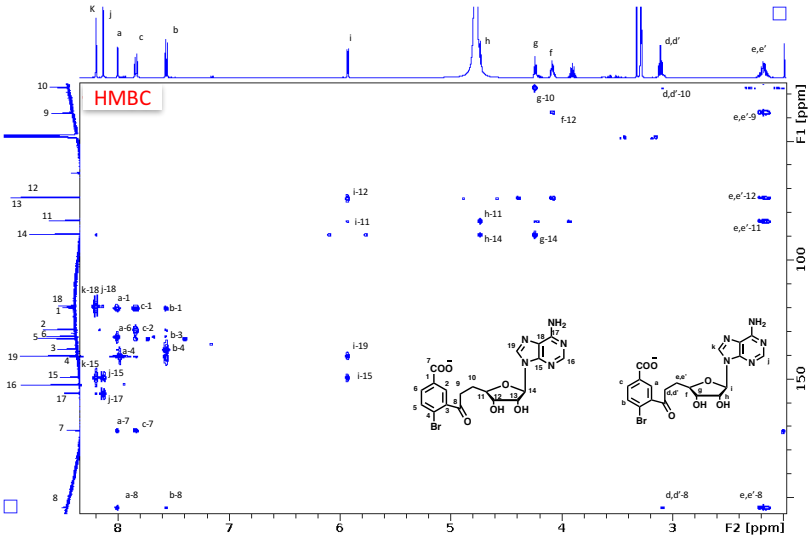

Figure 2.36 HMBC NMR spectrum of compound **50**.

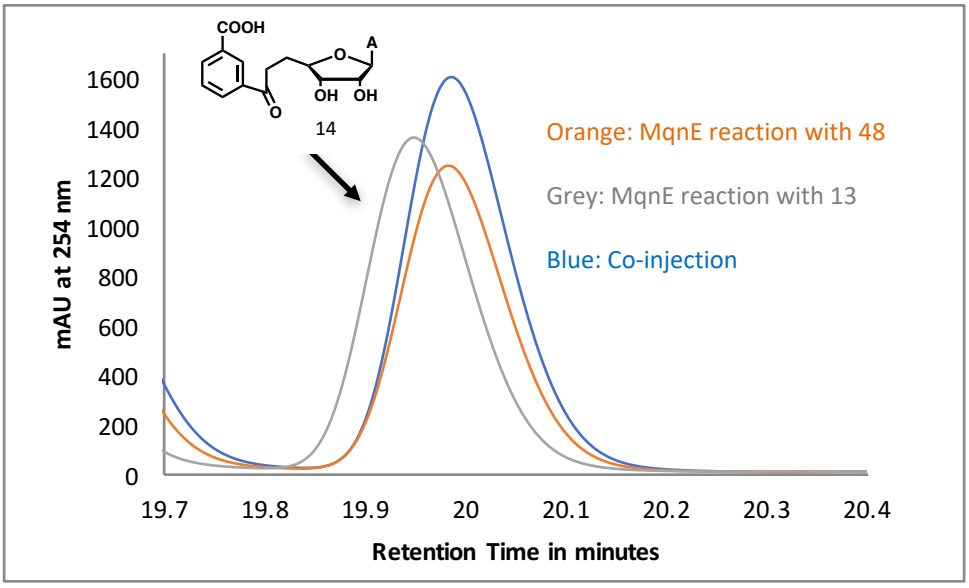

Figure 2.37 Co-elution study of the compound **14** with the authentic aminofutalosine **14** generated in the MqnE reaction with the native substrate **13**.

In summary, we have described three key experiments that support the mechanistic proposal for aminofutalosine synthase outlined in Figure 2.2. Bromo-analog **28** used the fragmentation of a C-Br bond beta to a radical center to trap the initially formed captodative radical **23**. While radical addition to double bonds has abundant precedent in organic synthesis, the addition of the adenosyl radical to a substrate double bond was unprecedented in biosynthesis. Addition of the 5'-deoxyadenosyl radical to a dehydroalanine containing pyruvate formate lyase variant[53] and the inactivation of glutamate mutase (B_{12}-dependent) by 2-methylene glutarate[54] are the closest examples of related chemistry in engineered systems. Analog **38** blocked the decarboxylation reaction resulting in the trapping of the captodative radical by a hydrogen atom transfer reaction. Bromo-analog **48** enabled the detection of the aryl radical anion intermediate by an $S_{RN}1$

type C-Br fragmentation reaction. These studies also demonstrate that the small, synthetically accessible C-Br bond is a highly sensitive radical probe with considerable potential for the detection of radical intermediates in enzyme-catalyzed reactions.

2.6. Experimental procedures

2.6.1. General materials and Methods

All chemicals were purchased from Sigma Aldrich (St. Louis, MO) unless otherwise stated and used without further purification. LB growth medium was obtained from Difco. Kanamycin, ampicillin, chloramphenicol antibiotics and isopropyl-β-D-thiogalactopyranoside (IPTG) were purchased from LabScientific Inc. Ni-Nitrilotriacetic acid (NTA) resin was from GE Life Sciences. Molecular biology manipulations were carried out as previously reported.[27] Centrifugal filters were obtained from Pall Life Sciences. HPLC grade solvents were obtained from Fisher Scientific.

2.6.2. HPLC parameters

An Agilent 1260 HPLC equipped with a quaternary pump was used. The system included a diode array UV-Vis detector and eluted compounds were detected by absorbance at 225, 254, 260, 280, 320, 340, and 475 nm. The parameters for the fluorescence detector were: excitation at 385 nm and emission at 484 nm. The HPLC analysis was performed on a ZORBAX Eclipse XDB-C18 column (15 cm x 4.6 mm, 5 μm particles, Agilent Technologies). Typical injection volumes were in the range of 10-50 μl. Data was processed using ChemStation ver. B.04.01 SP1 (Agilent technologies).

HPLC conditions:

A- Water

B- 100mM Potassium phosphate buffer, pH 6.6 or 10 mM Ammonium acetate pH 6.6

C- Methanol

HPLC method:

0 min – 100% B, 5min – 100% B, 14 min – 7% A 70% B 23% C, 25 min – 25% A 0% B 75% C, 28 min - 25% A 0% B 75% C, 32 min - 100% B, 36 min - 100%B.

or

0 min – 100% B, 5min – 100% B, 12 min – 48% A 40% B 12% C, 14 min – 50% A 30% B 20% C, 18 min - 30% A 10% B 60% C, 20 min - 100% B, 25 min - 100%B.

2.6.3. LCMS parameters

LC-ESI-TOF-MS was performed using an Agilent 1260 HPLC system equipped with a binary pump and a 1200 series diode array detector followed by a MicroToF-Q II mass spectrometer (Bruker Daltonics) using an ESI source either in negative mode or positive mode. The analysis was performed on an LC-18-T column (15 cm x 3 mm, 3 μm particles, Supelco). Typical injection volumes were in the range of 20-80 μl. The data was processed using DataAnalysis 4.0 SP1 (Bruker Daltonics).

LC conditions:

A- 5 mM ammonium acetate buffer, pH6.6

B- 75% Methanol and 25% Water.

LC method: (for negative mode on MS)

0min – 100% A, 7min – 100% A, 10min – 80% A 20%B, 27 min – 100%B, 29min – 100% B, 30min – 100% A, 40min – 100% A.

MS parameters: (for all LC-MS experiments)

Capillary, -4500 V; capillary offset, -500 V; nebulizer gas, 3.0 bar; dry gas, 10 L/min; dry gas temperature, 200 ^{o}C; funnel 1 RF, 250.0 Vpp; funnel 2 RF, 300.0 Vpp; ISCID, 0.0 eV; hexapole RF, 200 Vpp; quadrapole ion energy, 3.0 eV; collision cell, collision energy, 8.0 eV; collision RF, 150.0 Vpp, transfer time, 80.0 µs; prepulse storage, 5.0 µs.

2.6.4. NMR analysis

NMR spectra of all the synthetic samples were recorded on Bruker Avance III 400 MHz instrument. NMR characterization of samples collected by HPLC was performed on Bruker Avance III 500 MHz instrument with H-C-N cryoprobe in 3 mm Wilmad labglass (328-PP-7) high precision NMR tubes.

2.6.5. Expression and purification of MqnE

The mqnE gene from *T. Thermophilus* was cloned into the pTHT vector (derivative of pET28b vector with TEV protease cleavage site after N-terminal His-tag). MqnE was co-expressed with a plasmid encoding the suf operon[55] in *E. coli* BL 21(DE3) for in vivo assembly of the [4Fe-4S] cluster. A starter culture was grown overnight in LB media containing kanamycin (40µg/ml) and chloramphenicol (34µg/ml). 90 ml of this culture was added to 9 L LB media (6 x 1.5 L flasks) with antibiotics and grown at 37 °C with shaking (220 rpm) till OD_{600} ~ 0.6. The flasks were then incubated at 4 °C for ~1 h without

shaking. Each flask (1.5 L) was supplemented with 200 mg ferrous ammonium sulfate and 200 mg L-cysteine. Cultures were then induced with 500 μM IPTG followed by incubation at 15 °C for ~16-18 h with shaking (120 rpm). The cells were harvested by centrifugation and stored in liquid nitrogen until further use. Typical yields were 18-20 g of cell pellet (wet weight) from 9 L cell culture. All steps for MqnE purification were carried out in an anaerobic chamber (COY laboratories). Cell pellets were thawed and re-suspended in 60-70 ml of lysis buffer (100 mM Tris-HCl, pH 7.5) at room temperature in the presence of lysozyme (10-12 mg) and benzonase (1000 units). The suspension was stirred for ~1 h on an ice bath and further sonicated to lyse the cells. Cell debris was removed by centrifugation and the lysate was loaded onto a Histrap column pre-equilibrated with lysis buffer. The column was washed with 10 column volumes of wash buffer (100 mM Tris-HCl, 30 mM imidazole, 300 mM NaCl, pH 7.5). The protein was then eluted from the histrap column with elution buffer (100 mM Tris-HCl, 250 mM imidazole, 300mM NaCl, pH 7.5). The dark colored fractions were pooled and buffer exchanged to 100 mM potassium phosphate, 30% glycerol, pH 7.5 using an Econo-Pac 10DG desalting column. Typical yields were ~ 8 mg per liter of cell culture. The purified enzyme was stored submerged in liquid nitrogen until further use. Protein concentration was measured by the absorbance at 280 nm (A280) with an extinction coefficient calculated using the ProtParam tool of the ExPASy proteomics server. Iron content was determined using the ferrozine assay while sulfide content was determined using the methylene blue assay.[27, 30]

2.6.6. Assay of MqnE reaction with substrate analogs

Each reaction mixture (150 µL) contained chemically synthesized analog **9** (2 mM), S-adenosylmethionine, **29** (1 mM), purified MqnE (200 µM) and excess sodium dithionite in 100 mM Kpi buffer, pH 7.5. The reaction was allowed to proceed anaerobically for about 4-6 hrs. The reaction was repeated multiple times to give sufficient product for analysis. The reactions were quenched by ultrafiltration using 10 kDa centrifugal filters (Pall Life Sciences). Reaction products were purified from the reaction mixture by HPLC. The purified product was concentrated using a Freeze-dryer (Labconco), dissolved in suitable solvent and characterized by ^{1}H and ^{13}C NMR and mass spectrometry.

2.6.7. Steady state kinetics measurements on the MqnE reaction

The initial velocity for the Aminofutalosine formation by MqnE was determined using discontinuous HPLC assay. The concentrations of MqnE used in the assays was 5µM. To measure K_M for the substrate VOBA **13**, concentration of 13 was varied from 50 µM – 10 mM keeping concentration of SAM constant at 2mM. To measure K_M for the substrate SAM, concentration of SAM was varied from 10 µM – 2 mM keeping concentration of **13** constant at 2mM.

2.6.8. Electron recycling in MqnE reaction

To study the dithionite concentration dependence of Aminofutalosine **14** formation; MqnE (50uM) was incubated with varying concentrations of sodium dithionite (5 - 500 uM), S-adenosylmethionine, **19** (1.5 mM), and substrate **13** (1.5 mM) in 100 mM Kpi buffer, pH 7.5. The reaction was allowed to proceed anaerobically for about 4 hours.

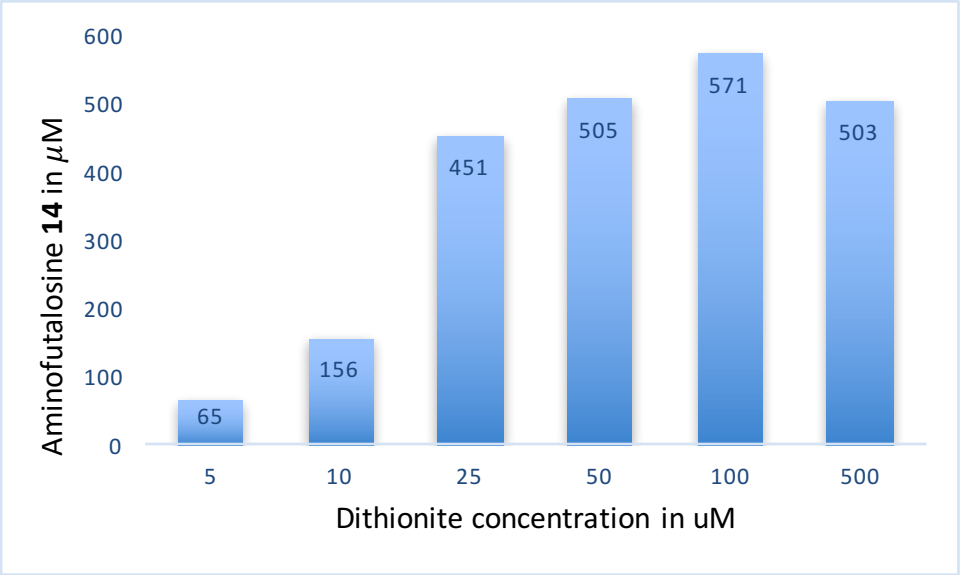

Figure 2.38 Dithionite concentration dependence of formation of aminofutalosine **14**. Multiple enzymatic turnovers (~10) are observed with one equivalent of dithionite.

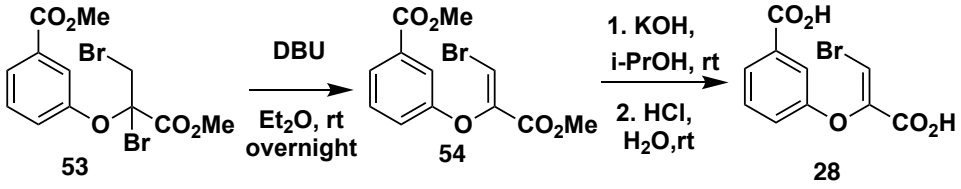

Figure 2.39 Synthetic scheme for (Z)-3-((2-bromo-1-carboxyvinyl)oxy)benzoic acid 9.

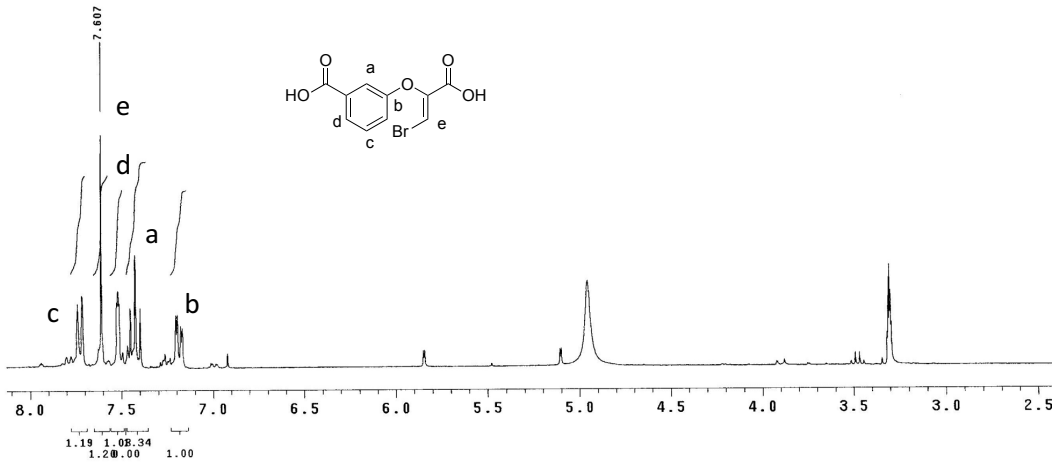

Figure 2.40 : ^{1}H NMR (300 MHz, CD_3OD) of (Z)-3-((2-bromo-carboxyvinyl)oxy)benzoic acid **28**.

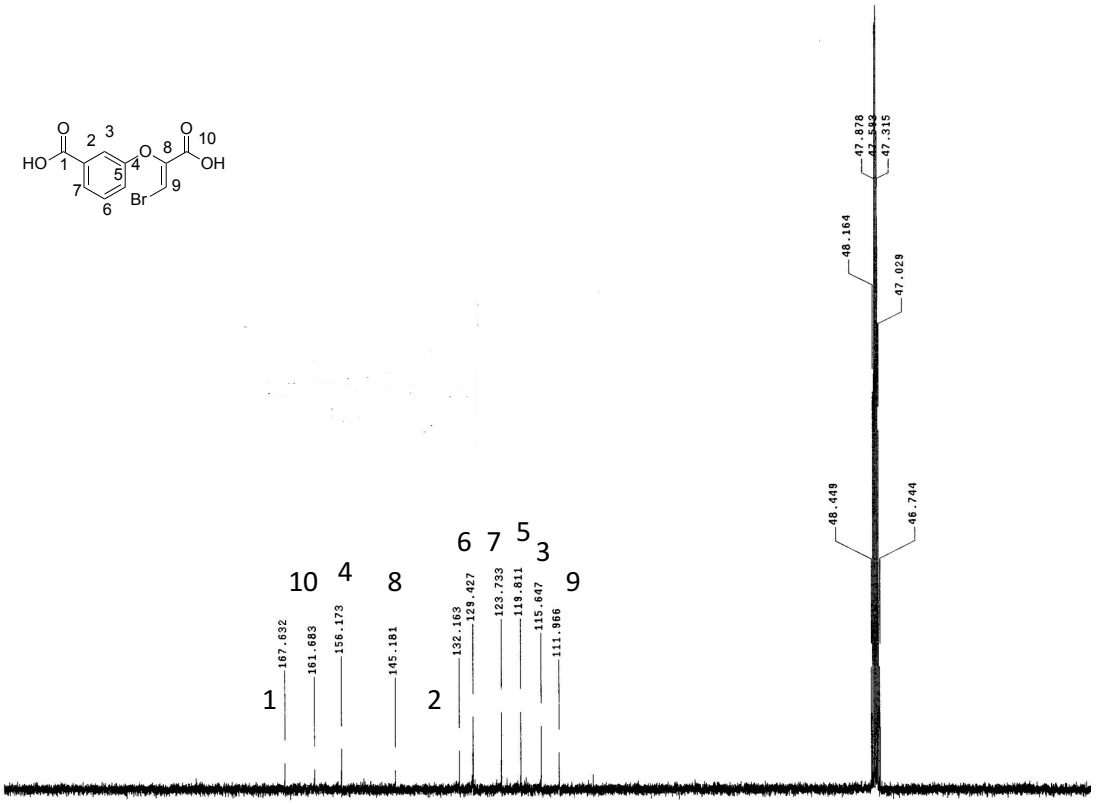

Figure 2.41 ^{13}C NMR (100 MHz, CD_3OD) of (Z)-3-((2-bromo-1-carboxyvinyl)oxy)benzoic acid **28**.

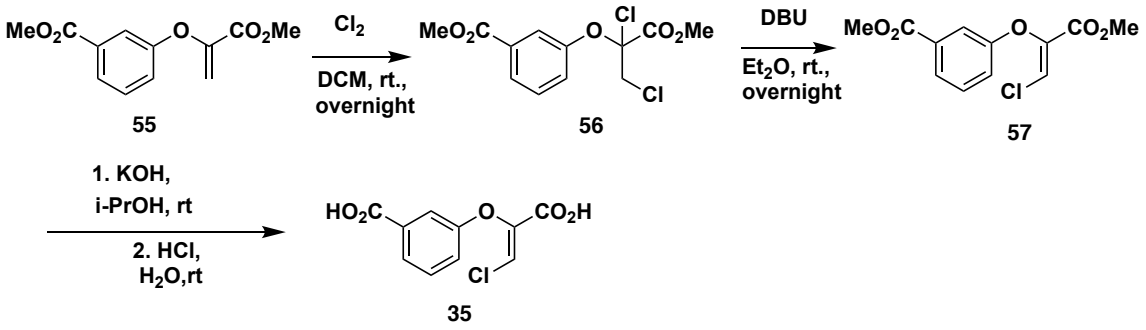

Figure 2.42 Synthetic scheme for (Z)-3-((1-carboxy-2-chlorovinyl)oxy)benzoic acid **35**

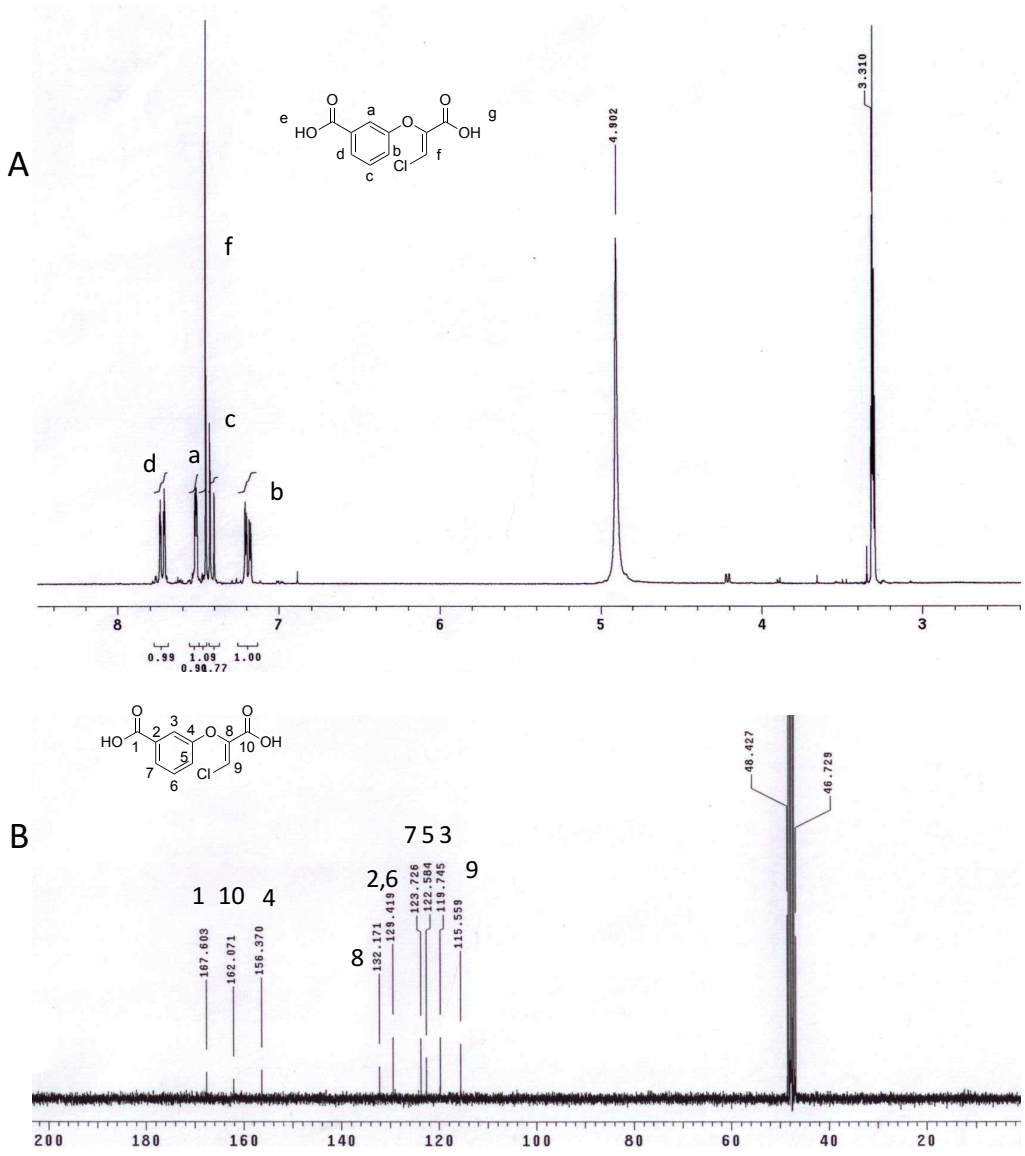

Figure 2.43 A) ^{1}H NMR (300 MHz, $CDCl_3$) and B) ^{13}C NMR (75 MHz, $CDCl_3$) of (Z)-3-((1-carboxy-2-chlorovinyl)oxy)benzoic acid **35**.

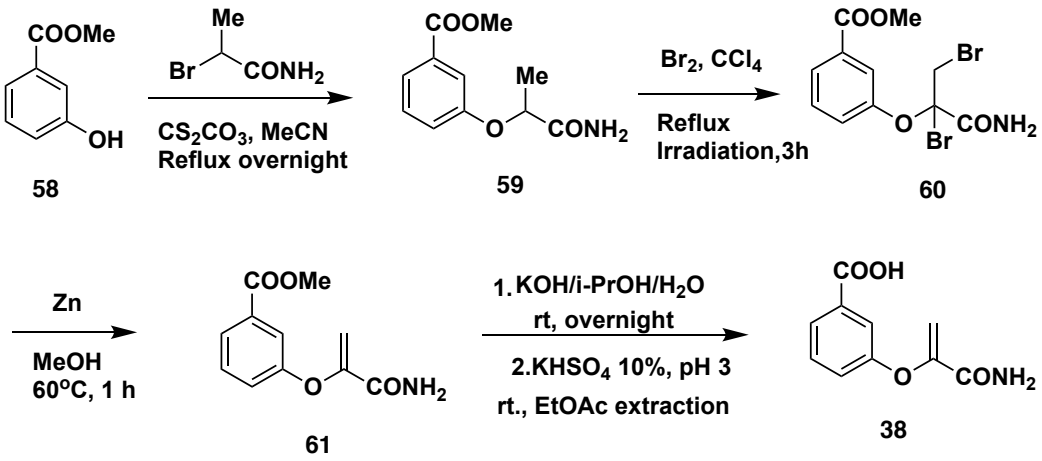

Figure 2.44 Synthetic scheme for 3-((3-Amino-3-oxoprop-1-en-2-yl)oxy)benzoic acid **38**.

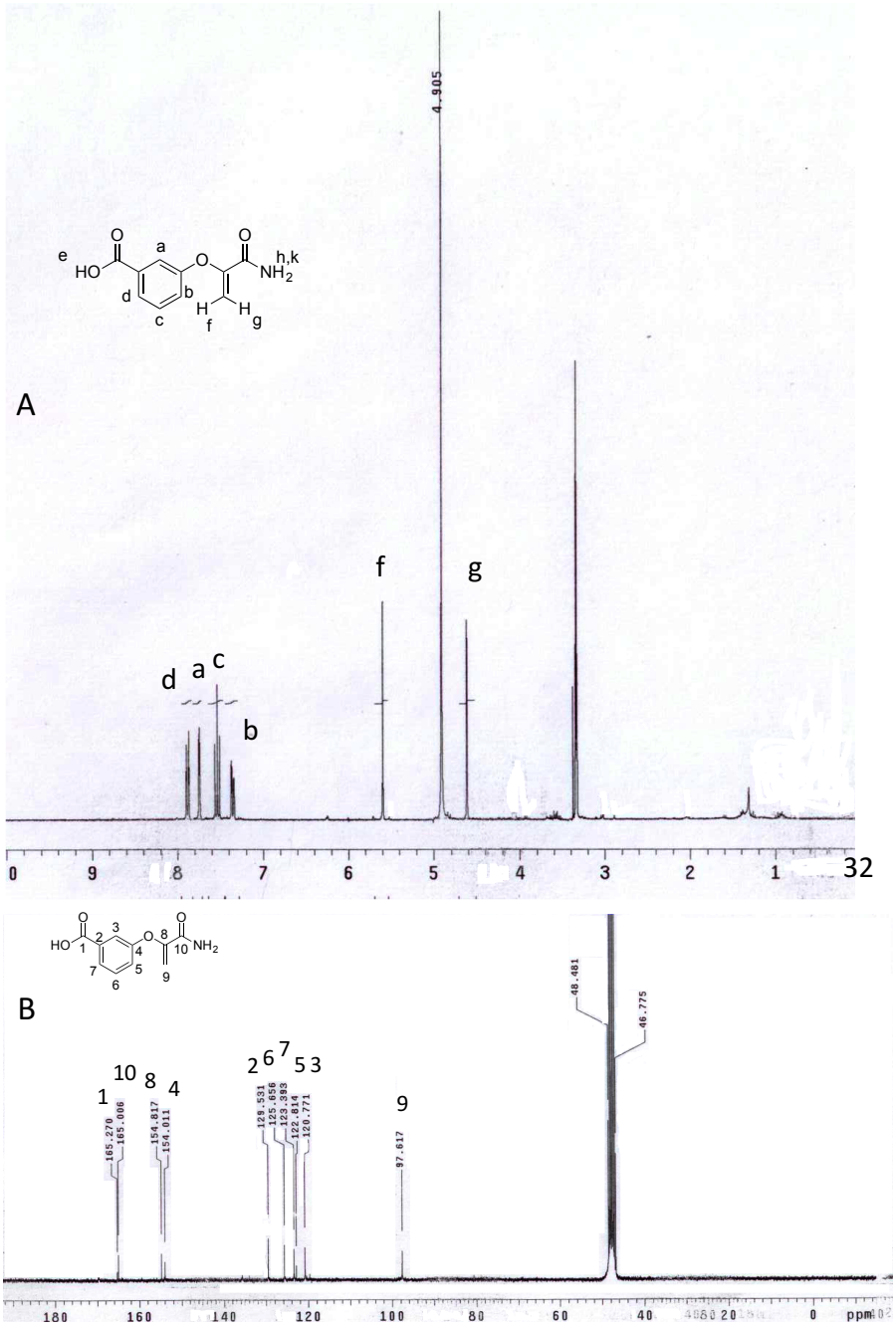

Figure 2.45 1H NMR (300 MHz, CDCl3) and B) 13C NMR (75 MHz, CDCl3) of 3-((3-amino-3-oxoprop-1-en-2-yl)oxy)benzoic acid 14.

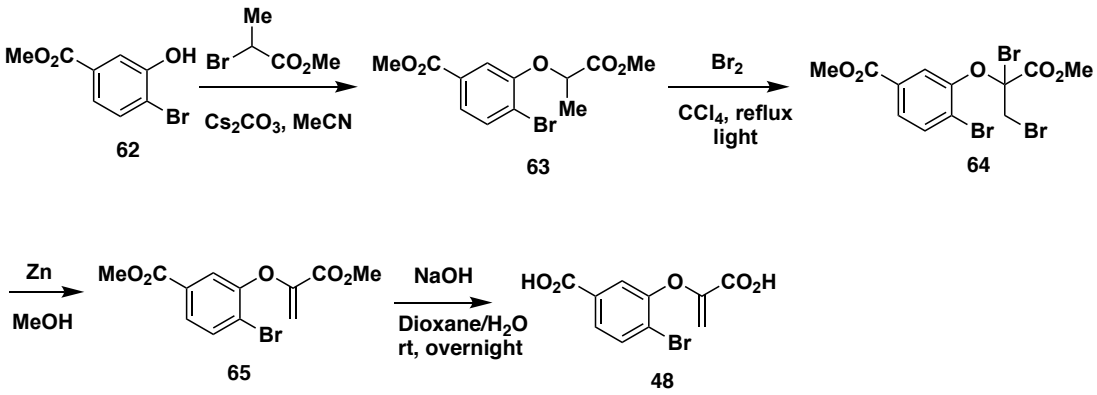

Figure 2.46 Synthetic scheme for 4-bromo-3-((1-carboxyvinyl)oxy)benzoic acid **48**.

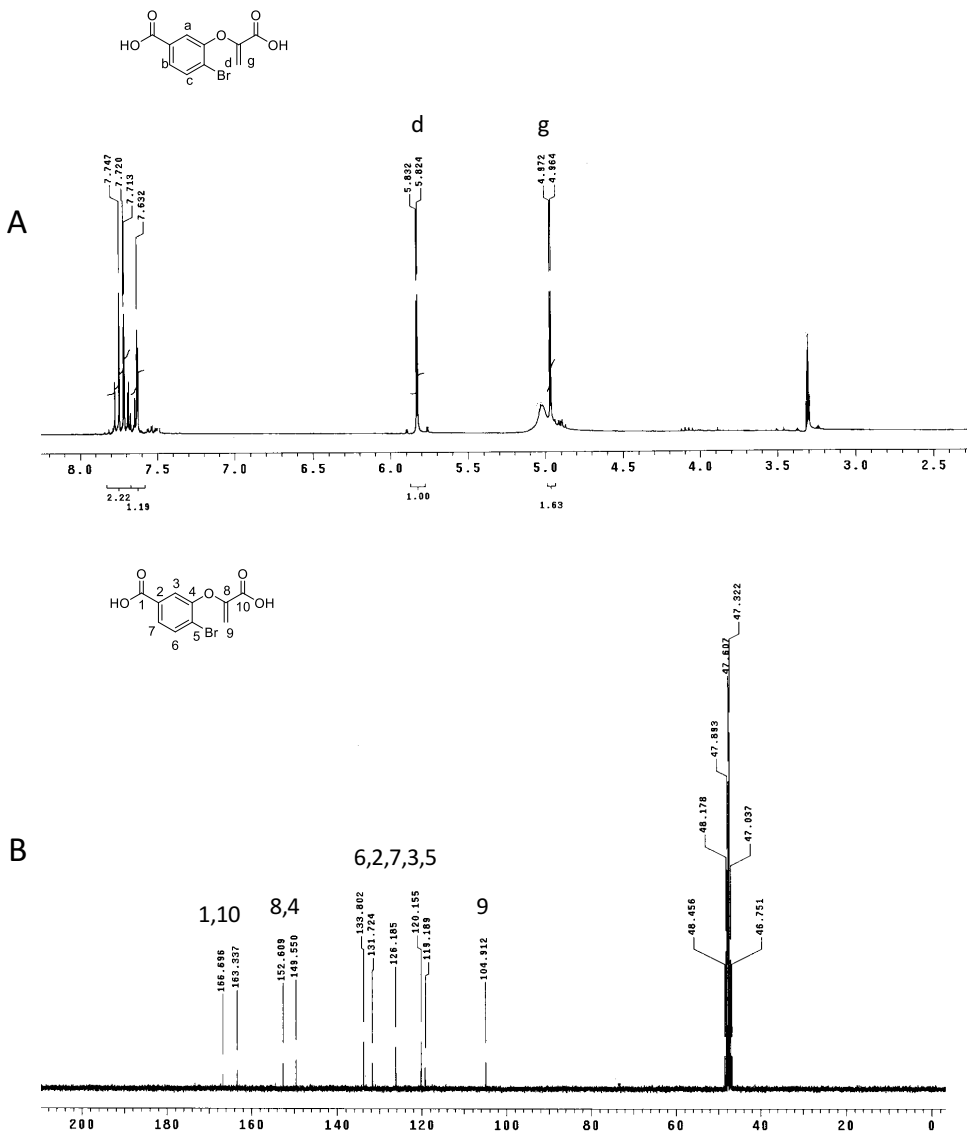

Figure 2.47 A) ^{1}H NMR (300 MHz, $CDCl_3$) and B) ^{13}C NMR (75 MHz, $CDCl_3$) of 4-bromo-3-((1-carboxyvinyl)oxy)benzoic acid **48**.

3. RADICAL TRAPPING AND INHIBITION STUDIES IN MQNE CATALYZED REACTION‡

3.1. MqnE reaction with the methylene analog

We hypothesized that replacing the bridging oxygen of the native substrate **13** with a methylene group (compound **66**) would block the conversion of **68** to **70/69** due to the instability of a primary carbanion (or radical). This would allow the accumulation of **67**, which after hydrogen atom abstraction would result in the formation of the shunt product **71** (Figure 3.1).

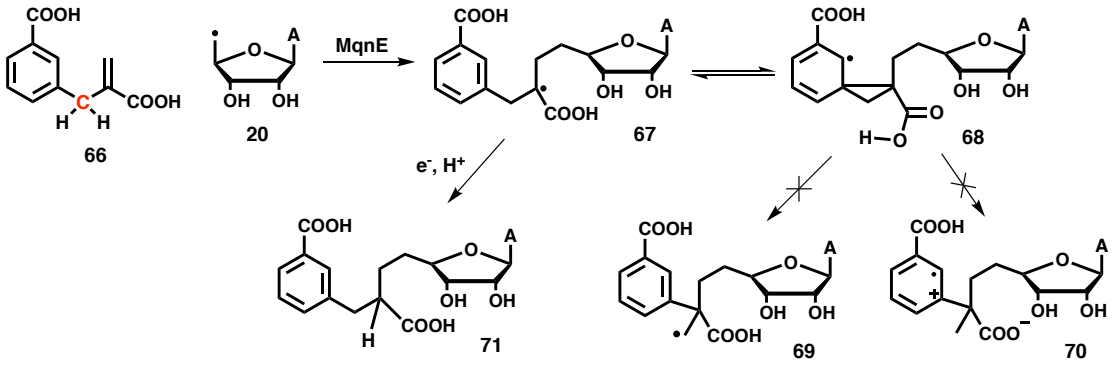

Figure 3.1 Mechanistic proposal for MqnE reaction with **66**

The methylene analog **66** was synthesized as shown in Figure S1[1-2] and tested with the *Thermus thermophilus* ortholog of MqnE. HPLC analysis of the reaction mixture indicated the formation of two major products that were absent in the controls (Figure

‡ Figures 3.1-3.9, 3.23-3.26 and text are adapted and reprinted in parts with permission from "Antibacterial Strategy against H. pylori: Inhibition of the Radical SAM Enzyme MqnE in Menaquinone Biosynthesis" by Joshi S., Fedoseyenko D., Mahanta N., Ducati R., Feng M., Schramm V., Begley T. ACS Med. Chem. Lett. 2019, 10, 3, 363-366. Copyright 2019 American Chemical Society.

3.2). The peak eluting at 19 minutes had a molecular ion m/z of 456 Da consistent with the mass of the shunt product **71** (Figure 3.3). This structure was confirmed using MS fragmentation and NMR analysis (Figure 3.3- 3.9). On running the reaction in 95% D_2O buffer, this peak showed one deuterium incorporation implying that the abstracted proton in **71** originated from solvent or a solvent exchangeable protein residue (Figure 3.3).

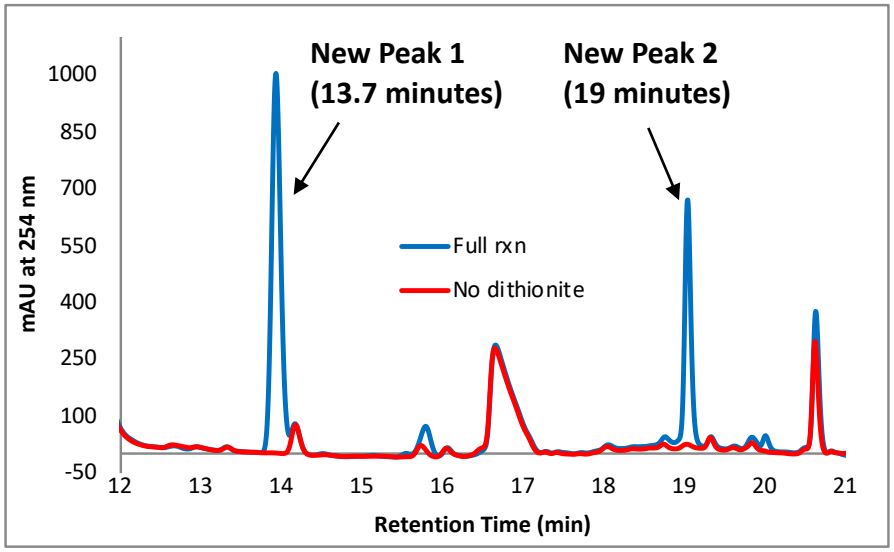

Figure 3.2 HPLC chromatogram of MqnE reaction with **66**

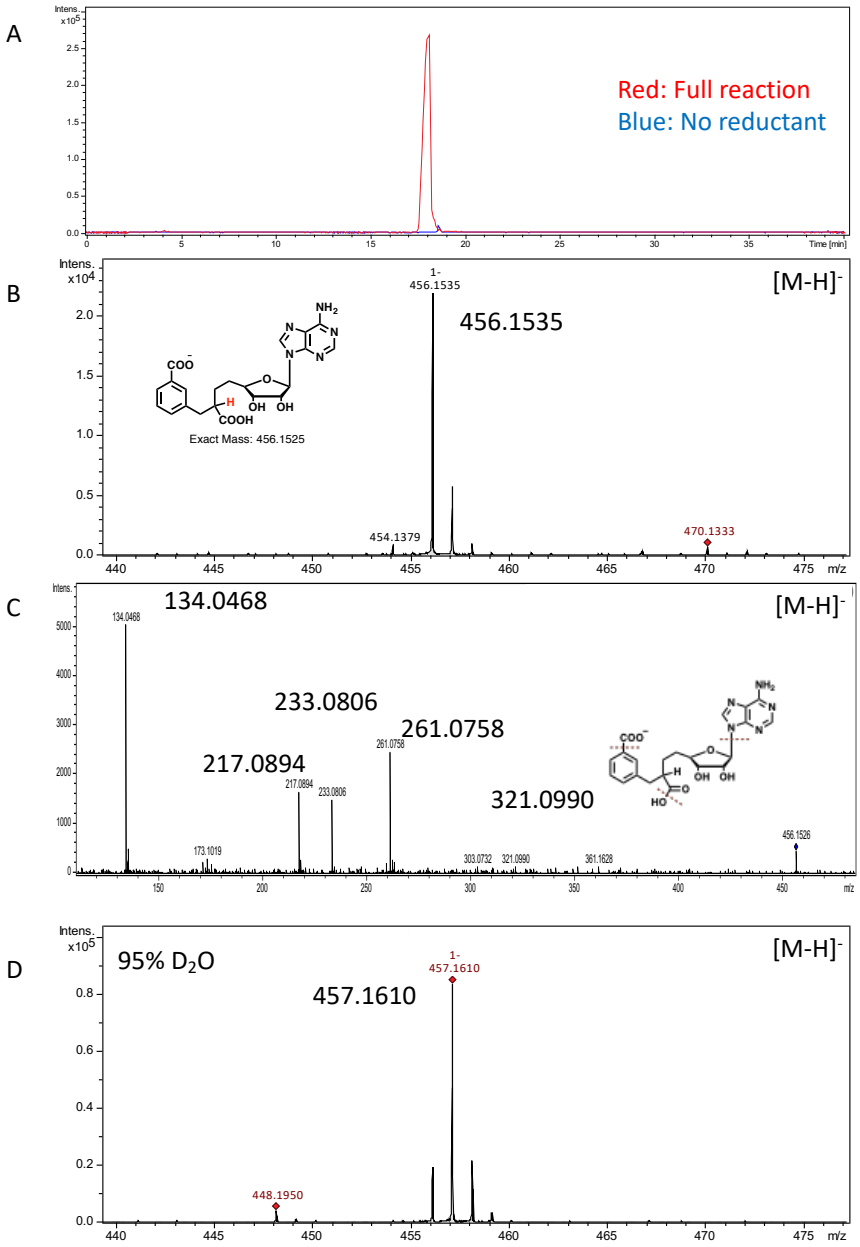

Figure 3.3 LC-MS analysis of the formation of **71** in the MqnE-catalyzed reaction of **66**. A) LC-MS analysis showing EIC [M-H]- = 456.1535 Da consistent with structure **71**. B) MS of **71**. C) MS-MS fragmentation analysis of **71**. D) LC-MS analysis of the reaction run in a deuterated buffer (95% D_2O) showing EIC [M-H]- = 457.1610 Da demonstrating the incorporation of one deuterium into compound **71**

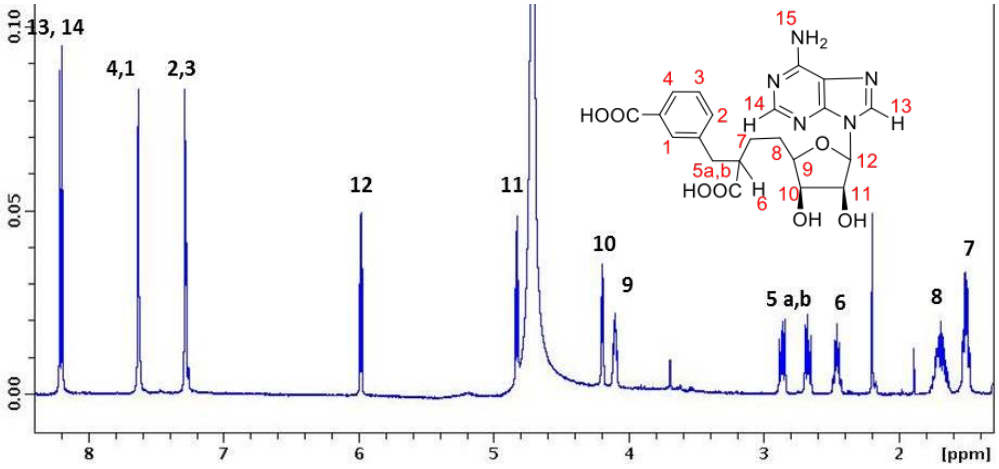

Figure 3.4 ^{1}H NMR (500 MHz, D_2O) of compound **71.**

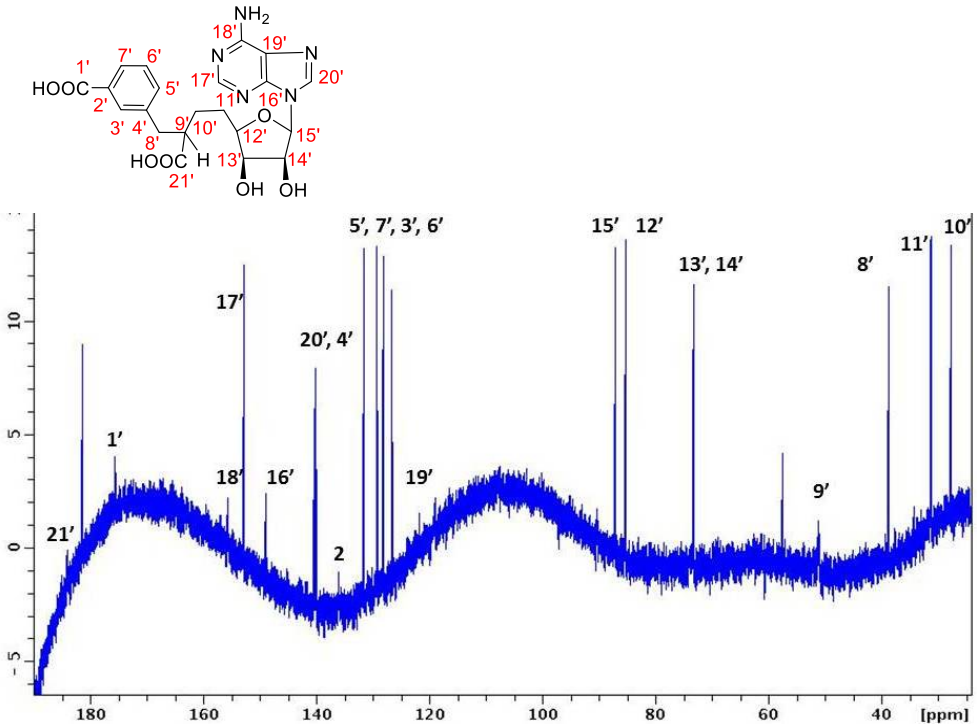

Figure 3.5 : ^{13}C NMR (125 MHz, D_2O) spectrum of compound **71**.

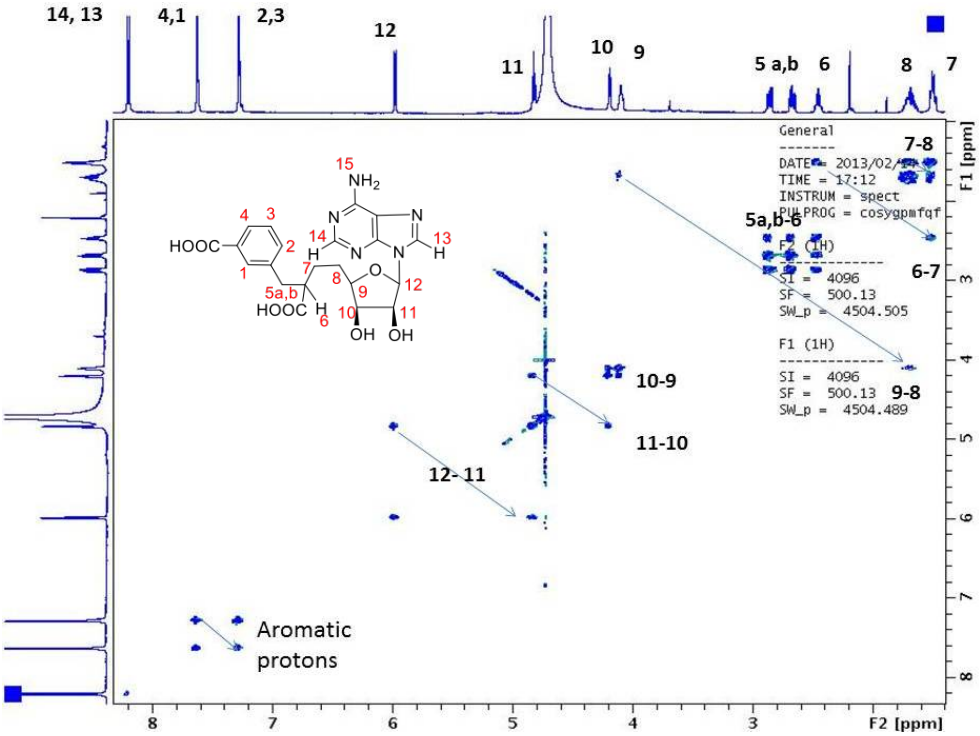

Figure 3.6 ^{1}H COSY spectrum of compound **71**.

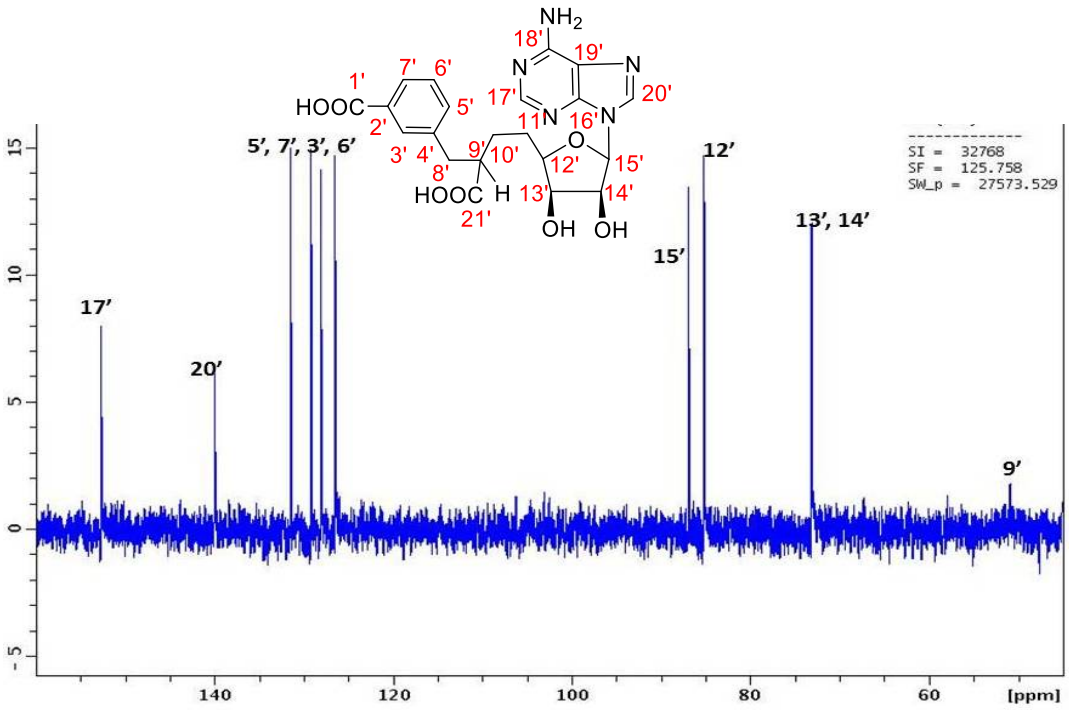

Figure 3.7 ^{13}C DEPT-90 NMR (125 MHz, D_2O) spectrum of compound **71**.

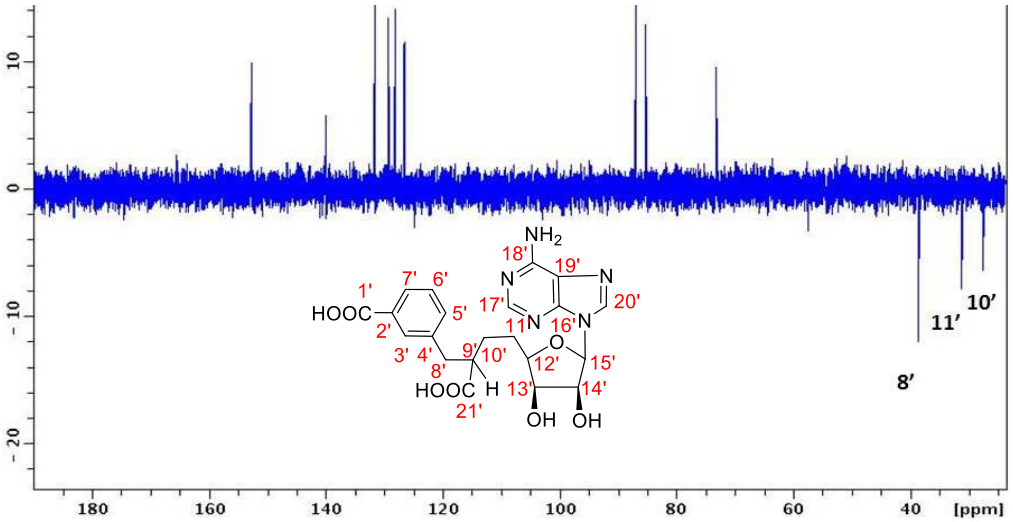

Figure 3.8 : ^{13}C DEPT-135 NMR (125 MHz, D_2O) spectrum of compound **71**

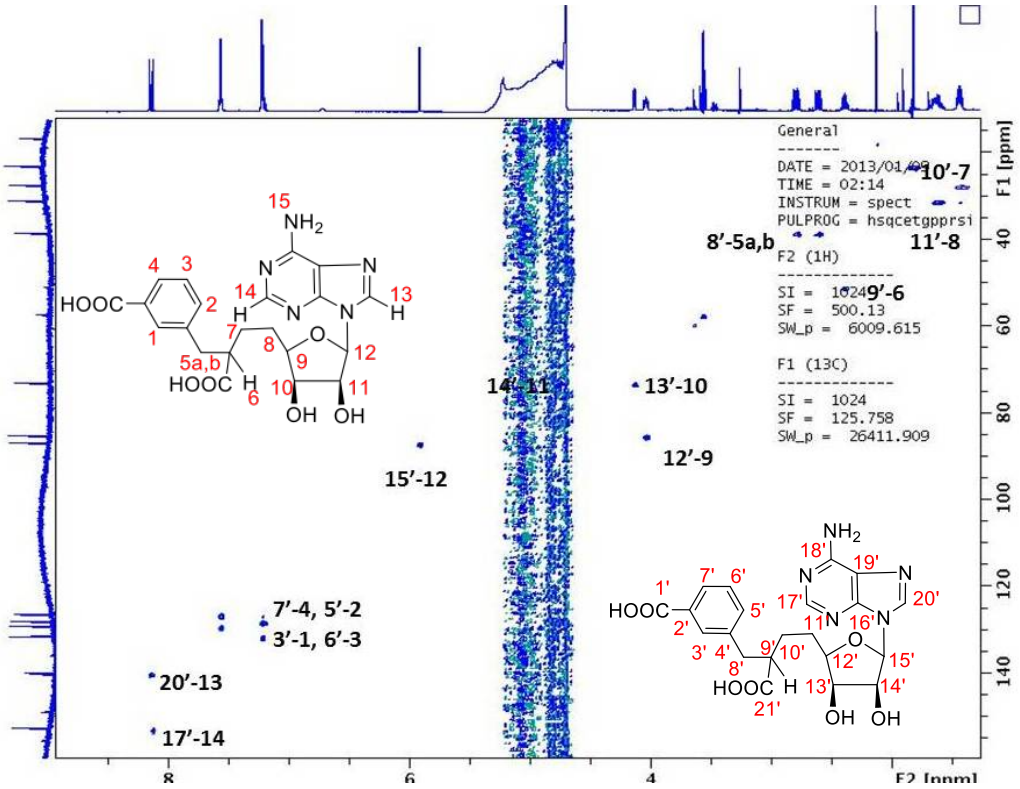

Figure 3.9 HSQC spectrum of compound **71**.

3.2. Characterization of the sulfinate adduct

The other new peak, eluting at 13.7 minutes had a molecular ion peak at $[M-H]^-$: 520 (Figure 3.10). The MS fragmentation analysis of this peak exhibited a neutral loss of 64 Da (equivalent to a SO_2 fragment) from the parent ion (Figure 3.10). Additionally, this peak didn't show any deuterium incorporation when the reaction was carried out in 95% D_2O buffer. We proposed this product to be the sulfinate adduct **72** generated by radical recombination of radical **67** with the sulfinate radical anion in the enzyme active site (Figure 3.11). Sulfinate radical anions are generated by dissociation of sodium dithionite which is the reductant used in this reaction. It has been reported that sodium dithionite oxygens are solvent exchangeable; thus we expected that if the reaction is run in $H_2{}^{18}O$,

we would see incorporation of two ^{18}O atoms in the sulfinate adduct. Consistent with this prediction, when we performed this reaction in 50% $H_2{}^{18}O$ we could detect an isotope pattern consistent with the incorporation of two ^{18}O atoms in the product.

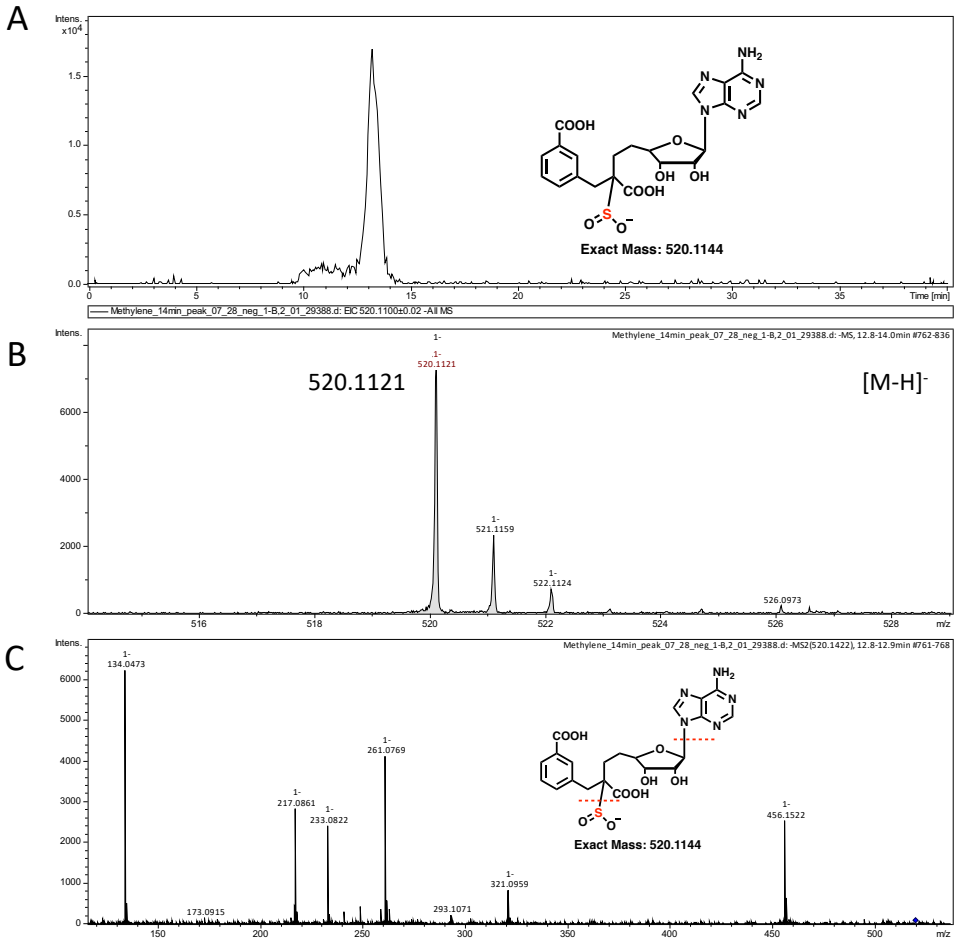

Figure 3.10 LC-MS analysis of the formation of **72** in the MqnE-catalyzed reaction of 66. A) LC-MS analysis showing EIC [M-H]- = 520.11 Da consistent with structure **72**. B) MS of **72**. C) MS-MS fragmentation analysis of **72.**

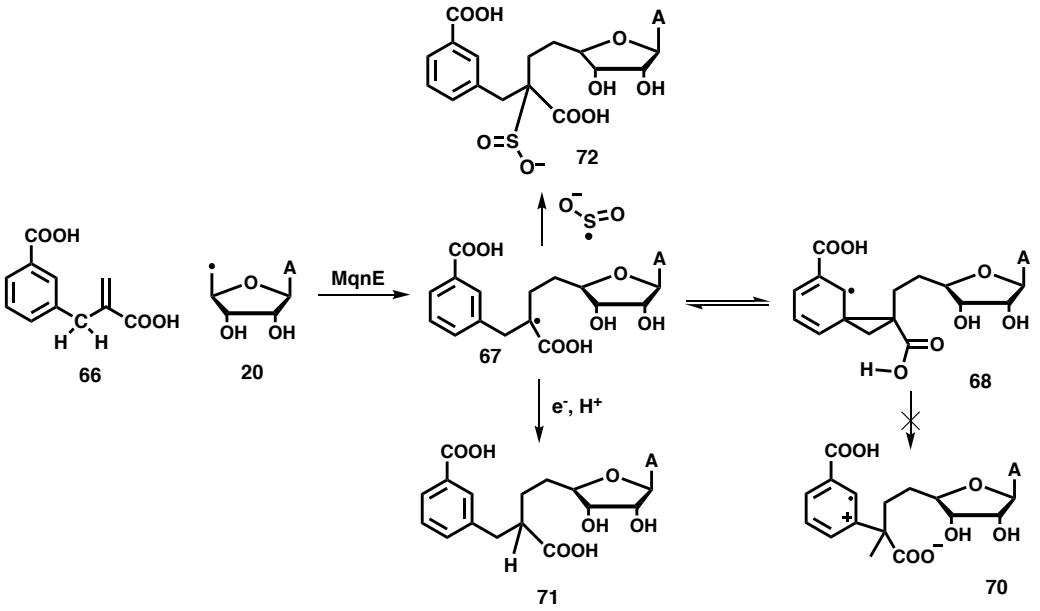

Figure 3.11 Mechanistic proposal for the formation of sulfinate adduct **72**

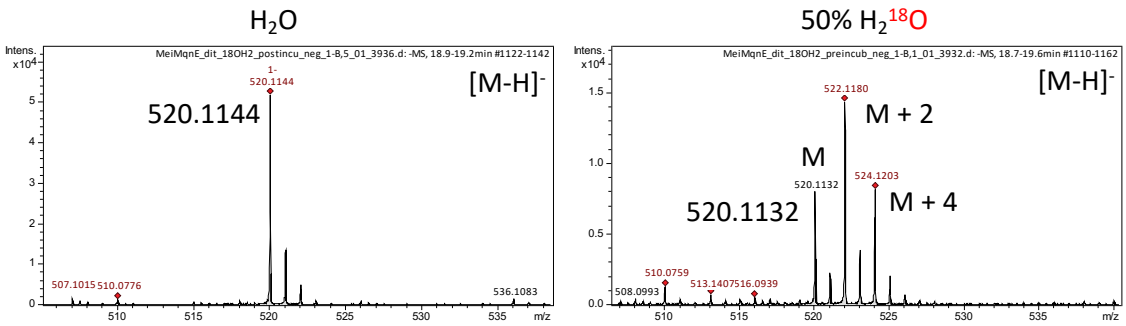

Figure 3.12 ^{18}O incorporation in **72** when reaction is performed in 50% $H_2{}^{18}O$

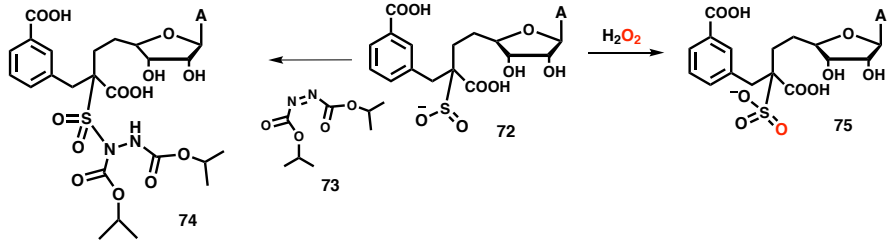

Figure 3.13 Chemical derivatization of sulfinate adduct **72**

This putative sulfinate adduct **72** was stable under anaerobic conditions over 4 weeks but degraded non-enzymatically under aerobic conditions within 4-6 hours yielding a mixture of degradation products. As a characterization strategy, we explored sulfinic acid specific, electron-deficient diazene trapping agent developed by Carroll lab[56] (Figure 3.13). This reagent covalently links to the sulfinic acid moiety leading to the formation of a stable sulfonamide adduct. Treating the MqnE reaction mixture with di-isopropyl azodicarboxylate reagent **73** led to the quantitative conversion of **72** to the corresponding sulfonamide **74** (Figure 3.14). Additionally, **72** was oxidized with H_2O_2 leading to the quantitative conversion of the putative sulfinate adduct to a single new product having mass 16 Da higher indicating the formation of the corresponding sulfonate adduct **75** (Figure 2C, S#).

Characterization of the sulfinate adducts is emerging as an efficient tool for the mechanistic study of radical SAM enzymes[40], but oxygen and hydrolytic instability of these sulfinate adducts can restrict their detection and structural characterization[57]. Thus converting sulfinate adducts to the corresponding sulfonamides or sulfonic acid would improve their stability and facilitate their chromatographic detection.

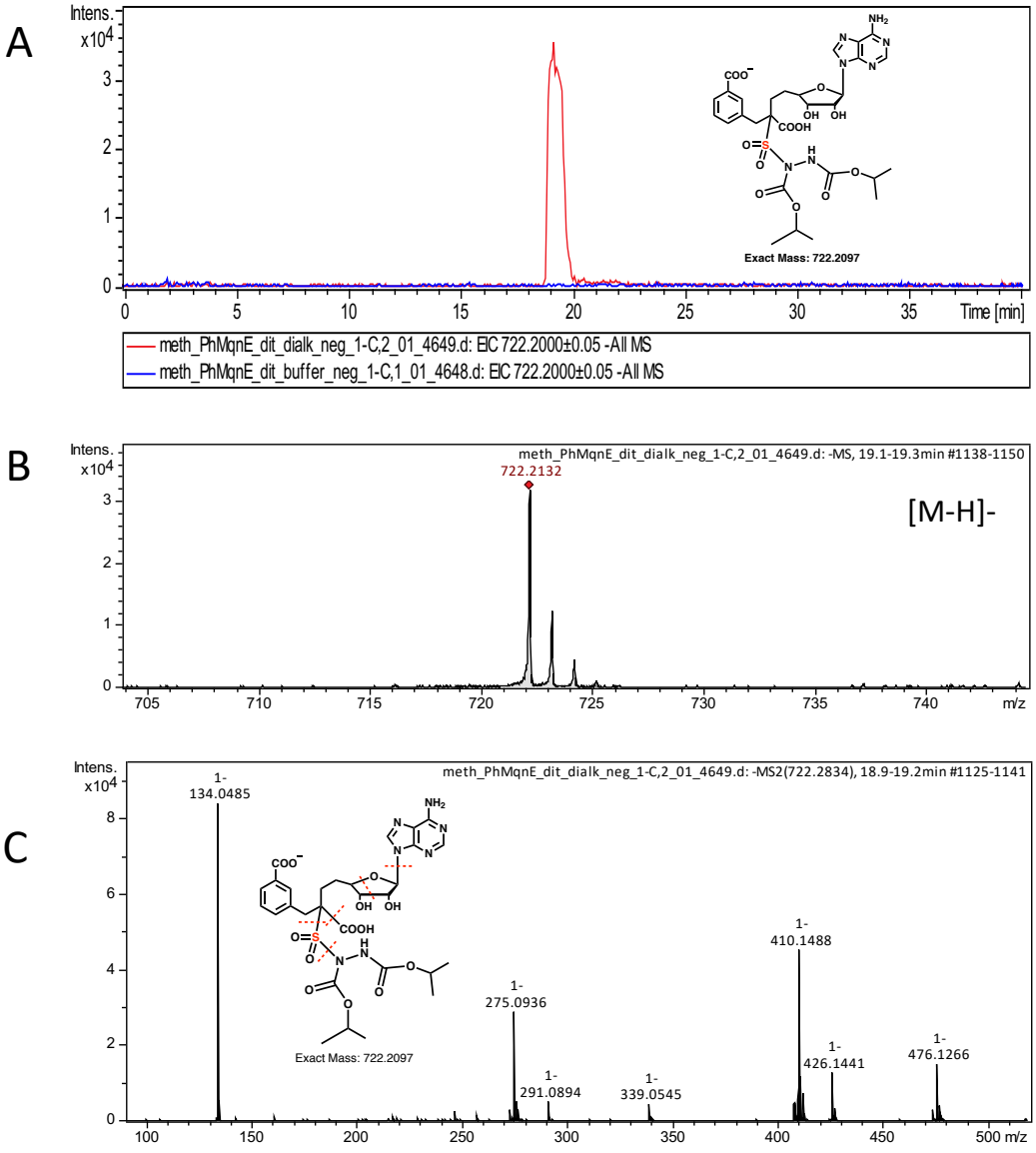

Figure 3.14 LC-MS analysis of the formation of **74** after treating **72** with reagent **73** A) LC-MS analysis showing EIC [M-H]- = 722.21 Da consistent with structure **74**. B) MS of **74**. C) MS-MS fragmentation analysis of **74**.

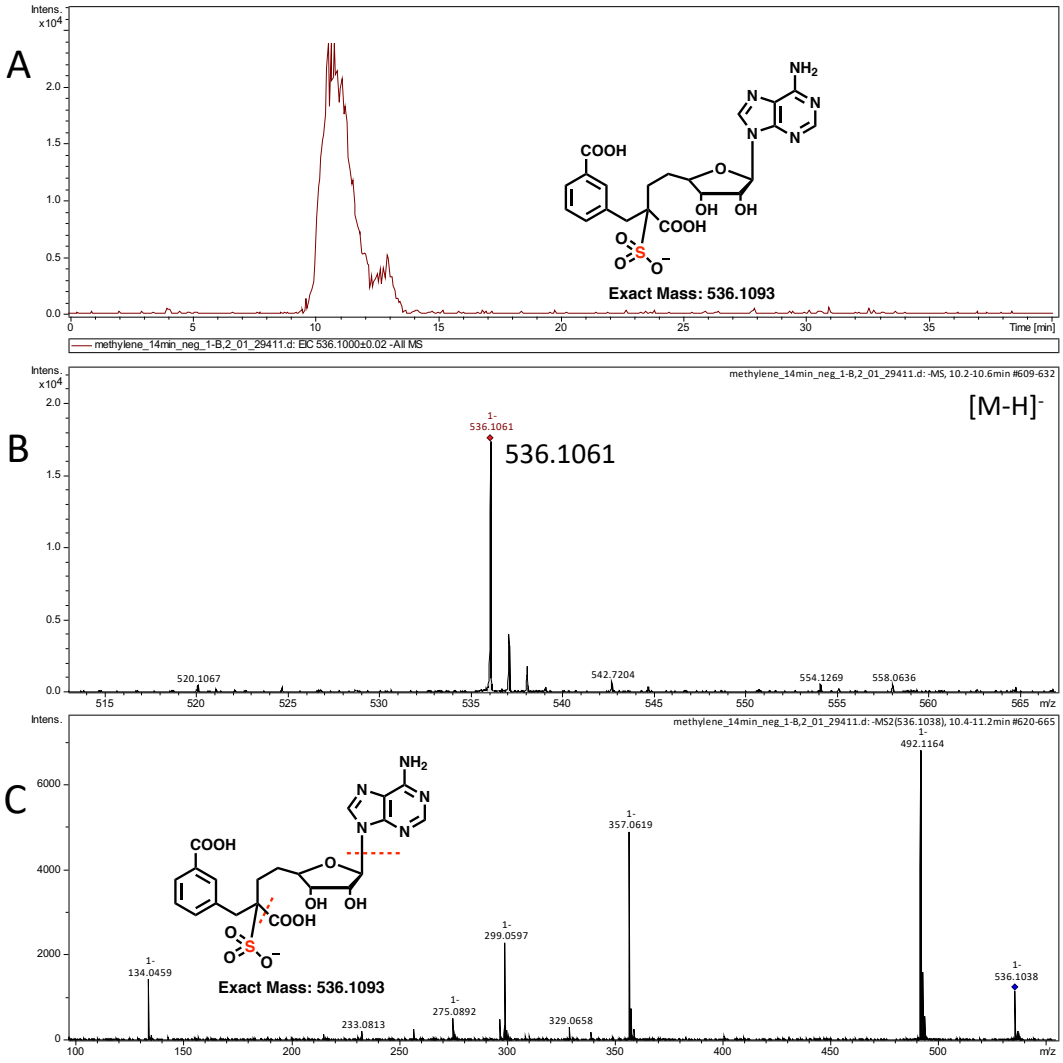

Figure 3.15 LC-MS analysis of the formation of **75** after treating **72** with H_2O_2 A) LC-MS analysis showing EIC [M-H]- = 536.10 Da consistent with structure **75**. B) MS of **75**. C) MS-MS fragmentation analysis of **75.**

3.3. MqnE reaction with the methylene analog with Flavodoxin/Flavodoxin reductase and Ti (III) citrate as reductants

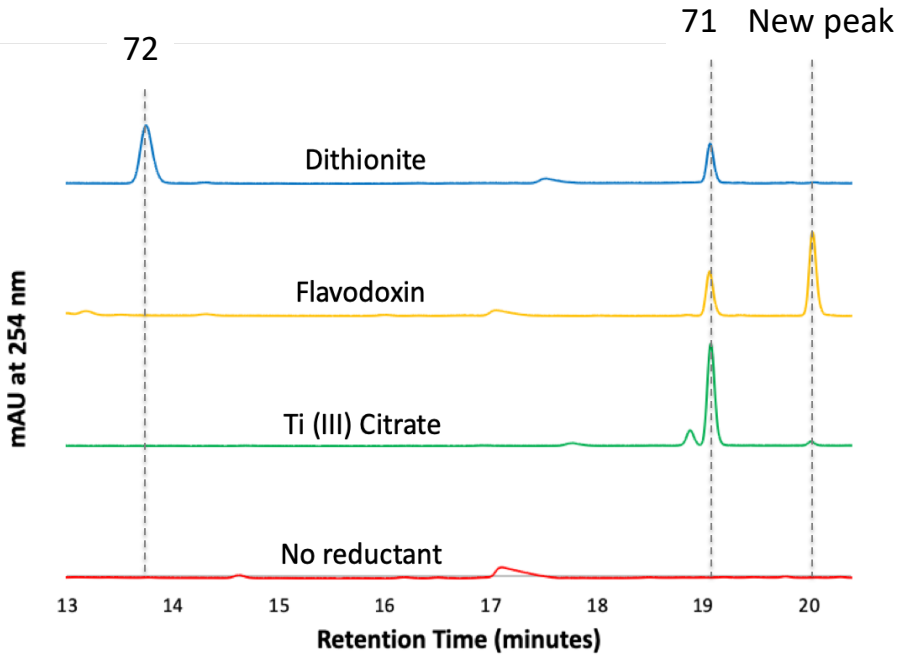

Figure 3.16 MqnE reaction of methylene analog **66** with different reducing agents

When the MqnE reaction with the methylene analog **66** was performed with the biological reducing agent- flavodoxin/flavodoxin reductase; as expected, the sulfinate adduct **72** was not observed; but surprisingly a new reaction product eluting at 20 minutes was observed in addition to the shunt product **71** (Figure 3.16). LCMS analysis revealed that this new peak had m/z: 426 (Figure 3.17). To gain insight into the structure of this unknown product; we performed ^{2}H, ^{13}C, ^{18}O labeling studies which revealed that the vinylic carboxylate group from the substrate is lost and a new oxygen atom from solvent-

water is incorporated into the unknown product (Figure 3.18). On reduction with $NaBH_4$, this peak showed the formation of 2 new peaks having mass 2 Da higher indicating the presence of a single carbonyl moiety in the structure. Based on these studies, the structure of the unknown product was proposed as **78**. A mechanistic hypothesis for the formation of **78** is shown in Figure 3.18. This involves initial one-electron oxidation of radical **67** to form α-hydroxy acid **77** which would undergo oxidative decarboxylation to yield **78** as the end product. Later we could observe similar reducing agent dependent product distribution with other substrate analogs having bulky substituents at the 2 position of **13** viz. 2-bromo-3-((1-carboxyvinyl)oxy)benzoic acid and 3-((1-carboxyvinyl)oxy)-2-methylbenzoic acid (Data not shown).

This study reveals the intrinsic reactivity of the captodative radical intermediate wherein if the spirocyclization is blocked, this intermediate can undergo reductive and oxidative radical quenching chemistry to yield corresponding shunt products. Analogous oxidative and reductive and re-combinative quenching of the radical intermediate has been observed in the C141A mutant of the radical SAM enzyme spore photoproduct lyase[58-59].

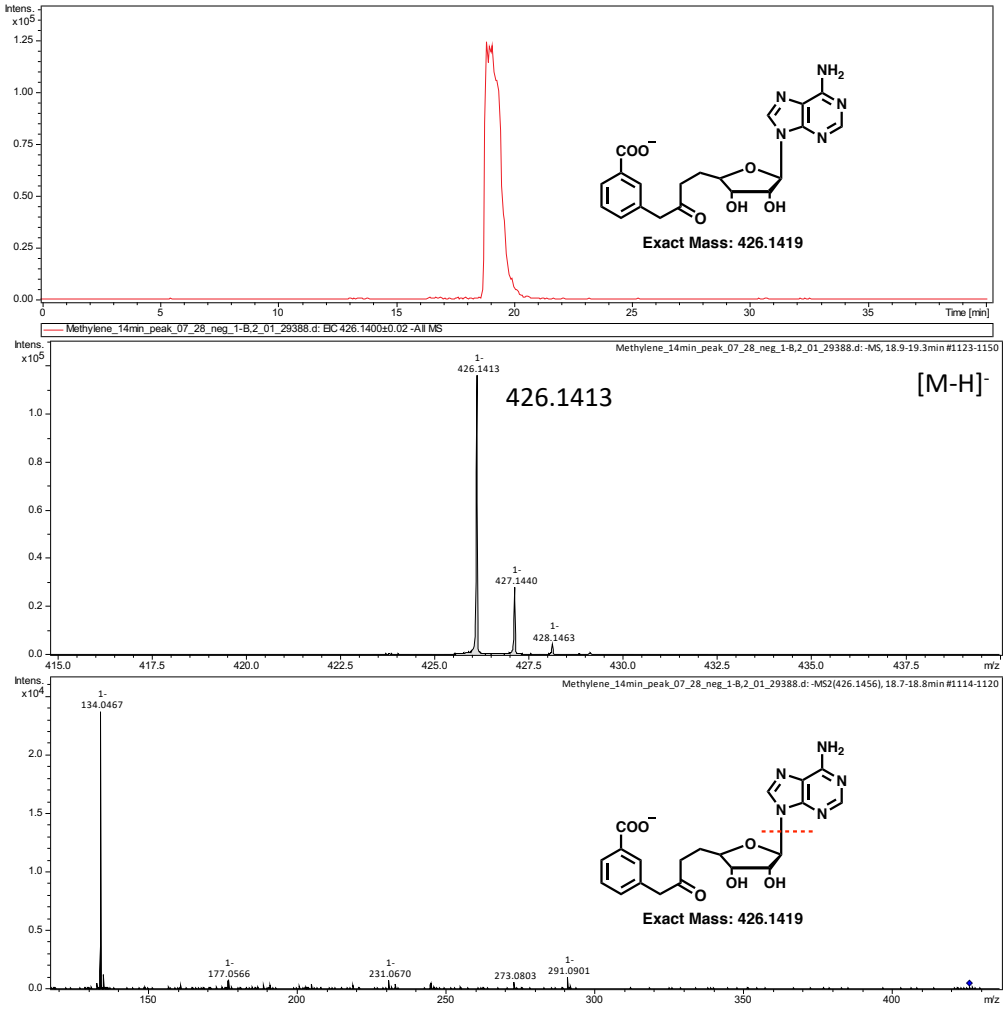

Figure 3.17 LC-MS analysis of the formation of **78** in the MqnE-catalyzed reaction of **66.** A) LC-MS analysis showing EIC [M-H]- = 426.14 Da consistent with structure **78**. B) MS of **78**. C) MS-MS fragmentation analysis of **78.**

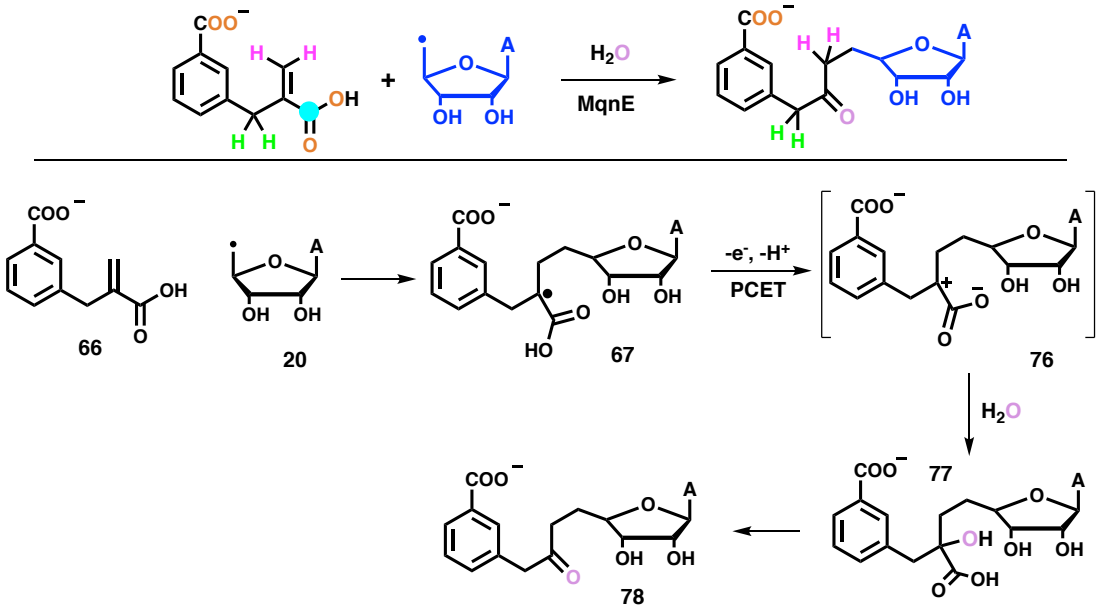

Figure 3.18 Labeling studies and mechanistic hypothesis for the formation of **78**

3.4. Spin trapping of radical intermediate in MqnE

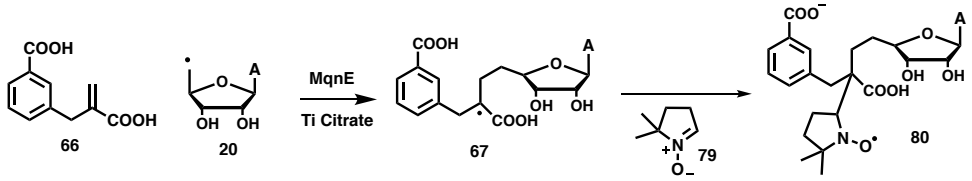

Figure 3.19 Spin trapping in MqnE catalyzed reaction

When MqnE reaction with the methylene analog **66** was performed in the presence of 5,5-Dimethyl-1-Pyrroline-N-Oxide (DMPO) **79** four new peaks were observed in the HPLC chromatogram (Figure 3.20). LCMS analysis of the new peaks revealed that all the four peaks have the mass corresponding to the spin trapping of the radical intermediate **80** (Figure 3.21). These peaks are proposed to be the two pairs of diastereomers of spin adduct **80** resulting from 2 new stereocenters generated on spin adduct formation (Figure 3.19). It is generally believed that the enzyme-generated radical intermediates are effectively

shielded from the solvent environment by the enzyme active site shell, but the lack of stereocontrol in the spin adduct formation indicates that the adduct formation might be taking place outside the active site. To the best of our knowledge, this is the first example of spin trapping of radical intermediate in radical SAM enzymes.

In this study, we have shown that the methylene captodative radical **67** can undergo quenching by reduction-protonation, oxidation-fragmentation, radical recombination or addition to spin trap depending on the reaction conditions to generate a diverse set of products (Figure 3.22).

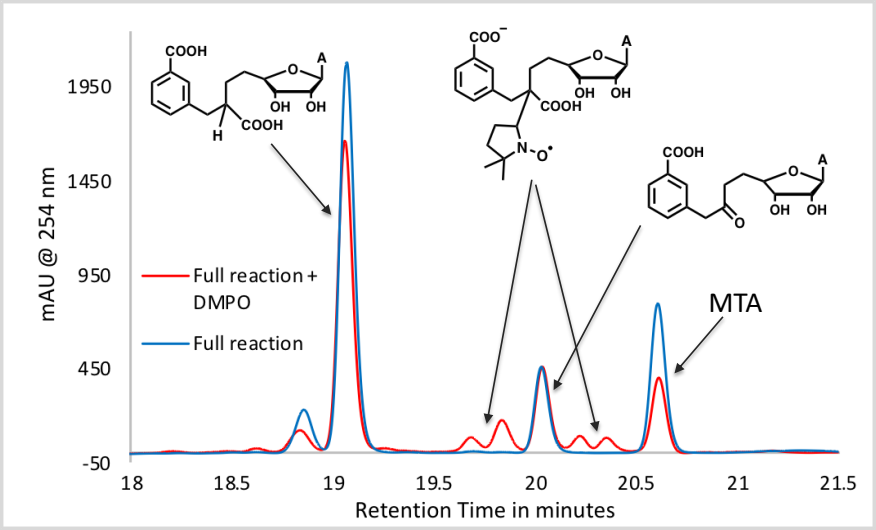

Figure 3.20 HPLC chromatogram of MqnE reaction with methylene analog **66** in presence of DMPO

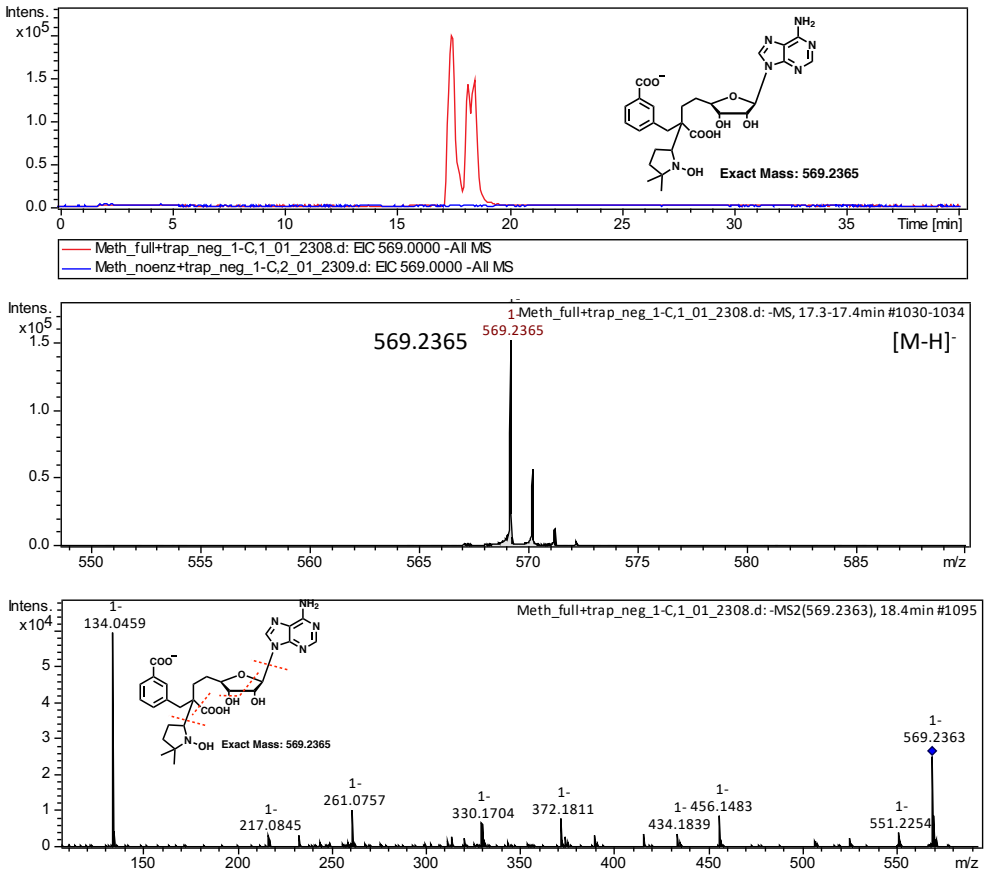

Figure 3.21 LC-MS analysis of the formation of **80** in the MqnE-catalyzed reaction of 66. A) LC-MS analysis showing EIC [M-H]- = 569.23 Da consistent with structure **80**. B) MS of **80**. C) MS-MS fragmentation analysis of **80**.

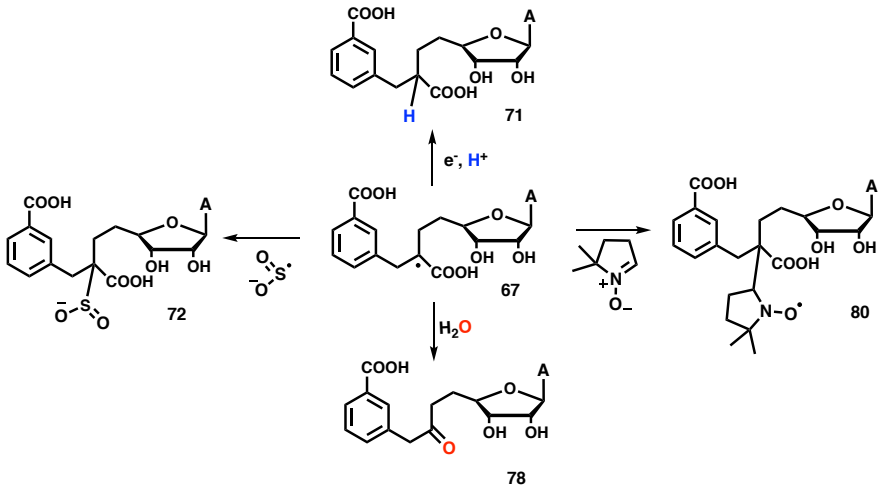

Figure 3.22 Novel trapping strategies for radical intermediate **67**

3.5. Antibiotic Potential of inhibiting menaquinone biosynthesis

The classical pathway to menaquinone has been validated as a target for antibiotic development and antibiotic compounds targeting the enzymes of this pathway have been reported against Gram-positive organisms such as *Mycobacterium tuberculosis*, *Staphylococcus aureus*, and *Plasmodium falciparum*.[60-66] Hence, there is considerable interest in the development of new herbicides and antibiotics targeting the futalosine-dependent pathway. Human pathogens such as *H. pylori* (causes gastric ulcers and cancer), *Campylobacter jejuni* (causes diarrhea), *Chlamydia* strains (causes urethritis and respiratory tract infections), *Spirochetes* (causes syphilis and Lyme disease) utilize the futalosine pathway for menaquinone biosynthesis.[67] Since the pathway is absent in humans and in many commensal bacteria, antibiotics targeting this pathway could prevent the growth of these important human pathogens without seriously damaging the gut microbiome.[67-68] Schramm and co-workers have targeted MTAN to develop transition-state analog inhibitors[69-71] against *Helicobacter pylori* while Dairi and co-workers, as well as other groups, have targeted the later steps of this pathway.[68, 72-74] The antibiotic potential of the other enzymes on the futalosine pathway, including the two radical SAM enzymes – MqnE and MqnC – has not been explored.

3.6. Inhibitor development against MqnE

High throughput screening for inhibitors of radical SAM enzymes is technically demanding because these enzymes are extremely oxygen-sensitive and have low turnover. We, therefore, undertook a mechanism guided approach for the development of an

inhibitor of MqnE. The captodative radical intermediate **23** is expected to be the most stable radical intermediate in the conversion of **13** to **14**. We, therefore, anticipated that a structural analog of this intermediate might act as a substrate or transition state mimic and form bi-substrate inhibitor of MqnE. A bi-substrate inhibitor is a molecule that is chemically synthesized or enzymatically generated by covalent linking of two substrates of a bi-substrate enzyme reaction and mimics the ternary enzyme-substrate complex[75]. This inhibitor design strategy has been demonstrated to be effective in achieving enhanced potency and selectivity and has led to the development of FDA approved therapeutics such as finasteride, mupirocin and isoniazid[75].

The *T. thermophilus* MqnE enzyme catalyzed >25 turnovers under our *in vitro* conditions with the native substrate. The MqnE reaction was slow with the methylene analog **66**, providing a single turnover. Encouraged by this result, we used competitive inhibition experiments in which MqnE-[4Fe-4S]$^{2+}$ was preincubated with variable concentrations of the methylene analog **66** in the presence of excess SAM and substrate **13**. Reactions were then initiated by reducing the enzyme with Ti(III) citrate and the rate of aminofutalosine **14** formation was followed by a discontinuous HPLC analysis. The normalized relative initial reaction rates were plotted as a function of inhibitor concentration to generate a dose-response curve and an IC_{50} value of 38.7 ± 3.4 μM was obtained. (Figure 3.23). Since this IC_{50} value was within 5-fold of the enzyme concentration used, the dose-response curve data was fitted to the Morrison equation for tight-binding inhibition[76] which gave an inhibition constant K_i of 3.1 ± 0.1 μM (Figure 3.24). Irreversible inhibition was

eliminated by demonstrating full restoration of enzyme activity after the enzyme was preincubated with **9** for one hour, followed by removal of the inhibitor by gel filtration. The bi-substrate analog **71** was enzymatically synthesized and also tested as a competitive inhibitor. This compound was a weaker inhibitor of MqnE with an IC_{50} value of 839 ± 187 µM (Figure 3.23). This suggests that the enzyme undergoes a major conformational change after the formation of **23** resulting in reduced affinity of the enzyme for **71** and avoiding product inhibition by **14**.

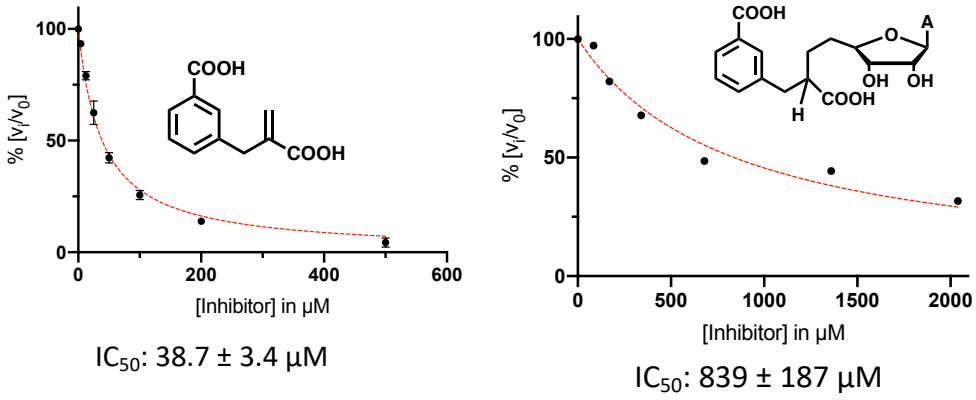

Figure 3.23 Dose response curves for **66** and **71**

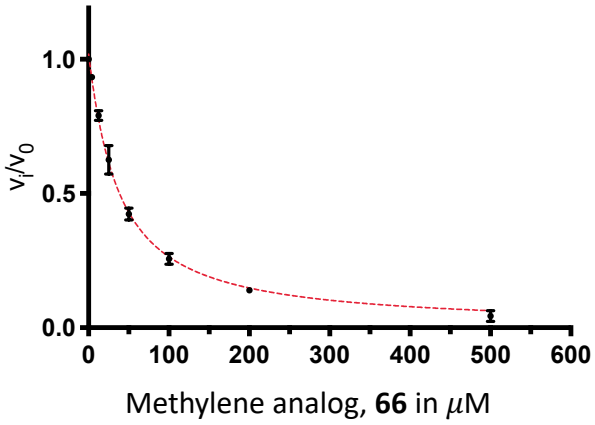

Figure 3.24 Tight binding inhibition kinetics of analog **66**

3.7. *In vivo* inhibition studies

The human pathogens *H. pylori* and *C. jejuni* were selected to test the antibiotic activity of the methylene analog **66** and the bi-substrate analog **71**. The effect of these inhibitors on *C. jejuni* and *H. pylori* growth was measured using the 96-well plate liquid culture method.[77-79] As shown in Figure 3.25, the IC_{50} for the methylene analog **66** and the bi-substrate analog **71** on *C. jejuni* were 13.6 ± 1.5 μM and 83.3 ± 3.4 μM, respectively. Gentamicin was used as a control and had an IC_{50} value of 1.9 ± 0.2 μM (Figure 3.25). The measured IC_{50} values for methylene analog **66** and bi-substrate analog **71** on *H. pylori* were 1.8 ± 0.4 μM and 16.1 ± 3.9 μM, respectively. BTDIA, a transition state analog of the *H. pylori* MTAN (Figure 3.25),[70] was tested as a control and displayed an IC_{50} of 0.012 ± 0.001 and 1.4 ± 0.3 μM for *H. pylori* and *C. jejuni*,[14] respectively (Figure 3.25). Radical SAM enzymes are widespread in cofactor biosynthesis pathways.[42] While these enzymes are reasonable targets for antibiotic development, technical difficulties working with highly oxygen sensitive low turnover enzymes has retarded the development of inhibitors against this family of enzymes. The methylene analog **66** is a potential lead compound as an antibiotic against *H. pylori*. It has a comparable antibacterial activity to amoxicillin and clarithromycin, currently approved antibiotics in the treatment of *H. pylori* infections.[80] In addition, this compound is resistant to acid hydrolysis, making it a suitable lead compound for the development of an orally available antibiotic against an acidophile like *H. pylori*.

	71 IC_{50} in μM	66 IC_{50} in μM	Gentamicin IC_{50} in μM	BTDIA IC_{50} in μM
C. jejuni	83.3 $\pm$ 3.4	13.6 $\pm$1.5	1.9 $\pm$ 0.2	1.4 $\pm$ 0.3
H. pylori	16.1 $\pm$ 3.9	1.8 $\pm$ 0.4	0.26	0.012 $\pm$ 0.0001

Figure 3.25 Summary of *in vivo* inhibition studies

In summary, we have identified methylene analog **66** as an inhibitor of MqnE and have demonstrated its antibacterial activity against *H. pylori* (IC_{50} = 1.8 ± 0.4 μM). These studies set the stage for the future development of antibiotics against *H. pylori* with MqnE as the target.

3.8. Experimental Procedures

3.8.1. Synthesis of methylene analog 66

Compound 66 was synthesized as reported previously using the synthetic scheme shown in Figure 3.26

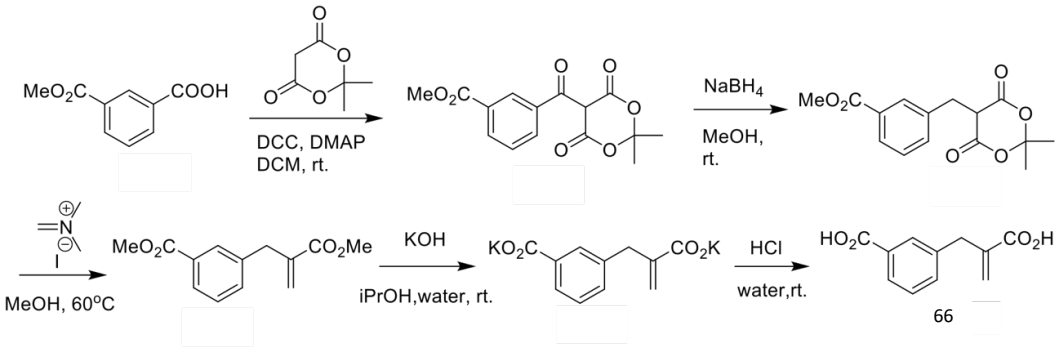

Figure 3.26 Synthetic scheme for compound **66**[1-2].

3.8.2. Protocol for competitive inhibition of MqnE

All the inhibition studies were done with the *T. thermophilus* ortholog of MqnE. MqnE (9 μM) was preincubated for 15 minutes with excess SAM (2 mM) and native substrate **13** (2 mM) and variable concentrations of the methylene analog **66** (4 μM-500 μM) at pH 7.5, 25^0C. The reaction was then initiated by adding the reducing agent- Ti (III) citrate and the rate of aminofutalosine formation was followed by a discontinuous HPLC assay. The normalized relative initial rates were plotted as a function of inhibitor concentration to generate a dose-response curve using GraphPad-Prism 8. The concentration of the bi-substrate inhibitor **71** was estimated based on the extinction coefficient ε_{260} = 13,517 M^{-1} cm^{-1}. (The extinction coefficient was estimated by adding the experimental extinction coefficients of 5'-deoxyadenosine and 3-(2-carboxypropyl)benzoic acid). The dose response curve was obtained as described above for **66**.

3.8.3. Experimental procedures for the *in vivo* inhibition studies with 66 and 71

The methylene analog **66** and bi-substrate analog **71** inhibitors were dissolved in sterile distilled water pH 7.0 and had their concentrations estimated based on the extinction coefficients (ε_{275} = 814 M^{-1} cm^{-1} and ε_{260} = 13,517 M^{-1} cm^{-1}, respectively). Solutions were further diluted with media prior to addition into the corresponding culture wells in the antibacterial activity assays. All chemicals were of analytical or reagent grade, or were of the highest purity commercially available, and were not subject to additional purification. Culturing Conditions. Each liter (distilled water) of *C. jejuni* culture media contained 21 g of Mueller-Hinton broth (Oxoid), and the final solution was sterilized by autoclaving at

121 ˚C for 15 min and stored at room temperature. The pH was 7.0. The culture media was warmed to 42 ˚C before use. Freeze-dried *C. jejuni* (ATCC strain AS-83-79; item number 33560) was hydrated with culture media (1.5 mL) and aseptically transferred to a 75 cm^2 blue plug seal cap tissue culture treated flask (Falcon) containing culture media (25 mL). *C. jejuni* was subject to routine *in vitro* culturing at 42 ˚C under microaerophilic conditions (5% O_2, 10% CO_2 and 85% N_2). The media was changed daily, and cultures were maintained under constant agitation using a Belly Button mini-orbital shaker (Sigma). The optical density was monitored daily and maintained under 1.5 absorbance units (λ = 600 nm).

H. pylori (ATCC 700392; strain 26695) was cultured in the presence of 5% CO_2 at 37 ˚C in brain heart infusion media (Oxoid; 37 g per liter of media) with 10% fetal bovine serum (Gibco) and DENT supplement (Oxoid) as described previously.[77-78] The media was warmed to 37 ˚C before inoculation.

3.8.4. *C. jejuni* Antibacterial activity assays

C. jejuni Antibacterial Activity Assays. The effect of methylene analog **66** and bi-substrate analog **71** on *C. jejuni* growth was measured to determine IC_{50} values using liquid culture media.[81] *C. jejuni* (ATCC strain AS-83-79; item number 33560) cultures (200 µL/well in a 96-well plates) with an initial optical density of 0.005 absorbance units (λ = 600 nm) were grown in the presence of increasing concentrations of either methylene analog **66** or bi-substrate analog **71**. Inhibitor concentrations were subject to 3-fold dilutions, ranging from 27.4 nM to 540 µM or 7.9 nM to 155 µM, respectively. Wells containing no inhibitor served as controls, and Gentamicin was used as a positive control, at concentrations

ranging from 1.5 μM to 30 mM. All culture media flasks were kept in a sealed gas chamber. *C. jejuni* susceptibility to these compounds was determined after 16.4 h in culture by measuring the cell growth based on optical density (600 nm) using a SpectraMax M5 microplate reader (Molecular Devices). Statistical analysis to determine the IC_{50} values were performed with GraphPad Prism 6.07 using a nonlinear regression curve fitting.

3.8.5. *H. pylori* Antibacterial activity assays

The effects of the methylene analog **66** and the bi-substrate analog **71** on *H. pylori* (ATCC 700392; strain 26695) growth were measured to determine IC_{50} values using liquid culture media. *H. pylori* cultures (200 μL/well in a 96-well plate) with an initial optical density of 0.02 absorbance units (λ = 600 nm) were grown in the presence of increasing concentrations of either the methylene analog **66** or the bi-substrate analog **71**. Inhibitor dilutions of 2-fold for the methylene analog **66** or 1.5-fold dilutions for the bi-substrate analog **71** were prepared in each assay. The inhibitor concentrations for the methylene analog **66** or the bi-substrate analog **71** ranged from 0.2 μM to 48 μM and from 0.9 μM to 34.5 μM, respectively. Media without inhibitor supplementation served as controls. BTDIA was prepared in 1.5-fold dilutions from 0.2 nM to 8 nM as quality controls. The *H. pylori* susceptibility to these compounds was determined after 72 h in culture by measuring the cell growth based on optical density (600 nm) using a SpectraMax M5 microplate reader (Molecular Devices). Statistical analysis to determine the IC_{50} values were performed with GraphPad Prism 6.07 using a nonlinear regression curve fitting.

4. MECHANISTIC STUDIES ON THIAMIN PYRIMIDINE SYNTHASE (THIC) AND 5-HYDROXYBENZIMIDAZOLE SYNTHASE (BZAF) CATALYZED REACTIONS

4.1. Introduction to bacterial Thiamin biosynthesis

Thiamin pyrophosphate is an essential cofactor in all forms of life. Thiamin-dependent enzymes play an important role in carbohydrate and branched-chain amino acid metabolism and include transketolase, α-ketoacid decarboxylase, α-ketoacid oxidases and acetolactate synthase. In all the cases Thiamin stabilizes an acyl carbanion biosynthon.

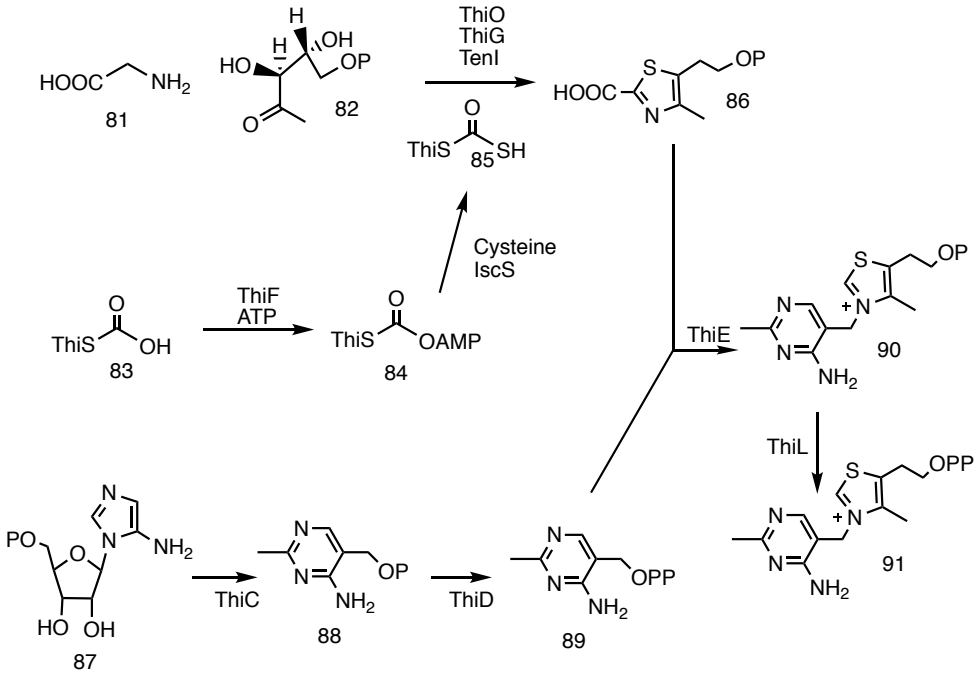

Figure 4.1 Bacterial Thiamin biosynthesis pathway

The biosynthesis of thiamin pyrophosphate in bacteria is summarized in Figure 4.1.[82-85] The thiazole moiety **86** is formed from deoxy-D-xylulose-5-phosphate **82**, glycine

81, and a 66 amino acid peptide carrying the sulfide as a thiocarboxylate at its carboxy terminus (ThiS-COSH, **85**). This sulfur donor is formed by activation of ThiS-COOH **83** with ATP followed by sulfur transfer from cysteine. A different thiazole assembly strategy, involving the ThiH protein, is used by *E. coli* and a small number of other bacteria. The hydroxymethyl pyrimidine phosphate (HMP-P **88)**, formed from 5-aminoimidazole ribonucleotide (AIR, **87**) in a complex rearrangement reaction, is converted to the corresponding pyrophosphate **89**, and then coupled with the thiazole phosphate **86** to give thiamin phosphate **90**. Final phosphorylation gives thiamin pyrophosphate **91**, the biologically active form of the cofactor.

Our understanding of the enzymology of Thiamin thiazole biosynthesis, thiazole/ pyrimidine coupling enzyme and the various kinases is at an advanced stage. Thiamin pyrimidine synthases (ThiC) has been reconstituted, but the mechanism of this reaction is still poorly understood and is the major remaining unsolved mechanistic problem in the biosynthesis of this important metabolite.

4.2. Thiamin Pyrimidine Synthase (ThiC)

The bacterial thiamin pyrimidine synthase, ThiC, a radical SAM enzyme, catalyzes a remarkable rearrangement reaction where it converts aminoimidazole ribonucleotide (AIR, **87**) to the thiamin pyrimidine - 4-amino-5-hydroxymethyl-2-methylpyrimidine phosphate (HMP-P, **88**) as shown in Figure 4.2. Detailed labeling studies with ^{2}H and ^{13}C isotopologues of AIR have established the origin of all of the atoms of HMP-P **88** and have identified carbon monoxide and formate as reaction products. It has been determined

that the proS hydrogen at C5' of AIR **87** is abstracted by the adenosyl radical and replaced by a hydrogen atom from 5'-deoxyadenosine **20** with the retention of stereochemistry. Studies have demonstrated that the same adenosyl radical also abstracts the hydrogen atom from C4' of AIR. High-resolution crystal structures of ThiC from *Arabidopsis Thaliana* (AtThiC) have been solved showing bound S-adenosyl homocysteine, AIR, the iron-sulfur cluster and a novel second iron site involved in SAM binding[86]. In spite of these extensive efforts over the past decade, the mechanism of ThiC catalyzed reaction remains poorly understood.

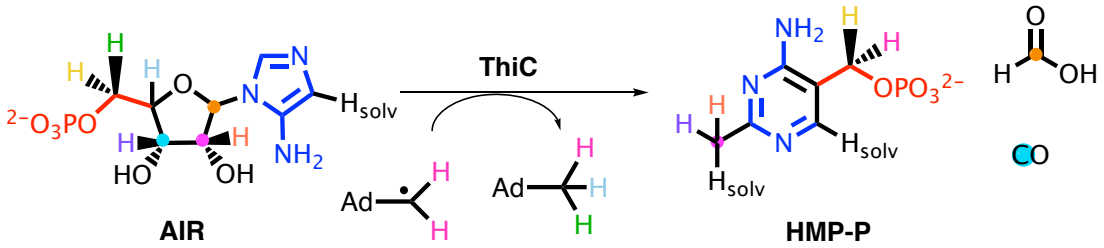

Figure 4.2 ThiC catalyzed reaction

4.3. ThiC reaction with the substrate analog IRN

One of the major reasons for the slow progress on the mechanistic studies of ThiC has been the failure to detect any shunt products using substrate analogs of AIR. We decided to renew the efforts on this front. Our lab has previously reported high resolution crystal structures of ThiC from *Arabidopsis Thaliana* bound to the substrate analog imidazole ribonucleotide (IRN **92)** (PDB IDs: 4S25, 4S26)[86]. These structures demonstrate that IRN binds in ThiC active site in a similar binding mode as the native substrate AIR. Thus we decided to test this substrate analog as a starting point for our mechanistic studies.

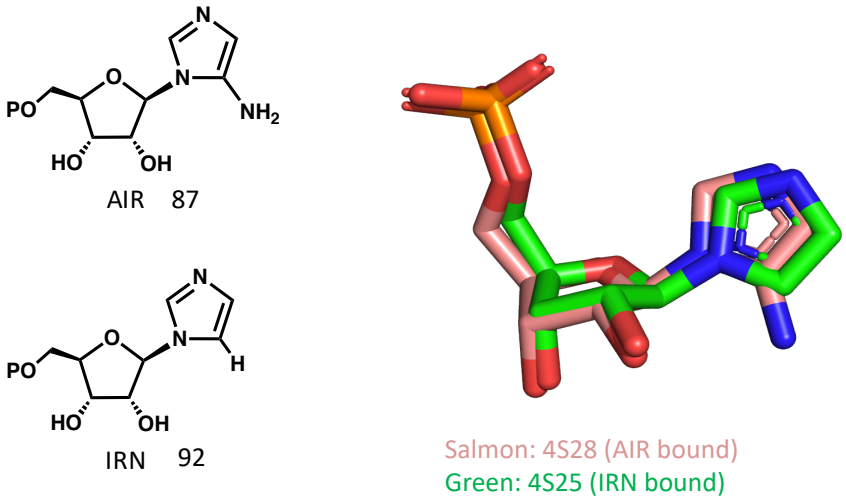

Figure 4.3 Overlay of crystal structures of AIR and IRN bound in the ThiC active site

Imidazole ribonucleoside (IRNs) was synthesized following a previously reported procedure. IRNs was phosphorylated enzymatically to get IRN which was HPLC purified before use in the ThiC reaction. IRN was incubated with ThiC under standard reaction conditions and on HPLC analysis >40% substrate consumption was observed (Figure 4.4 A). 5'dA formation was more than 2 fold higher in the full reaction as compared to the control reaction in the absence of the substrate IRN. Both of these observations indicated that IRN is accepted as a substrate by ThiC. A closer look at the initial region in the HPLC chromatogram at 215 nm revealed formation of 4 new peaks which were absent in all the controls. The major product eluting at 2.01 minutes was confirmed to be imidazole by co-migration with the commercial standard of imidazole (Figure 4.4 B,C).

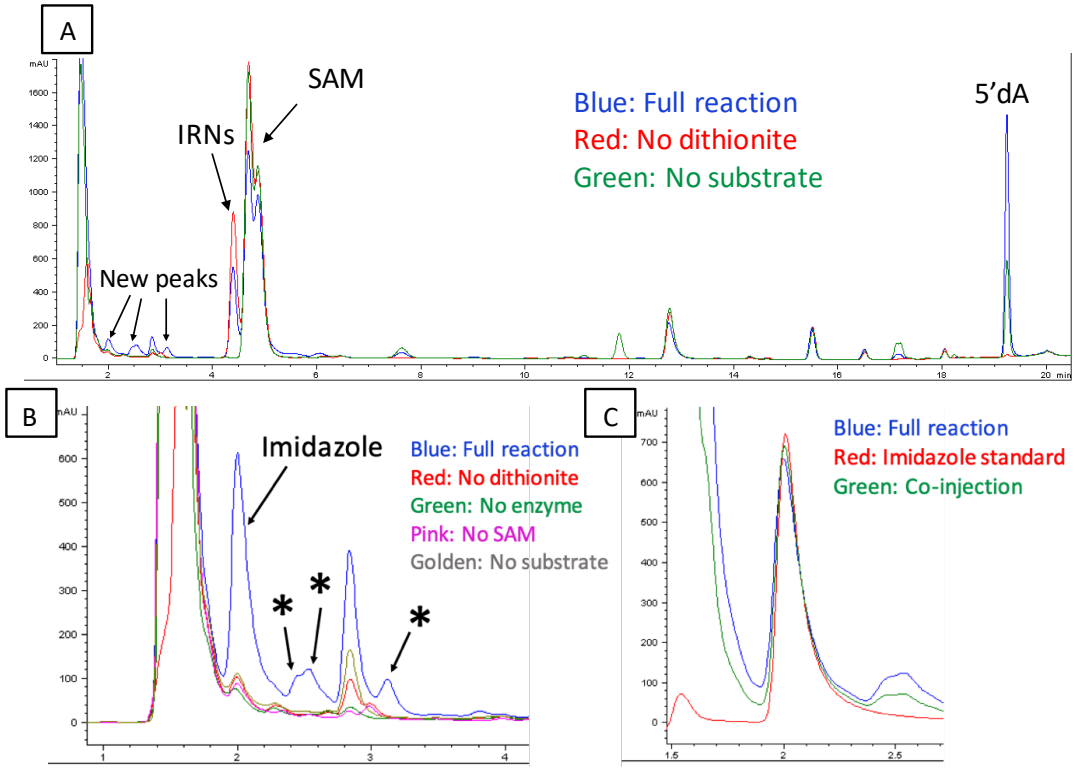

Figure 4.4 [A] HPLC chromatogram of ThiC reaction with IRN at 225 nm
[B] Zoomed in initial region at 215 nm showing the formation of new peaks
[C] Co-migration of the imidazole standard with the reaction product

To get more insight into the other 3 unknown products, ThiC reaction with IRN was analyzed before and after phosphatase treatment (Figure 4.5). The data revealed that imidazole and the peaks eluting at 2.4, 2.55 minutes are formed even without the phosphatase treatment. The peak at 3.1 minutes, on the other hand, didn't form in the absence of phosphatase treatment, indicating that this peak originates from a phosphate-containing precursor. An attempt was made to isolate these products by HPLC and analyze by mass spectroscopy without any success. The identity of these minor reaction products eluting at 2.4, 2.55 and 3.1 minutes remains to be established.

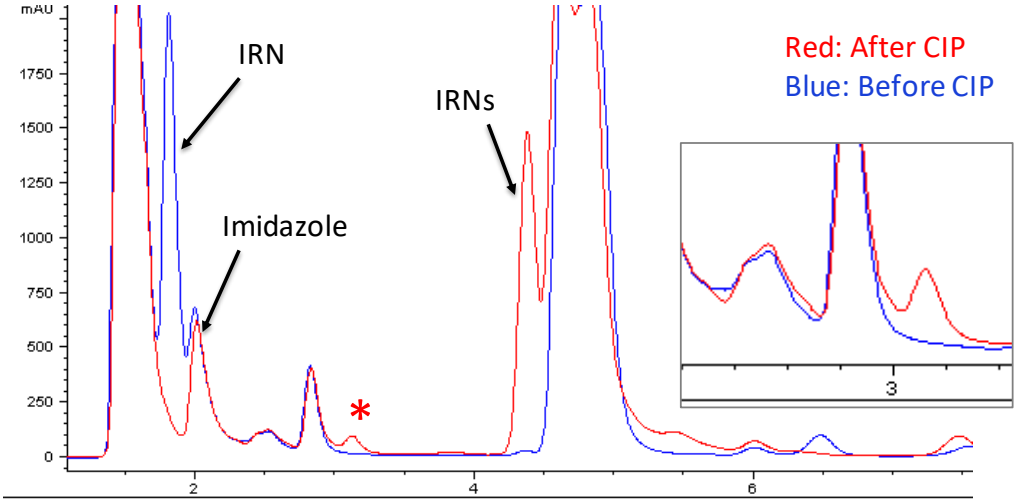

Figure 4.5 ThiC reaction with IRN before and after phosphatase treatment

We also looked for the formation of the expected final product of this reaction-desamino-HMP, but could not detect it using HPLC or LCMS analysis. The detection limit for desamino-HMP under our chromatographic conditions was estimated to be 5 μM (2% of the total products formed) based on the experiments with the commercial standard of desamino-HMP.

In order to establish the site of H atom abstraction on IRN, we chemo-enzymatically synthesized 5'-D_2-IRN isotopologue. When ThiC reaction was performed with the 5'-D_2-IRN isotopologue, >80% deuterium incorporation was observed in the 5'dA formed (Figure 4.6). This confirmed that the chemistry is initiated by abstracting 5' hydrogen atom of IRN similar to the native substrate AIR.

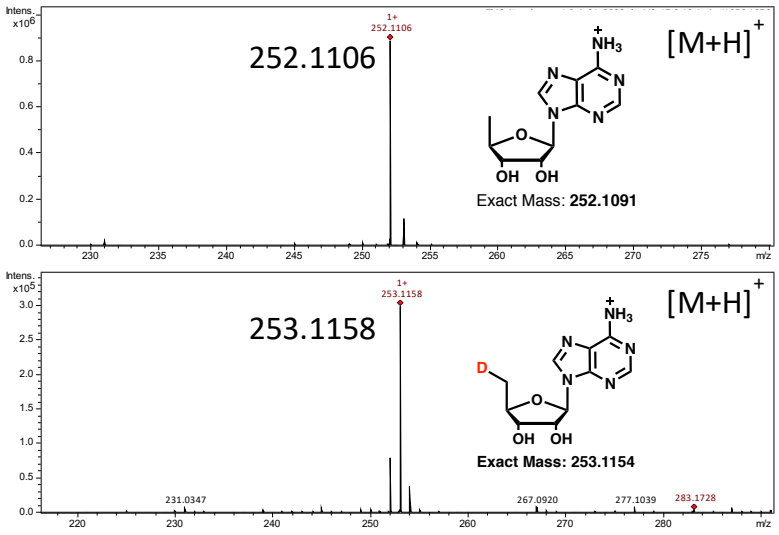

Figure 4.6 Mass analysis of 5'dA formed in the ThiC reaction with IRN and IRN-D_2

Detection of imidazole as a shunt product demonstrates N-glycosidic bond cleavage in the course of ThiC reaction with IRN. Examination of the crystal structure of AtThiC with IRN (PDB ID: 4S25) reveals that N3 of the imidazole of IRN is within the hydrogen bond distance of the Asp 383. This substrate binding mode is similar to that observed in the glycosidase enzyme- methyl thioadenosine nucleosidase (MTAN)[87]. In MTAN, the active site aspartate residue activates the substrate by protonating the N7 of the adenine ring for the hydrolytic cleavage of the N-glycosidic bond. Mutation of this aspartate to asparagine retains substrate binding but leads to the complete loss of catalytic activity in the case of MTAN. To test the role of Asp 383 in the N-glycosidic bond cleavage of IRN in ThiC reaction, we tested D383N and D383A mutants of AtThiC. As shown in Figure 4.7, both the mutants showed the formation of imidazole in the reaction

with IRN in the end point assay. This indicates that the observed cleavage of the N-glycosidic bond of IRN is not strictly dependent on Asp 383 residue.

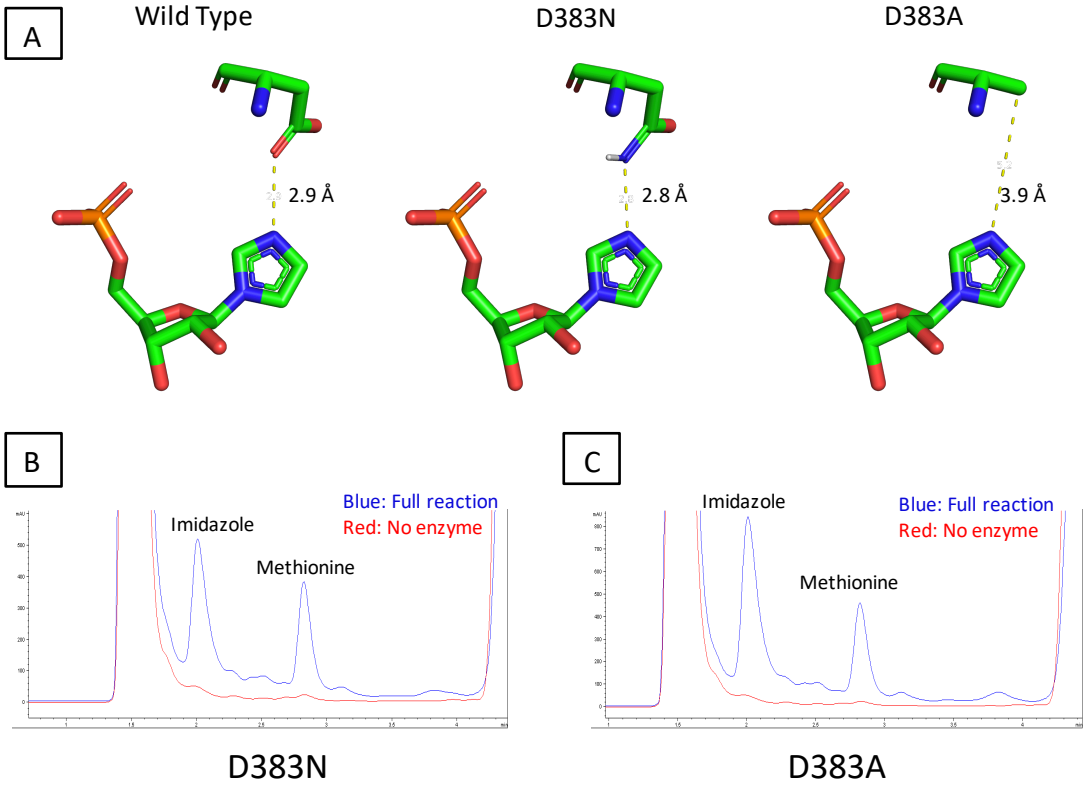

Figure 4.7 [A] Aspartate 383 interaction with IRN in the wild type ThiC (PDB ID: 4S25) and the model of ThiC D383N and D383A mutants of ThiC [B] & [C] HPLC chromatograms of ThiC D383N and D383A reactions with IRN

These experiments suggested that ThiC accepts IRN as a substrate and imidazole is the major detectable product. As a corollary, a corresponding sugar fragment should also be formed. Sugar fragment is likely to be very polar and non-chromophoric, and hence difficult to detect using spectroscopic detection techniques on HPLC. MTAN catalyzed N-glycosidic bond cleavage generates ribosyl moiety having an aldehyde group. Since the

sugar fragment generated in the ThiC reaction with IRN is also formed by hydrolysis of N-glycosidic bond, we hypothesized that this sugar fragment could also have an aldehyde group present. We hence attempted to trap this fragment using aldehyde trapping agents which would generate a chromophoric product and facilitate its detection.

We tested several hydroxylamine and hydrazine aldehyde trapping agents viz. O-(2,3,4,5,6-Pentafluorobenzyl)hydroxylamine (PFBHA), *O*-(4-Nitrobenzyl)hydroxylamine, 4-Hydrazino-7-nitro-benzofurazan (NBD-hydrazine), 2,4-dinitrophenylhydrazine (DNP). When ThiC reaction with AIR was performed in the presence of these aldehyde trapping agents the enzymatic activity was severely inhibited e.g. the 5'dA formed was <10% of the levels in the absence of the trapping agent. Thus it was not possible to perform ThiC reaction in the presence of these trapping reagents. We hence tried alternate aldehyde trapping agent: o-Phenylenediamine (OPDA). ThiC reaction with AIR showed no inhibition in 5'dA formation in the presence of 10 mM OPDA. Thus we decided to use OPDA as the aldehyde trapping agent to trap sugar fragment in the ThiC reaction with IRN.

OPDA **93** reacts with aldehydes & 1,2-dicarbonyl compounds to generate corresponding benzimidazoles & quinoxalines under aerobic conditions. We tested glyceraldehyde & pyruvaldehyde as a model compound for the aldehyde trapping experiment. Incubation of glyceraldehyde & pyruvaldehyde (500 μM) with 10 mM OPDA under aerobic conditions led to the formation of the corresponding benzimidazole & quinoxaline which showed absorbance at 300 nm & 316 nm respectively (Figure 4.8).

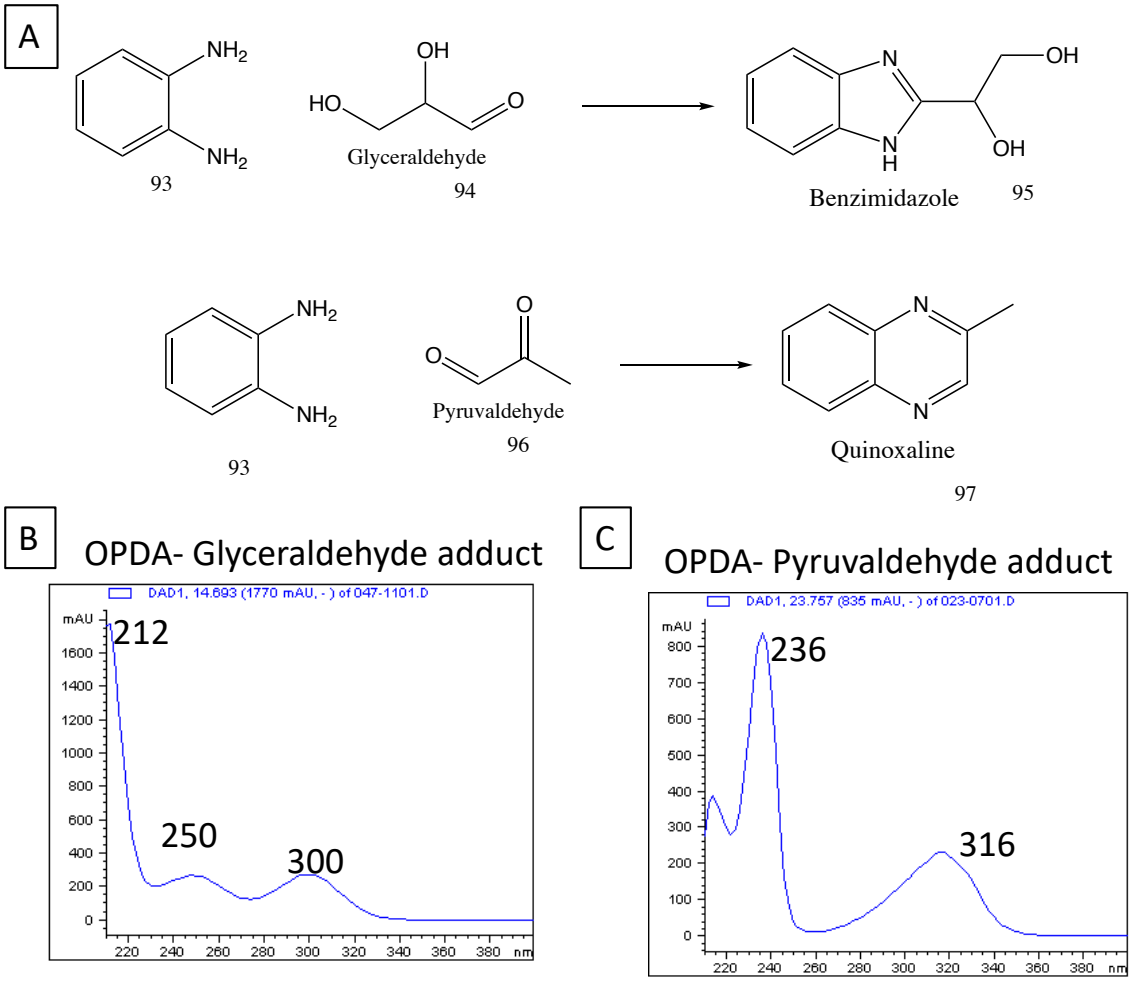

Figure 4.8 [A]Trapping chemistry of OPDA [B] UV-vis spectrum of **95** [C] UV-vis spectrum of **97**

We tested ThiC reaction with IRN in the presence of 10 mM OPDA and analyzed the reaction after CIP treatment by HPLC. We could detect the formation of a new peak eluting at 17.5 minutes which was absent in all the control reactions (Figure 4.9). The formation of this peak was dependent on the concentration of OPDA and it had UV spectrum similar to that of OPDA-glyceraldehyde adduct. We termed this new peak as Compound X.

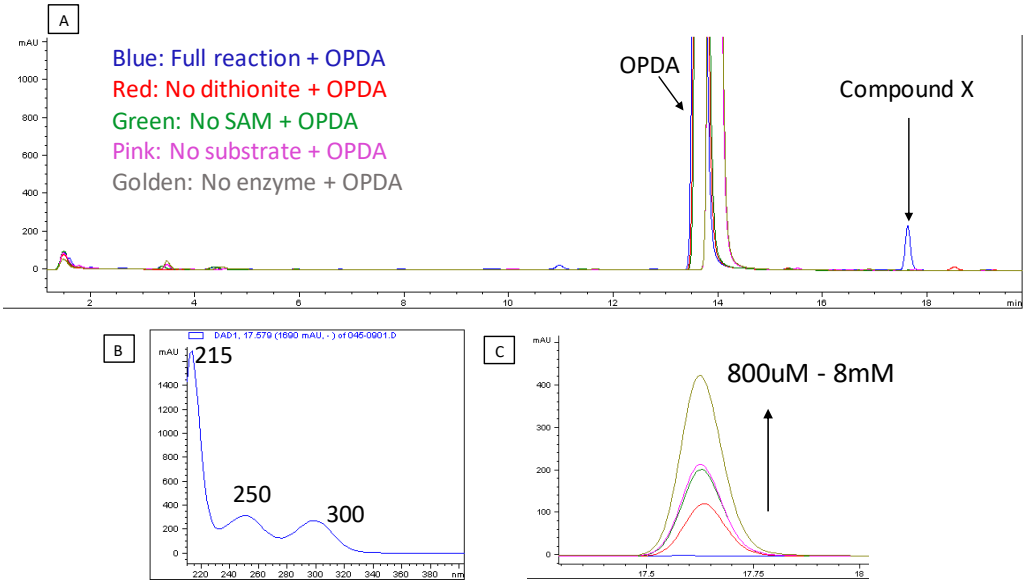

Figure 4.9 [A] HPLC chromatogram of ThiC reaction with IRN in presence of OPDA at 300nm; [B] UV-Vis spectrum of Compound X; [C] Concentration dependent formation of compound X

To test if Compound X originated from a phosphate containing precursor, we analyzed the ThiC reaction mixture before and after CIP treatment. Compound X was absent before CIP treatment and a new peak could be detected eluting at 21.2 minutes (Figure 4.10).

This new peak was consumed after CIP treatment hinting that this could be the phosphate containing precursor of Compound X.

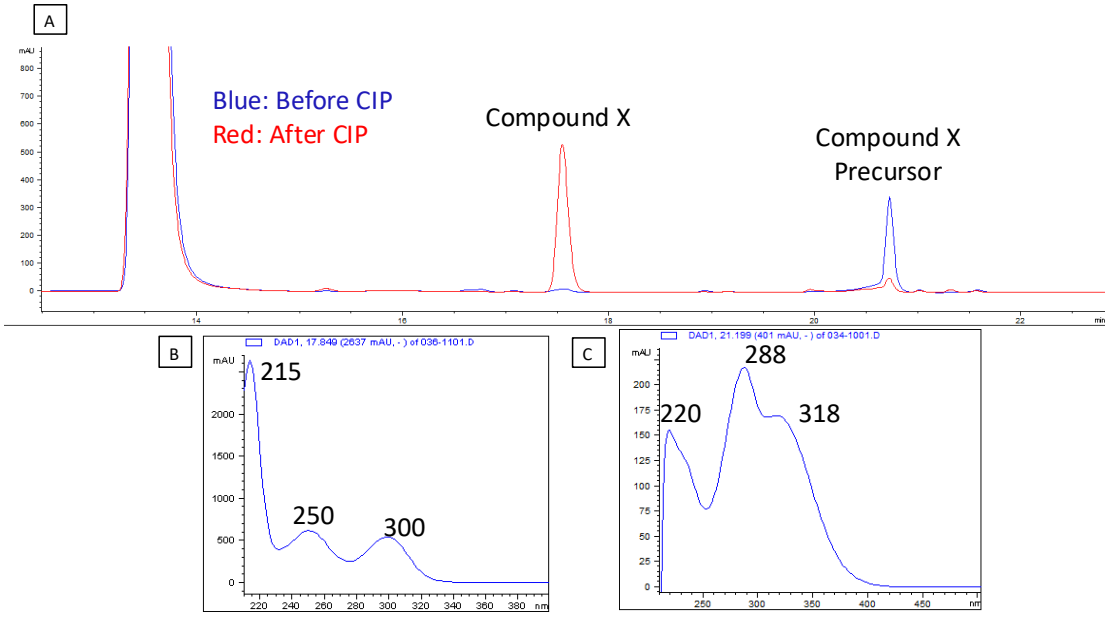

Figure 4.10 HPLC chromatogram of ThiC reaction with IRN, before and after CIP treatment; [B] UV-Vis spectrum of Compound X; [C] UV-Vis spectrum of Compound X precursor

LCMS analysis revealed that Compound X had m/z of 239.050 in the negative mode (Figure 4.11). Based on the accurate mass analysis, we could predict $C_{10}H_{11}N_2O_3S^-$ as the molecular formula of Compound X. Assuming OPDA trapping of sugar fragment to form benzimidazole moiety, we can predict that 6 carbon atoms, 4 hydrogen atoms and 2 nitrogen atoms would originate from OPDA. Remaining 4 carbons could have originated from the sugar fragment, hinting loss of one carbon atom from the ribose moiety. The source of the sulfur atom could be the [4Fe-4S] cluster or sodium dithionite reductant used in the reaction. When we tested 5'-D_2-IRN isotopologue under similar reaction conditions,

we observed 1 Da increment in the mass of Compound X, confirming that the Compound X is indeed derived from the ribose moiety of IRN.

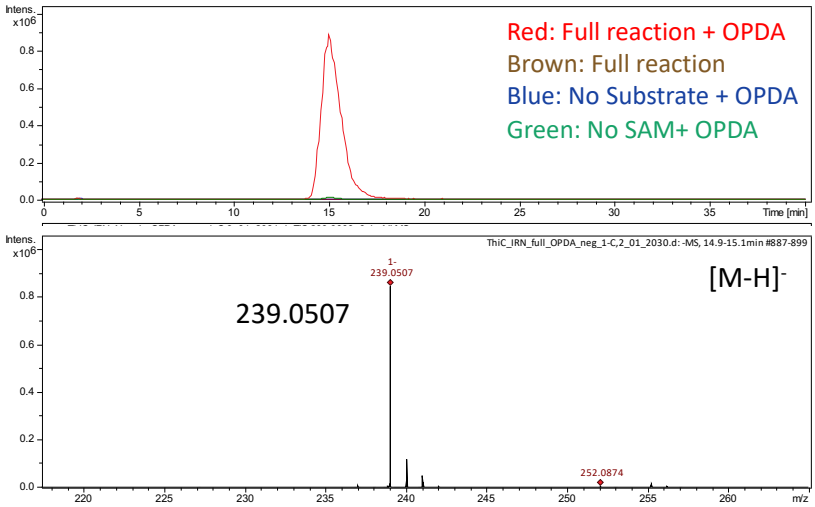

Figure 4.11 LCMS analysis of Compound X

In order to further characterize Compound X, we first isolated Compound X using HPLC and tested its stability. When purified and lyophilized sample of Compound X was re-analyzed on HPLC, we could detect the formation of 2 degradation products of Compound X (Figure 4.12). We termed these degradation products as Compound Y and Compound Z.

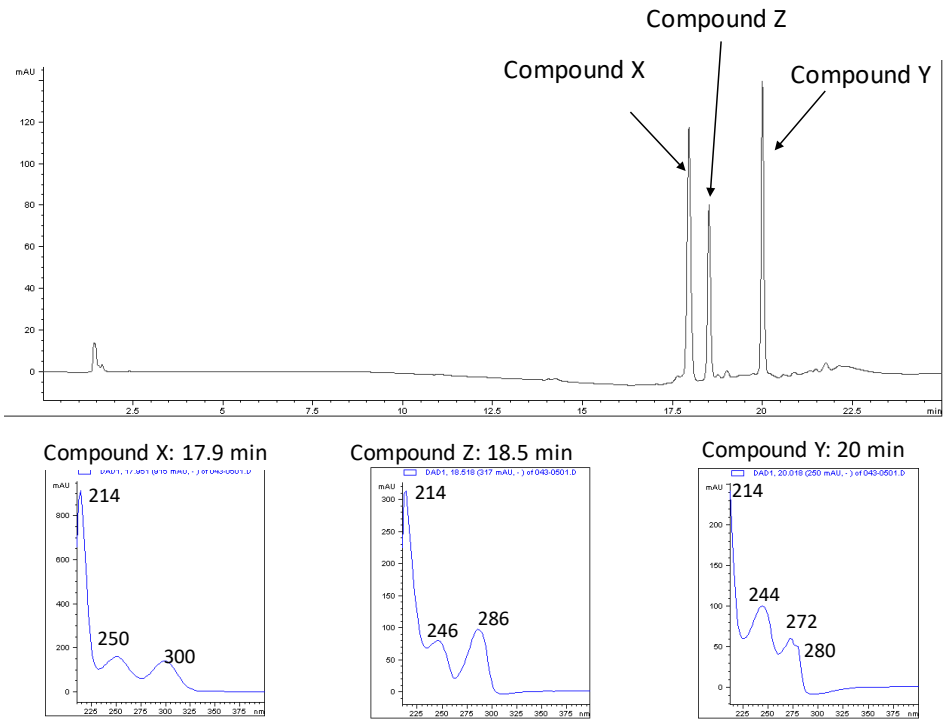

Figure 4.12Degradation of Compound X and UV-Vis spectra of the degradation products

These degradation products had UV-spectra significantly different from that of Compound X (Figure 4.12). We further analyzed this sample by mass spectrometry and could decipher the masses of these 2 degradation products. In the negative mode, Compound Y and Z had m/z of 237.03 and 253.02 respectively. Based on this data we could propose molecular formulae for these compounds and put forward an oxidative degradation pathway for the Compound X. Compound X would first undergo a $2e^-$ oxidation to Compound Y which could further oxidize to Compound Z by oxygen incorporation. Further structural characterization of Compound X has been challenging owing to its oxidatively instability.

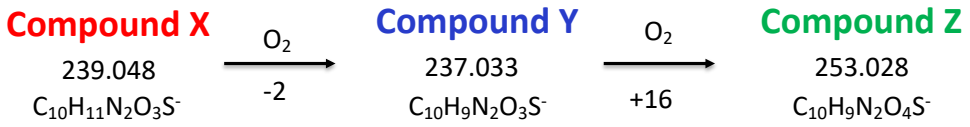

Figure 4.13 Oxidative degradation scheme of Compound X

All these experiments unequivocally established that IRN is accepted as a substrate by ThiC and the chemistry is initiated by H atom abstraction from the C5' of IRN. The expected final product desamino-HMP **99** is not formed. Instead, imidazole **100** and the corresponding sugar fragment are the major products. Imidazole **100** was directly detected using HPLC analysis whereas the sugar fragment was detected by trapping it with the aldehyde trapping reagent OPDA.

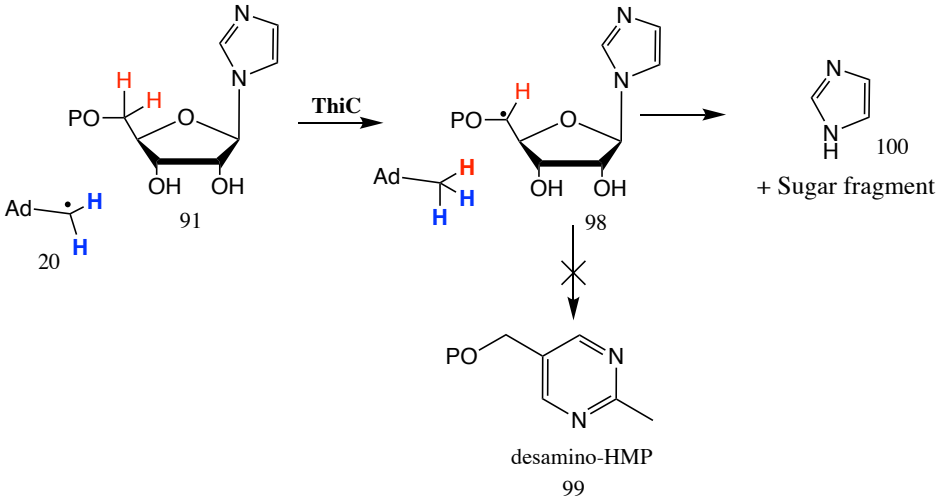

Figure 4.14 Reaction scheme of ThiC reaction with IRN

To test if the sugar fragment detected with the substrate analog IRN is relevant to the native ThiC chemistry, we decided to check for the presence of Compound X and 5-aminoimidazole as side products in the ThiC reaction with the native substrate AIR. When ThiC reaction with AIR in the presence of OPDA was analyzed by LCMS analysis,

Compound X was detected. The levels of Compound X were significantly lower than those observed in the case of IRN. This is expected since in the case native ThiC reaction, most of the reaction flux is directed towards the final product - HMP-P formation. Detection of Compound X in the native ThiC reaction indicates that the sugar fragment detected in the form of Compound X is likely to be a mechanistically relevant shunt product.

When we tested ThiC D383A mutant with AIR, no HMP formation was observed, but there was significant AIR consumption (Figure 4.15). This prompted us to check for the alternative products formed in this reaction. On running this reaction in the presence of OPDA, we could detect Compound X formation. The levels of Compound X formed with the D383A mutant were >10 fold higher than observed in the wild type reaction with AIR (Figure 4.16). Encouraged with this result, we tested AIR isotopologues to get insight into the structure of Compound X (Figure 4.17, A).

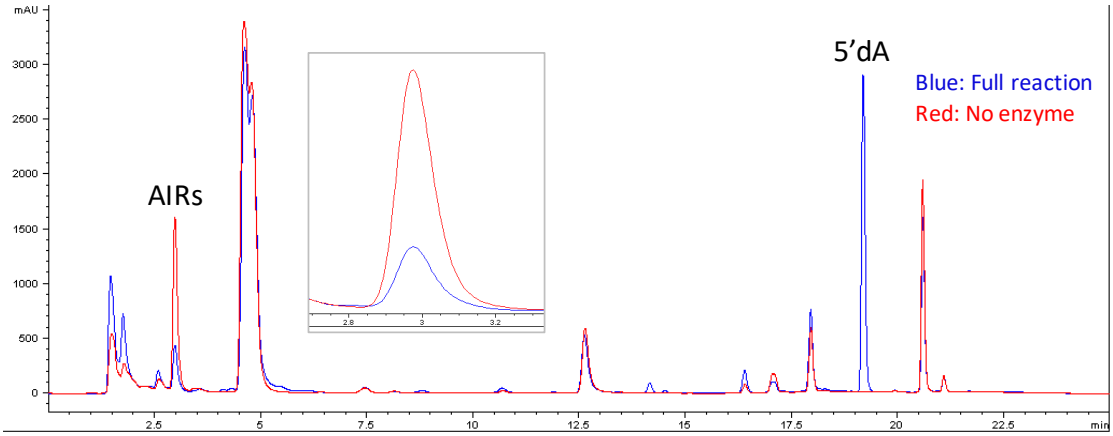

Figure 4.15 ThiC D383A reaction with AIR. Inset: consumption of AIR

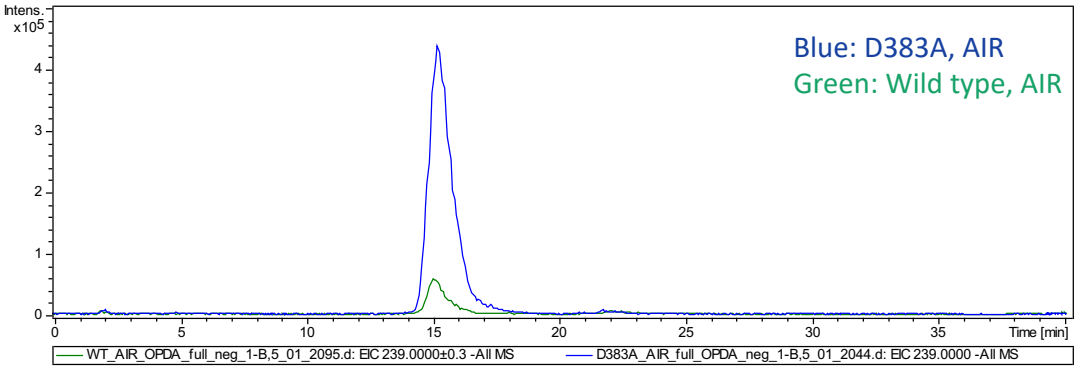

Figure 4.16 LCMS detection of Compound X in Wild type and D383A ThiC reaction with AIR

A

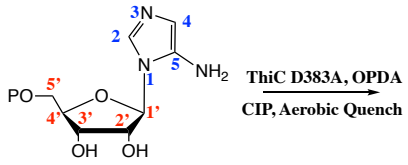

Isotopomer	Compound X
AIR	239
5'-D_2-AIR	240 (+1)
4'-D-AIR	240 (+1)
2',3',4',5',5'-D_5-AIR (4'- 50%)	242:243 (+4) (50:50)
50% D_2O	239:240 (+1) (50:50)

Isotopomer	Compound X
^{15}-NH2-AIR	239
2,4-D_2-AIR	239
U-^{13}C-AIR	243 (+4)
2'-^{13}C-AIR	240 (+1)
1'-^{13}C-AIR	239

B

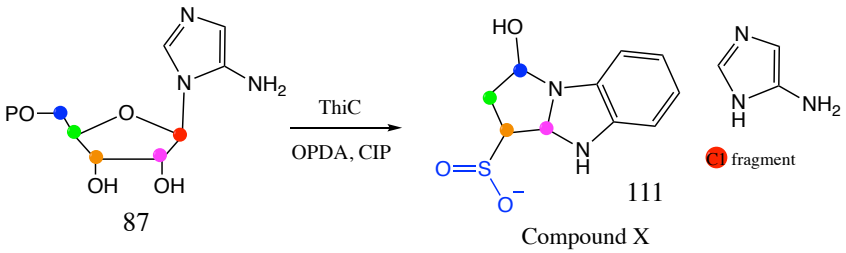

87 111 Compound X

Figure 4.17 [A] Isotope labeling studies for Compound X formation [B] Proposed structure for Compound X

The labeling studies established that C1' carbon and the aminoimidazole moiety is lost whereas 2',3',4',5' protons are retained and one proton is incorporated from solvent

in Compound X. Based on these isotope labeling studies and the oxidative degradation profile of Compound X, we can propose a structure for Compound X (Figure 4.17, B). Compound X **111** would have a tricyclic structure having a five membered ring fused to the benzimidazoline moiety. We can also write a mechanistic hypothesis for Compound X **111** formation(Figure 4.18). The chemistry initiates by hydrogen atom abstraction from C5'. This would undergo acid assisted heterolysis of carbon-oxygen bond leading to the alkene radical cation **102**. This is followed by intramolecular electron transfer from the imidazole moiety to alkene radical cation generating imidazolyl radical cation **103**. This will be followed by rapid mesolytic cleavage to generate formylated imidazole **106** and C2' radical **104** as fragments. This C2' radical **104** undergoes diol dehydratase type chemistry to lose water molecule and generates C3' radical **105**. This radical subsequently gets quenched by recombination with sulfinate radical anion to form a sulfinate adduct **107**. Formylated imidazole **106** would get hydrolyzed to corresponding imidazole and formate. This sugar fragment having sulfinate adduct is then trapped by OPDA to generate benzimidazoline adduct **108**. Phosphatase treatment will cleave off terminal phosphate to generate enol intermediate **109**, which can tautomerize to the aldehyde form **110**. The C5' aldehydic carbon can undergo intramolecular cyclization by nucleophilic attack from the benzimidazoline nitrogen generating Compound X **111**. Under aerobic conditions, Compound X can undergo a $2e^-$ oxidation to form the corresponding benzimidazole viz. Compound Y **112**. On prolonged air exposure, the sulfinic acid moiety of Compound Y can oxidize to sulfonic acid leading to Compound Z **113**.

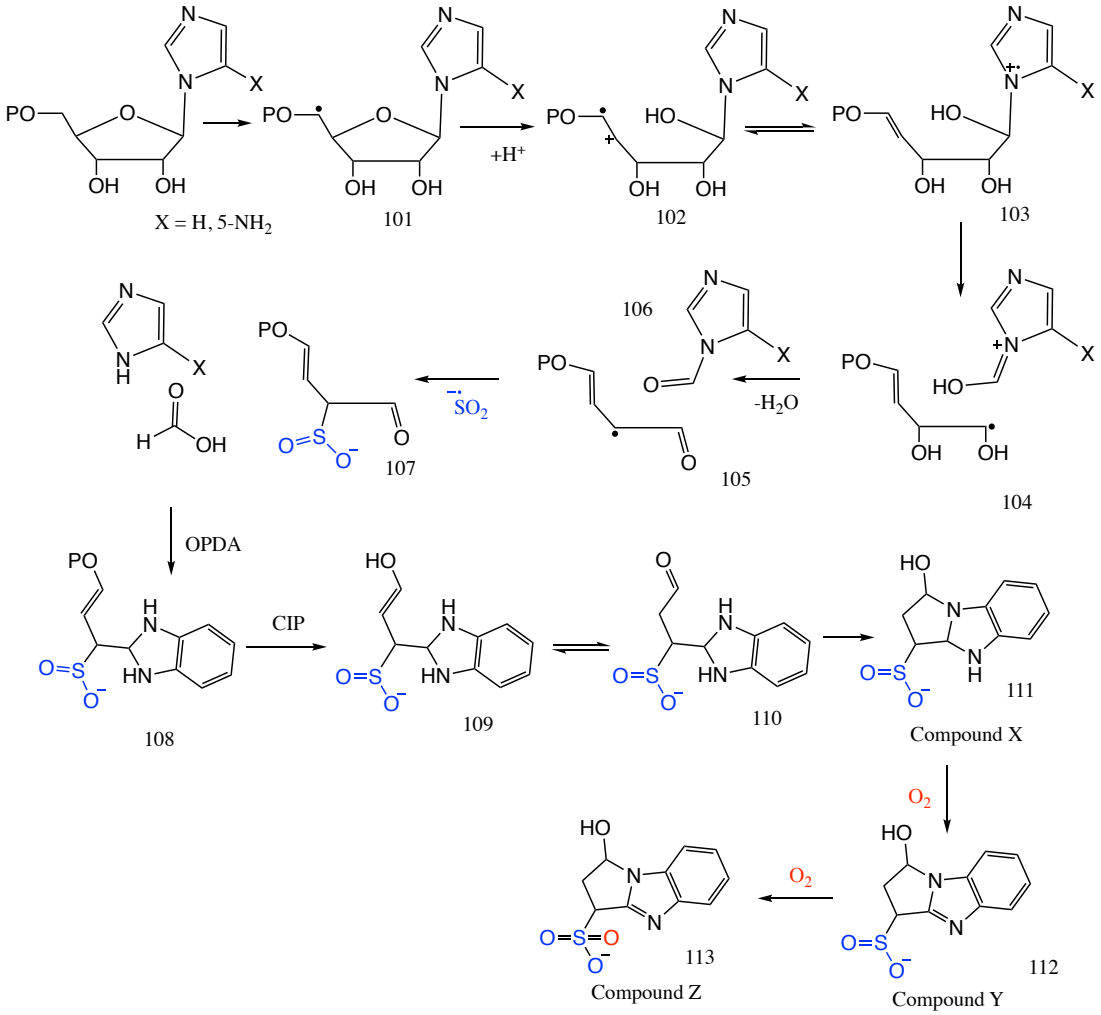

Figure 4.18 Mechanistic proposal for Compound X, Y, Z formation

Efforts are underway to synthesize synthetic reference compounds for Compounds X, Y and Z to confirm their proposed structures.

4.4. ThiC reaction with the other imidazole based substrate analogs

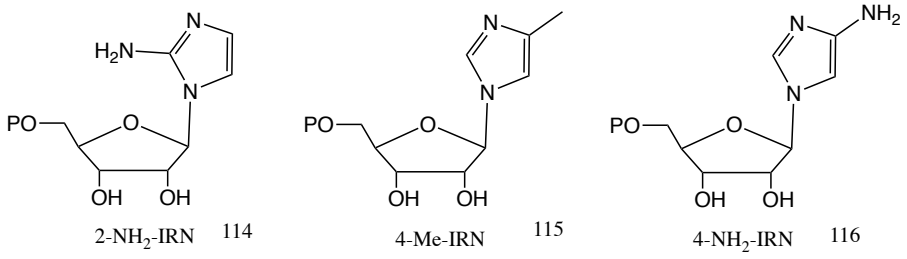

Figure 4.19 Imidazole based substrate analogs tested on ThiC

Encouraged with the results from the IRN, we tested more substrate analogs having imidazole modification: 2-NH_2-IRN **114**, 4-NH_2-IRN **116** and 4-Me-IRN **115**. 2-NH_2-IRN and 4-Me-IRN showed the formation of Compound X and corresponding imidazole as major products. No other new signal was detected by HPLC analysis. Surprisingly, 4-NH_2-IRN **116** was susceptible to dithionite mediated non-enzymatic degradation. We could still detect the formation of low levels of Compound X in the ThiC reaction with 4-NH_2-IRN using LCMS analysis.

4.5. Mechanistic proposal for the ThiC catalyzed reaction

Based on the results of ThiC reaction with substrate analogs and D383A mutant, we can propose a credible mechanistic hypothesis for the early steps of the ThiC catalyzed reaction. The reaction initiates by the abstraction of proS hydrogen from C5'. This radical undergoes acid assisted heterolysis of a carbon-oxygen bond leading to the alkene radical cation. This is followed by intramolecular electron transfer from the aminoimidazole moiety to the alkene radical cation generating aminoimidazolyl radical cation. This will be followed by rapid mesolytic cleavage[88] to generate formylated aminoimidazole and C2'

radical as fragments. C2' radical then would recombine with the C2 of aminoimidazole to generate aminoimidazole based radical which on further rearrangement would form HMP-P as the final product.

This proposal involves fragmentation and recombination of radical intermediates. The results with the substrate analogs and with D383A mutant indicate that recombination of C2' sugar radical with the C2 of imidazole moiety is a carefully orchestrated event. Active site Aspartate 383 residue and the 5-NH_2 substituent on the imidazole are critically important for the successful recombination. Modification of either of these leads to the generation of shunt products. Studies are in progress to decipher further details of the mechanism of this remarkable transformation.

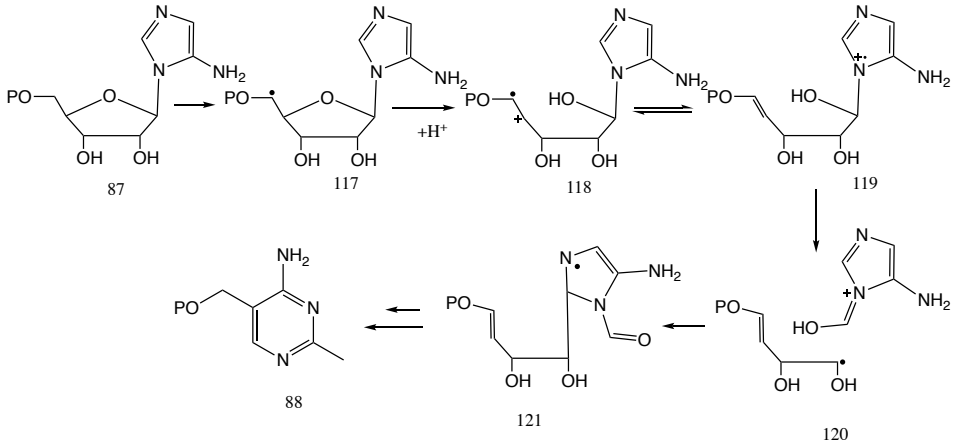

Figure 4.20 Mechanistic proposal for the early steps of the ThiC reaction

4.6. BzaF mediated Vitamin B_{12} biosynthesis

Vitamin B_{12}, or cobalamin, is a biological cofactor used in radical-initiated rearrangements, methyl transfers, and dehalogenation reactions. Organisms in all domains of life require vitamin B_{12}, but animals, plants, and fungi have to obtain it from the bacteria

& archaea. The B_{12} cofactor consists of a hexacoordinate cobalt ion equatorially ligated by the four nitrogens of the corrin. A number of ligands can bind the upper axial position (the R group). For methyl-transfer reactions, this ligand is a CH_3 group whereas for the radical rearrangement reactions, this position is occupied by 5'dA. The lower axial position is often occupied by the nitrogen of a 5,6 dimethylbenzimidazole (DMB) The biosynthesis of the complete corrinoid including DMB occurs via two distinct pathways- aerobic and anaerobic. In the anaerobic pathway *Eubacterium limosum* uses a set enzymes BzaA-BzaE to biosynthesize DMB from AIR. BzaA and BzaB are ThiC homologs and together catalyze conversion of AIR to 5-hydroxybenzimidazole (HBI). In *Desulfuromonas acetoxidans* and *Geobacter sulfurreducens*, BzaA & BzaB are replaced by a single enzymes- BzaF.

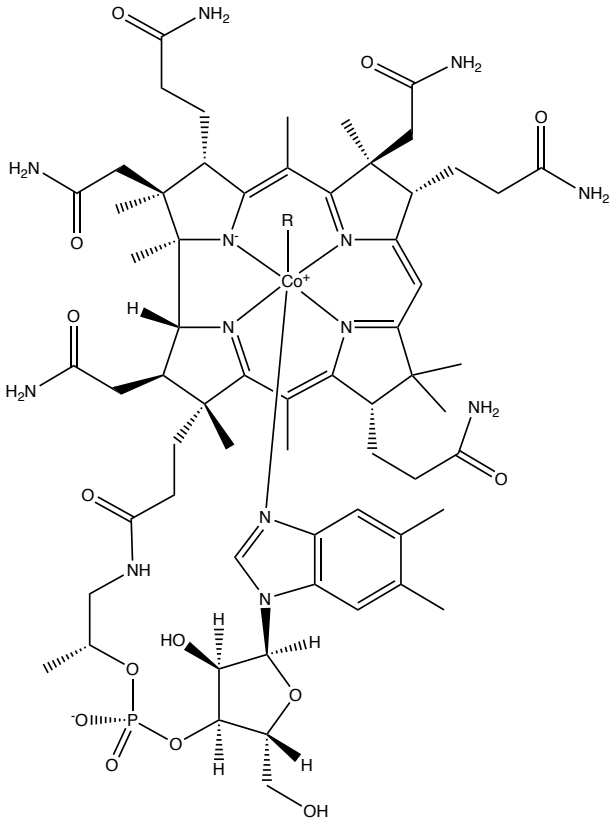

Figure 4.21 Structure of Vitamin B_{12}

4.7. BzaF catalyzed conversion of AIR to HBI

BzaF is a radical SAM enzyme and is a ThiC paralog. It catalyzes rearrangement of AIR to form 5-hydroxybenzimidazole.[89] Analogous to ThiC reaction on AIR, the BzaF catalyzed reaction is initiated by the abstraction of pro S hydrogen atom from C5' of AIR. Isotope labeling studies have demonstrated that four of the five ribose carbons of AIR form the benzyl portion of HBI. The 1′ carbon is lost as formate. The 2′ and 5′ carbons form bonds to the 4 and 5 carbons of the imidazole.[89] Early stage aminoimidazole based radical intermediate has been detected using EPR studies.[90] These studies indicate that the

early steps of BzaF and ThiC catalyzed reactions are similar. We can propose a mechanistic hypothesis as shown in Figure 4.23. In this proposal, the reaction is initiated by the abstraction of pro S hydrogen atom from C5' of AIR to generate **117**. This radical would follow the reaction course similar to ThiC mechanism to generate C2' radical **120** and formylated aminoimidazole. These 2 fragments would undergo recombination to generate adduct **123** where C2' of ribose forms a bond with C5 of aminoimidazole. **123** on subsequent rearrangement would yield 5-hydroxybenzimidazole **122** as the end product.

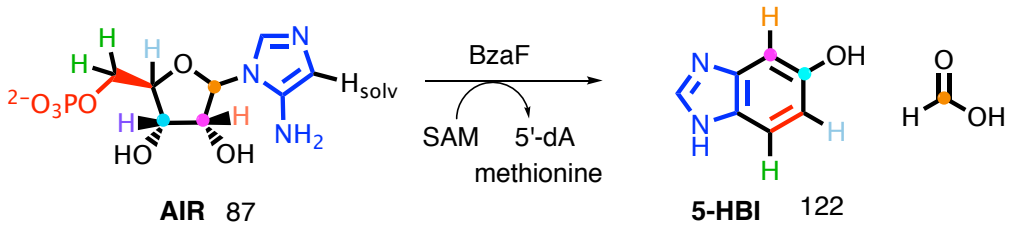

Figure 4.22 BzaF catalyzed conversion of AIR to 5-HBI

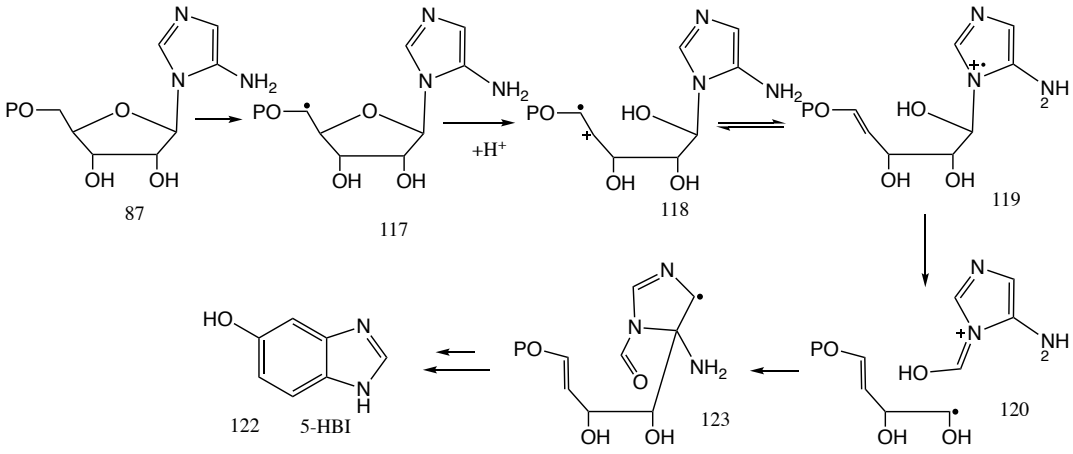

Figure 4.23 Mechanistic hypothesis for the early steps of BzaF catalyzed reaction

4.8. BzaF reaction with substrate analogs

Analogous to ThiC mechanism, recombination of radical intermediates would need careful orchestration by enzyme active site and thus could be a weak link in the mechanism. Thus we anticipated that imidazole based substrate analogs would yield Compound X and corresponding imidazole as products even in case of BzaF reaction. When we tested IRN & 2-NH_2-IRN as substrate analogs in BzaF reaction, we could detect the formation of imidazole and 2-NH_2-imidazole using HPLC analysis (Figure 4.24, 4.25).

This established that BzaF accepts substrate analogs with imidazole modification. Encouraged with this, we tried to trap the sugar fragment using OPDA. LCMS analysis of BzaF reaction with 2-NH_2-IRN in the presence of OPDA exhibited the efficient formation of Compound X (Figure 4.26). We also tried to detect Compound X formation in the BzaF native reaction with AIR. As shown in Figure 4.27 we could detect 2 peaks with the mass consistent with Compound X (Figure 4.27) Peak at 15.1 was Compound X based on the known retention time of Compound X. Identity of Peak at 18 minutes is not known but could be an isomer of Compound X.

These studies have established that early steps catalyzed by ThiC and BzaF reactions are indeed similar and both the enzymes follow fragmentation-recombination mechanisms. ThiC and BzaF diverge after fragmentation of radical intermediate **113**. Studies are in progress to identify evidence for the later steps in the BzaF catalyzed reaction.

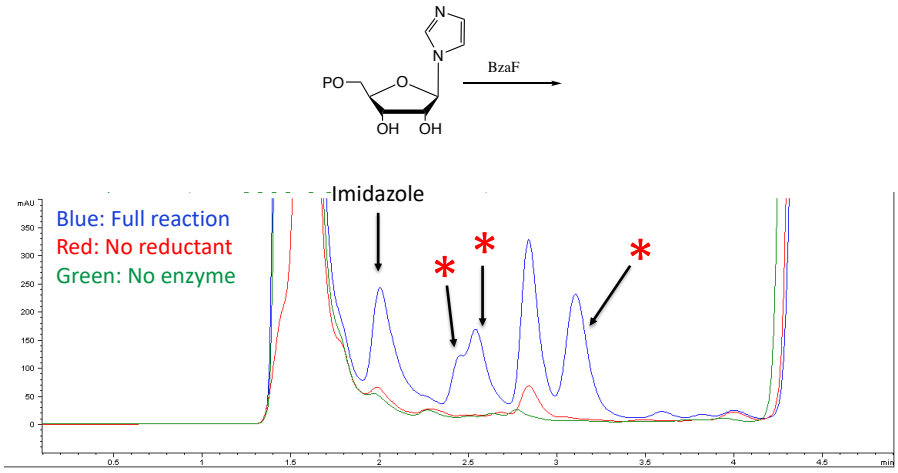

Figure 4.24 HPLC chromatogram of BzaF reaction with IRN

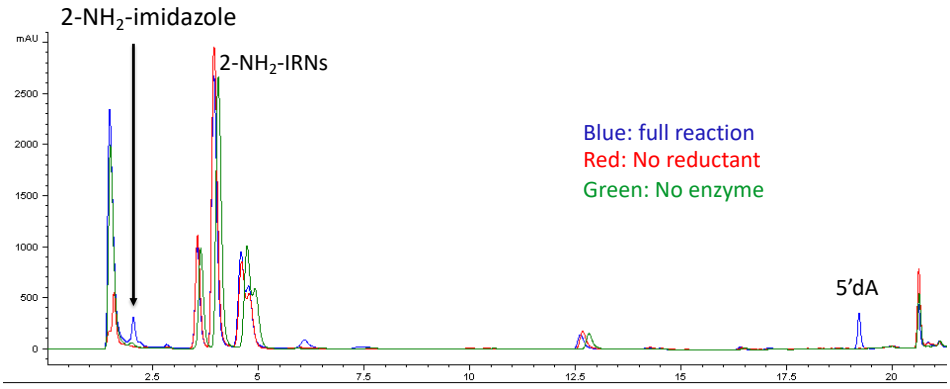

Figure 4.25 HPLC chromatogram of BzaF reaction with 2-NH2-IRN

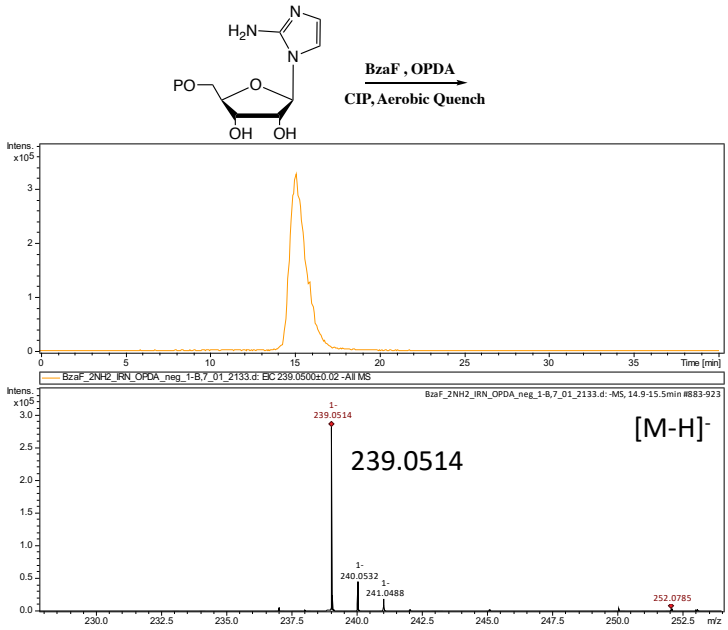

Figure 4.26 Compound X detection in BzaF reaction with 2-NH2-IRN

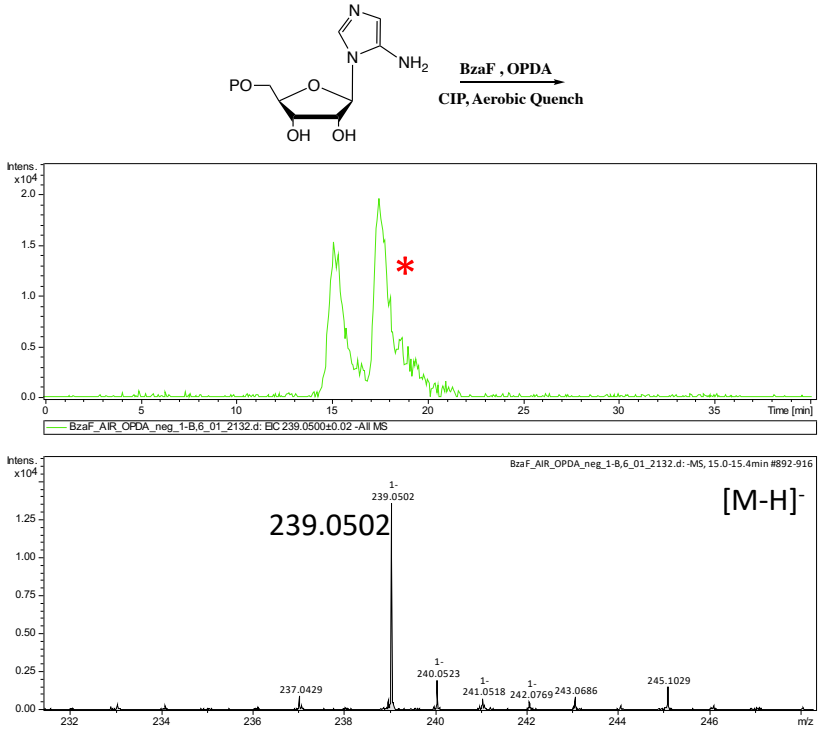

Figure 4.27 Compound X detection in the native BzaF reaction

4.9. Experimental procedures

4.9.1. HPLC parameters

An Agilent 1260 HPLC equipped with a quaternary pump was used. The system included a diode array UV-Vis detector and eluted compounds were detected by absorbance at 215, 225, 240, 254, 280, 320, 340 nm. The HPLC analysis was performed on a ZORBAX Eclipse XDB-C18 column (15 cm x 4.6 mm, 5 µm particles, Agilent Technologies). Typical injection volumes were in the range of 10-50 µl. Data was processed using ChemStation ver. B.04.01 SP1 (Agilent technologies).

HPLC conditions:

A- Water

B- 100mM Potassium phosphate buffer, pH 6.6 or 10 mM Ammonium acetate pH 6.6

C- Methanol

HPLC method:

0 min – 100% B, 5min – 100% B, 12 min – 48% A 40% B 12% C, 14 min – 50% A 30% B 20% C, 18 min - 30% A 10% B 60% C, 20 min - 100% B, 25 min - 100%B.

4.9.2. LCMS parameters

LC-ESI-TOF-MS was performed using an Agilent 1260 HPLC system equipped with a binary pump and a 1200 series diode array detector followed by a MicroToF-Q II mass spectrometer (Bruker Daltonics) using an ESI source either in negative mode or positive

mode. The analysis was performed on an LC-18-T column (15 cm x 3 mm, 3 μm particles, Supelco). Typical injection volumes were in the range of 20-80 μl. The data was processed using Data Analysis 4.0 SP1 (Bruker Daltonics). LCMS parameters used were similar to described in chapter 2.

4.9.3. Overexpression and purification of ThiC and BzaF

ThiC from *Arabidopsis thaliana* and BzaF from *pelobacter propionicus* were overexpressed and purified following a similar procedure as described for MqnE in Chapter 2.

4.9.4. Enzymatic synthesis of AIR from AIRs

AIRs kinase from *Salmonella enterica* was overexpressed in *E. coli* BL21(DE3) and purified using Ni-NTA chromatography as per published protocol.[91] All the stocks were prepared in 100mM Tris-HCl buffer (pH 7.5). A typical reaction mixture consisted of 2.5 mM AIRs, 4 mM ATP, 50mM $MgSO_4.7H_2O$, (pH 7.5) and 400 μM AIRs kinase. The reaction mixture was incubated at room temperature for 1 hour and analyzed by HPLC. AIR was then purified using HPLC and lyophilized to dryness. Lyophilized AIR was then transferred into the glove box and resuspended in degassed water to have final AIR concentration of 5-10 mM. This AIR stock was used for ThiC reactions. The concentration of AIR was measured by comparing the peak areas in HPLC of AIRs synthetic standard and phosphatase treated purified AIR stock.

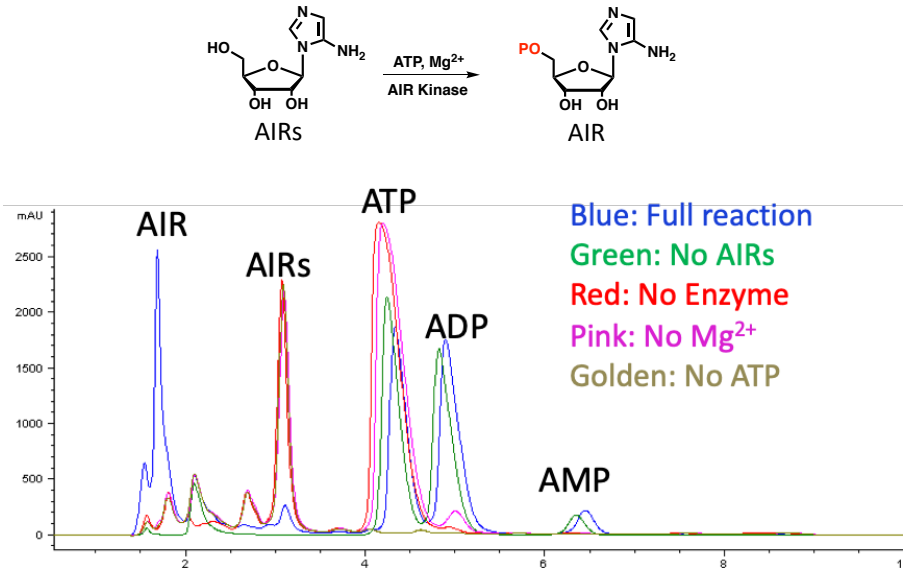

Figure 4.28 HPLC chromatogram for AIR kinase reaction

4.9.5. Enzymatic assay of ThiC reaction

A typical enzymatic reaction was performed in 100 mM Tris-HCl buffer (pH 7.5) containing 300 μM AtThiC, 500 μM AIR, 1 mM SAM and 2 mM dithionite. The reaction was incubated at room temperature anaerobically for 4-5 hours. The reaction mixture was then heat quenched at 90 °C for one minute and then centrifuged and filtered through a 10kDa cut-off filter before analyzed by HPLC or LC-MS.

4.9.6. Alkaline phosphatase treatment of ThiC reaction

Alkaline phosphatase, calf intestinal (New England Biolabs) 1µL (1000 units) was added to 100 - 200 µl of ThiC enzymatic reaction. The mixture was incubated at room temperature for 60 minutes and then quenched through 10kDa cut-off filter before it was analyzed by HPLC or LC-MS.

4.9.7. Chemo-enzymatic synthesis of IRNs

IRNs was chemo-enzymatically synthesized by N-transglycosylation of Adenosine using *E. coli* purine nucleoside phosphorylase (PNP).[92] All the stock solutions were prepared in Tris-HCl buffer (pH 7.5). 1mM Adenosine, 10mM potassium phosphate dibasic, 100 mM imidazole and 200 µg/ml *E. coli* purine nucleoside phosphorylase (sigma) were incubated at 37^0C for 18-24 hours. The reaction mixture was then analyzed using HPLC. After complete consumption of adenosine, the reaction was quenched using 10kDa cut-off filters and IRNs was purified using HPLC. 5'-D_2-IRNs isotopologue was obtained following the same protocol using 5-D_2-Adenosine (Cambridge isotope laboratories).

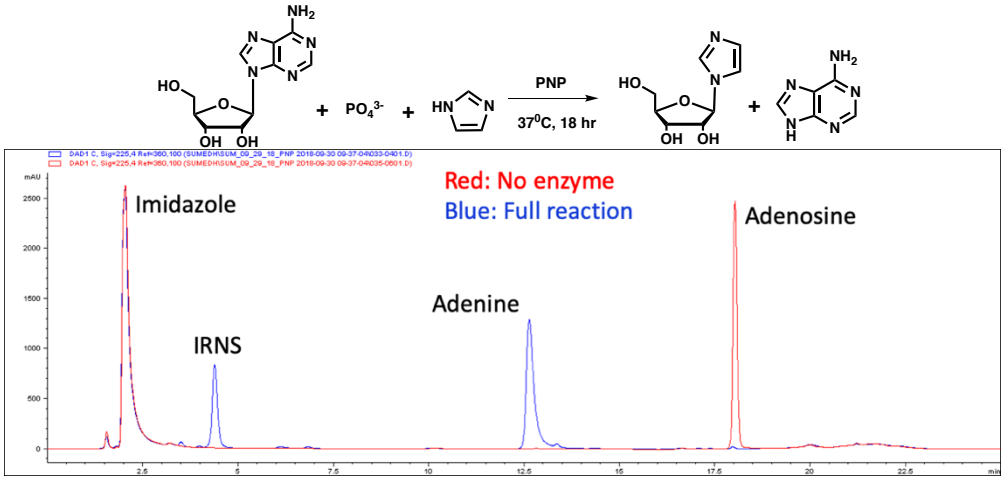

Figure 4.29 HPLC chromatogram for PNP catalyzed IRNs formation

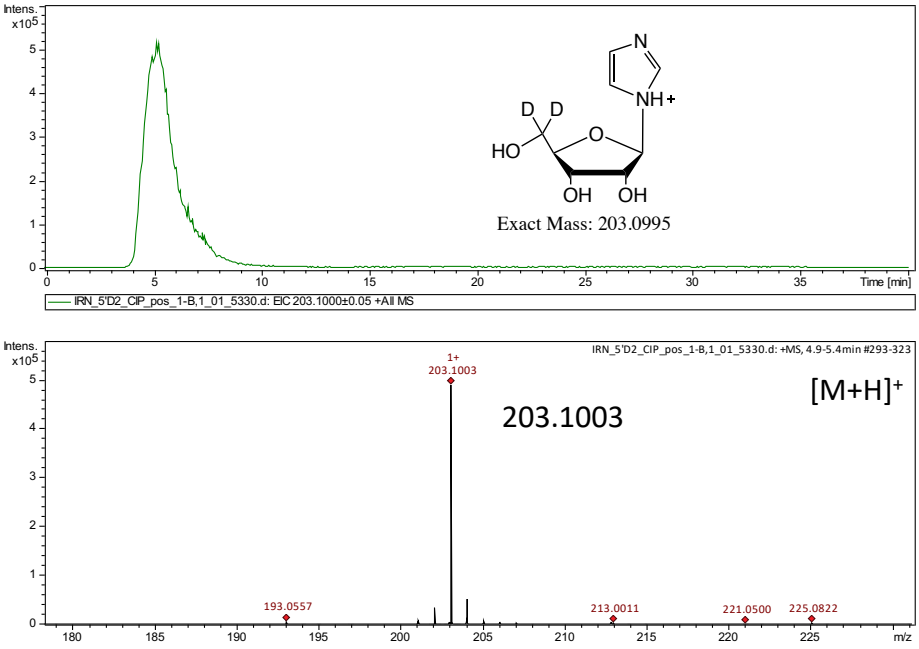

Figure 4.30 Mass analysis of 5'-D2-IRNs

5. SUMMARY

The majority of the work has been centered around mechanistic studies of on the radical SAM enzymes involved in menaquinone (Vitamin K), Thiamin (Vitamin B_1) and cobalamin (Vitamin B_{12}) biosynthesis. Aminofutalosine synthase (MqnE) catalyzes the important C-C bond formation reaction in futalosine dependent menaquinone biosynthesis pathway converting 3-((1-carboxyvinyl)oxy)benzoic acid (**13**) to Aminofutalosine (**14**) in menaquinone biosynthesis. We have proposed a novel reaction mechanism for the MqnE catalyzed radical rearrangement involving a radical addition to the stable benzene ring (Figure 5.1). Although well precedented in synthetic chemistry, such arene addition reactions are still poorly understood in biosynthesis. We have developed new radical trapping strategies based on using intramolecular, fast and radical triggered carbon-halogen bond fragmentation reactions (β-scission and $S_{RN}1$ fragmentation) to trap the captodative (**23**) and aryl radical anion (**27**) intermediates.

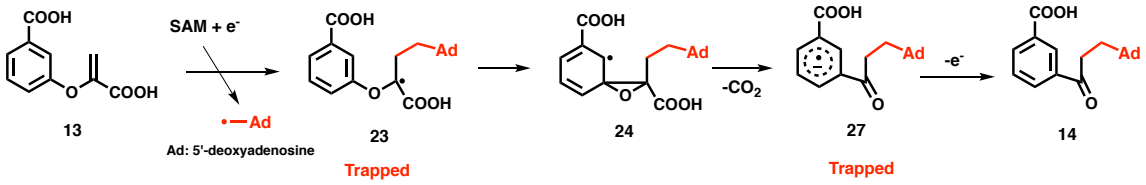

Figure 5.1 Summary of mechanistic studies on MqnE catalyzed reaction

It is generally not possible to trap the active-site radical intermediates using exogenous trapping agents because the enzyme active site effectively shields the radical intermediates from the environment. But contrary to this notion, we demonstrated efficient trapping of the radical intermediate (**67**) using radical trapping agents sodium dithionite and 5,5-

dimethyl-1-pyrroline-N-oxide (DMPO) (Figure 3.22). To the best of our knowledge, this is the first example of spin trapping of a radical intermediate in radical SAM enzymology. Using a mechanism-guided approach, we have identified potent inhibitors of MqnE and have demonstrated their inhibitory activity against important human pathogens - *Helicobacter pylori and Campylobacter jejuni.*

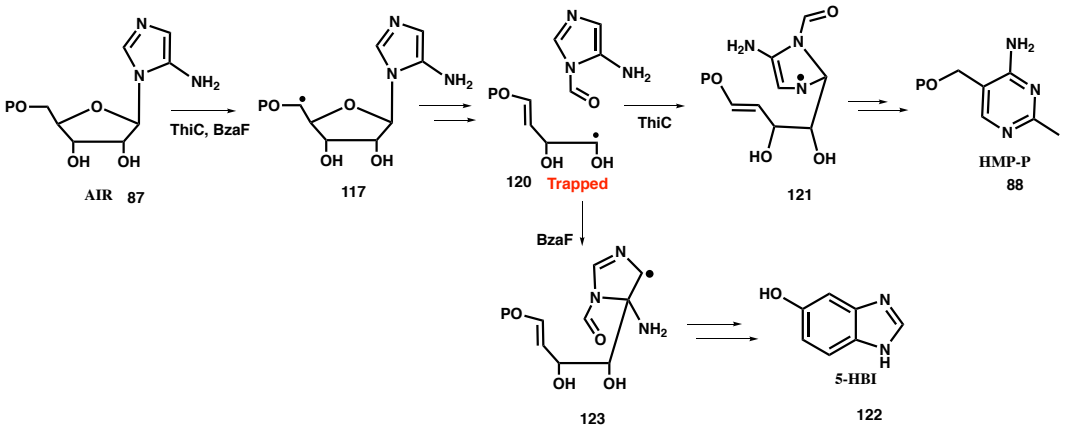

Figure 5.2 Summary of mechanistic studies on ThiC & BzaF catalyzed reaction

ThiC and BzaF are radical SAM enzymes which catalyze remarkable rearrangement reactions in the biosynthesis of Thiamin (Vitamin B_1) and cobalamin (Vitamin B_{12}) by converting 5-aminoimidazole ribonucleotide (AIR) to hydroxymethyl pyrimidine phosphate (HMP-P) and 5-hydroxybenzimidazole (5-HBI) respectively. Using sodium dithionite as a radical trapping agent, we have trapped a sugar-based radical intermediate in ThiC and BzaF catalyzed reactions. This has enabled us to propose credible mechanistic hypotheses for the early steps of these reactions.

REFERENCES

1. Hin, B.; Majer, P.; Tsukamoto, T., Facile synthesis of α-substituted acrylate esters. *The Journal of organic chemistry* **2002,** *67* (21), 7365-7368.

2. Majer, P.; Hin, B.; Stoermer, D.; Adams, J.; Xu, W.; Duvall, B. R.; Delahanty, G.; Liu, Q.; Stathis, M. J.; Wozniak, K. M., Structural optimization of thiol-based inhibitors of glutamate carboxypeptidase II by modification of the P1 'side chain. *Journal of medicinal chemistry* **2006,** *49* (10), 2876-2885.

3. Nowicka, B.; Kruk, J., Occurrence, biosynthesis and function of isoprenoid quinones. *Biochimica et Biophysica Acta (BBA) - Bioenergetics* **2010,** *1797* (9), 1587-1605.

4. Cranenburg, E. C. M.; Schurgers, L. J.; Vermeer, C., Vitamin K: the coagulation vitamin that became omnipotent. *Thromb. Haemostasis* **2007,** *98* (1), 120-125.

5. Plaza, S. M.; Lamson, D. W., Vitamin K2 in bone metabolism and osteoporosis. *Altern Med Rev* **2005,** *10* (1), 24-35.

6. Dowd, P.; Hershline, R.; Ham, S. W.; Naganathan, S., Vitamin K and energy transduction: a base strength amplification mechanism. *Science* **1995,** *269* (5231), 1684-1691.

7. Suttie, J. W., The importance of menaquinones in human nutrition. *Annu. Rev. Nutr.* **1995,** *15*, 399-417.

8. Meganathan, R.; Kwon, O., Biosynthesis of menaquinone (vitamin K2) and ubiquinone (coenzyme Q). *EcoSal Plus* **2009**, 1-24.

9. Meganathan, R., Menaquinone/Ubiquinone Biosynthesis and Enzymology. **2010**.

10. Hiratsuka, T.; Furihata, K.; Ishikawa, J.; Yamashita, H.; Itoh, N.; Seto, H.; Dairi, T., An alternative menaquinone biosynthetic pathway operating in microorganisms. *Science* **2008,** *321* (5896), 1670-1673.

11. Seto, H.; Jinnai, Y.; Hiratsuka, T.; Fukawa, M.; Furihata, K.; Itoh, N.; Dairi, T., Studies on a new biosynthetic pathway for menaquinone. *Journal of the American Chemical Society* **2008,** *130* (17), 5614-5615.

12. Dairi, T., Menaquinone biosyntheses in microorganisms. *Methods Enzymol.* **2012,** *515* (Natural Product Biosynthesis by Microorganisms and Plants, Part A), 107-122.

13. Begley, T. P.; Chatterjee, A.; Hanes, J. W.; Hazra, A.; Ealick, S. E., Cofactor biosynthesis—still yielding fascinating new biological chemistry. *Current opinion in chemical biology* **2008,** *12* (2), 118-125.

14. Dairi, T.; Kuzuyama, T.; Nishiyama, M.; Fujii, I., Convergent strategies in biosynthesis. *Nat. Prod. Rep.* **2011,** *28* (6), 1054-1086.

15. Dairi, T.; Kuzuyama, T.; Nishiyama, M.; Fujii, I., Convergent strategies in biosynthesis. *Natural product reports* **2011,** *28* (6), 1054-1086.

16. Kolappan, S.; Zwahlen, J.; Zhou, R.; Truglio, J. J.; Tonge, P. J.; Kisker, C., Lysine 190 is the catalytic base in MenF, the menaquinone-specific isochorismate synthase from Escherichia coli: Implications for an enzyme family. *Biochemistry* **2007,** *46* (4), 946-953.

17. Jirgis, E. N.; Bashiri, G.; Bulloch, E. M.; Johnston, J. M.; Baker, E. N., Structural views along the Mycobacterium tuberculosis MenD reaction pathway illuminate key

aspects of thiamin diphosphate-dependent enzyme mechanisms. *Structure* **2016,** *24* (7), 1167-1177.

18. Jiang, M.; Chen, X.; Wu, X.-H.; Chen, M.; Wu, Y.-D.; Guo, Z., Catalytic mechanism of SHCHC synthase in the menaquinone biosynthesis of Escherichia coli: identification and mutational analysis of the active site residues. *Biochemistry* **2009,** *48* (29), 6921-6931.

19. Thompson, T. B.; Garrett, J. B.; Taylor, E. A.; Meganathan, R.; Gerlt, J. A.; Rayment, I., Evolution of Enzymatic Activity in the Enolase Superfamily: Structure of o-Succinylbenzoate Synthase from Escherichia coli in Complex with Mg2+ and o-Succinylbenzoate. *Biochemistry* **2000,** *39* (35), 10662-10676.

20. Klenchin, V. A.; Taylor Ringia, E. A.; Gerlt, J. A.; Rayment, I., Evolution of Enzymatic Activity in the Enolase Superfamily: Structural and Mutagenic Studies of the Mechanism of the Reaction Catalyzed by o-Succinylbenzoate Synthase from Escherichia coli. *Biochemistry* **2003,** *42* (49), 14427-14433.

21. Chen, Y.; Jiang, Y.; Guo, Z., Mechanistic insights from the crystal structure of Bacillus subtilis o-succinylbenzoyl-CoA synthetase complexed with the adenylate intermediate. *Biochemistry* **2016,** *55* (48), 6685-6695.

22. Li, H.-J.; Li, X.; Liu, N.; Zhang, H.; Truglio, J. J.; Mishra, S.; Kisker, C.; Garcia-Diaz, M.; Tonge, P. J., Mechanism of the intramolecular Claisen condensation reaction catalyzed by MenB, a crotonase superfamily member. *Biochemistry* **2011,** *50* (44), 9532-9544.

23. Widhalm, J. R.; van Oostende, C.; Furt, F.; Basset, G. J. C., A dedicated thioesterase of the Hotdog-fold family is required for the biosynthesis of the naphthoquinone ring of vitamin K1. *Proc. Natl. Acad. Sci. U. S. A.* **2009,** *106* (14), 5599-5603.

24. Bentley, R.; Meganathan, R., Biosynthesis of vitamin K (menaquinone) in bacteria. *Microbiol. Rev.* **1982,** *46* (3), 241-80.

25. Meganathan, R., Biosynthesis of menaquinone (vitamin K2) and ubiquinone (coenzyme Q): A perspective on enzymatic mechanisms. *Vitam. Horm. (San Diego, CA, U. S.)* **2001,** *61*, 173-218.

26. Zhi, X.-Y.; Yao, J.-C.; Tang, S.-K.; Huang, Y.; Li, H.-W.; Li, W.-J., The futalosine pathway played an important role in menaquinone biosynthesis during early prokaryote evolution. *Genome biology and evolution* **2014,** *6* (1), 149-160.

27. Mahanta, N.; Fedoseyenko, D.; Dairi, T.; Begley, T. P., Menaquinone biosynthesis: formation of aminofutalosine requires a unique radical SAM enzyme. *Journal of the American Chemical Society* **2013,** *135* (41), 15318-15321.

28. Goble, A. M.; Toro, R.; Li, X.; Ornelas, A.; Fan, H.; Eswaramoorthy, S.; Patskovsky, Y.; Hillerich, B.; Seidel, R.; Sali, A., Deamination of 6-aminodeoxyfutalosine in menaquinone biosynthesis by distantly related enzymes. *Biochemistry* **2013,** *52* (37), 6525-6536.

29. Arakawa, C.; Kuratsu, M.; Furihata, K.; Hiratsuka, T.; Itoh, N.; Seto, H.; Dairi, T., Diversity of the early step of the futalosine pathway. *Antimicrobial agents and chemotherapy* **2011,** *55* (2), 913-916.

30. Cooper, L. E.; Fedoseyenko, D.; Abdelwahed, S. H.; Kim, S.-H.; Dairi, T.; Begley, T. P., In vitro reconstitution of the radical S-adenosylmethionine enzyme MqnC involved in the biosynthesis of futalosine-derived menaquinone. *Biochemistry* **2013,** *52* (27), 4592-4594.

31. Cotrim, C. A.; Weidner, A.; Strehmel, N.; Bisol, T. B.; Meyer, D.; Brandt, W.; Wessjohann, L. A.; Stubbs, M. T., A Distinct Aromatic Prenyltransferase Associated with the Futalosine Pathway. *ChemistrySelect* **2017,** *2* (29), 9319-9325.

32. Bentley, S. D.; Chater, K. F.; Cerdeno-Tarraga, A. M.; Challis, G. L.; Thomson, N. R.; James, K. D.; Harris, D. E.; Quail, M. A.; Kieser, H.; Harper, D.; Bateman, A.; Brown, S.; Chandra, G.; Chen, C. W.; Collins, M.; Cronin, A.; Fraser, A.; Goble, A.; Hidalgo, J.; Hornsby, T.; Howarth, S.; Huang, C. H.; Kieser, T.; Larke, L.; Murphy, L.; Oliver, K.; O'Neil, S.; Rabbinowitsch, E.; Rajandream, M. A.; Rutherford, K.; Rutter, S.; Seeger, K.; Saunders, D.; Sharp, S.; Squares, R.; Squares, S.; Taylor, K.; Warren, T.; Wietzorrek, A.; Woodward, J.; Barrell, B. G.; Parkhill, J.; Hopwood, D. A., Complete genome sequence of the model actinomycete Streptomyces coelicolor A3(2). *Nature (London, U. K.)* **2002,** *417* (6885), 141-147.

33. Ravcheev, D. A.; Thiele, I., Genomic analysis of the human gut microbiome suggests novel enzymes involved in quinone biosynthesis. *Frontiers in microbiology* **2016,** *7*.

34. Sofia, H. J.; Chen, G.; Hetzler, B. G.; Reyes-Spindola, J. F.; Miller, N. E., Radical SAM, a novel protein superfamily linking unresolved steps in familiar biosynthetic pathways with radical mechanisms: functional characterization using new

analysis and information visualization methods. *Nucleic acids research* **2001,** *29* (5), 1097-1106.

35. Broderick, J. B.; Duffus, B. R.; Duschene, K. S.; Shepard, E. M., Radical S-adenosylmethionine enzymes. *Chemical reviews* **2014,** *114* (8), 4229-4317.

36. Gerlt, J. A., Genomic Enzymology: Web Tools for Leveraging Protein Family Sequence–Function Space and Genome Context to Discover Novel Functions. *Biochemistry* **2017,** *56* (33), 4293-4308.

37. Finn, R. D.; Attwood, T. K.; Babbitt, P. C.; Bateman, A.; Bork, P.; Bridge, A. J.; Chang, H.-Y.; Dosztányi, Z.; El-Gebali, S.; Fraser, M., InterPro in 2017—beyond protein family and domain annotations. *Nucleic acids research* **2016,** *45* (D1), D190-D199.

38. Vey, J. L.; Drennan, C. L., Structural Insights into Radical Generation by the Radical SAM Superfamily. *Chemical Reviews* **2011,** *111* (4), 2487-2506.

39. Ruszczycky, M. W.; Zhong, A.; Liu, H.-w., Following the electrons: peculiarities in the catalytic cycles of radical SAM enzymes. *Natural product reports* **2018**.

40. Bhandari, D. M.; Fedoseyenko, D.; Begley, T. P., Tryptophan lyase (NosL): A cornucopia of 5′-deoxyadenosyl radical mediated transformations. *Journal of the American Chemical Society* **2016**.

41. Nicolet, Y.; Rohac, R.; Martin, L.; Fontecilla-Camps, J. C., X-ray snapshots of possible intermediates in the time course of synthesis and degradation of protein-bound Fe4S4 clusters. *Proceedings of the National Academy of Sciences* **2013,** *110* (18), 7188-7192.

42. Mehta, A. P.; Abdelwahed, S. H.; Mahanta, N.; Fedoseyenko, D.; Philmus, B.; Cooper, L. E.; Liu, Y.; Jhulki, I.; Ealick, S. E.; Begley, T. P., Radical S-adenosylmethionine (SAM) enzymes in cofactor biosynthesis: a treasure trove of complex organic radical rearrangement reactions. *Journal of Biological Chemistry* **2015,** *290* (7), 3980-3986.

43. Liu, W.; Sakr, E.; Schaeffer, P.; Talbot, H. M.; Donisi, J.; Härtner, T.; Kannenberg, E.; Takano, E.; Rohmer, M., Ribosylhopane, a novel bacterial hopanoid, as precursor of C35 bacteriohopanepolyols in Streptomyces coelicolor A3 (2). *ChemBioChem* **2014,** *15* (14), 2156-2161.

44. Bodlenner, A.; Liu, W.; Hirsch, G.; Schaeffer, P.; Blumenberg, M.; Lendt, R.; Tritsch, D.; Michaelis, W.; Rohmer, M., C35 Hopanoid Side Chain Biosynthesis: Reduction of Ribosylhopane into Bacteriohopanetetrol by a Cell-Free System Derived from Methylobacterium organophilum. *ChemBioChem* **2015,** *16* (12), 1764-1770.

45. Bietti, M.; Calcagni, A.; Cicero, D. O.; Martella, R.; Salamone, M., The O-neophyl rearrangement of 1,1-diarylalkoxyl radicals. Experimental evidence for the formation of an intermediate 1-oxaspiro[2,5]octadienyl radical. *Tetrahedron Lett.* **2010,** *51* (31), 4129-4131.

46. Baroudi, A.; Alicea, J.; Flack, P.; Kirincich, J.; Alabugin, I. V., Radical O→C Transposition: A Metal-Free Process for Conversion of Phenols into Benzoates and Benzamides. *J. Org. Chem.* **2011,** *76* (6), 1521-1537.

47. Baroudi, A.; Flack, P.; Alabugin, I. V., Metal-Free Transformation of Phenols into Substituted Benzamides: a Highly Selective Radical 1,2-O→C Transposition in O-

Aryl-N-phenylthiocarbamates. *Chem. - Eur. J.* **2010,** *16* (41), 12316-12320, S12316/1-S12316/40.

48. Tang, M.-C.; Zou, Y.; Watanabe, K.; Walsh, C. T.; Tang, Y., Oxidative cyclization in natural product biosynthesis. *Chem. Rev* **2017,** *117* (8), 5226-5333.

49. Wagner, P. J.; Lindstrom, M. J.; Sedon, J. H.; Ward, D. R., Photochemistry of δ-haloketones: anchimeric assistance in triplet-state γ-hydrogen abstraction and β-elimination of halogen atoms from the resulting diradicals. *J. Am. Chem. Soc.* **1981,** *103* (13), 3842-9.

50. Rossi, R. A.; Pierini, A. B.; Peñéñory, A. B., Nucleophilic substitution reactions by electron transfer. *Chemical reviews* **2003,** *103* (1), 71-168.

51. Tanner, D. D.; Chen, J. J.; Chen, L.; Luelo, C., Fragmentation of substituted acetophenones and halobenzophenone ketyls. Calibration of a mechanistic probe. *Journal of the American Chemical Society* **1991,** *113* (21), 8074-8081.

52. Ruszczycky, M. W.; Choi, S.-h.; Liu, H.-w., Stoichiometry of the redox neutral deamination and oxidative dehydrogenation reactions catalyzed by the radical SAM enzyme DesII. *Journal of the American Chemical Society* **2010,** *132* (7), 2359-2369.

53. Wagner, A. V.; Demand, J.; Schilling, G.; Pils, T.; Knappe, J., A Dehydroalanyl Residue Can Capture the 5′-Deoxyadenosyl Radical Generated fromS-Adenosylmethionine by Pyruvate Formate-Lyase-Activating Enzyme. *Biochemical and biophysical research communications* **1999,** *254* (2), 306-310.

54. Huhta, M. S.; Ciceri, D.; Golding, B. T.; Marsh, E. N. G., A novel reaction between adenosylcobalamin and 2-methyleneglutarate catalyzed by glutamate mutase. *Biochemistry* **2002,** *41* (9), 3200-3206.

55. Hänzelmann, P.; Schindelin, H., Crystal structure of the S-adenosylmethionine-dependent enzyme MoaA and its implications for molybdenum cofactor deficiency in humans. *Proceedings of the National Academy of Sciences of the United States of America* **2004,** *101* (35), 12870-12875.

56. Akter, S.; Fu, L.; Jung, Y.; Conte, M. L.; Lawson, J. R.; Lowther, W. T.; Sun, R.; Liu, K.; Yang, J.; Carroll, K. S., Chemical proteomics reveals new targets of cysteine sulfinic acid reductase. *Nature chemical biology* **2018,** *14* (11), 995-1004.

57. Dong, M.; Horitani, M.; Dzikovski, B.; Pandelia, M.-E.; Krebs, C.; Freed, J. H.; Hoffman, B. M.; Lin, H., Organometallic Complex Formed by an Unconventional Radical S-Adenosylmethionine Enzyme. *Journal of the American Chemical Society* **2016,** *138* (31), 9755-9758.

58. Chandor-Proust, A.; Berteau, O.; Douki, T.; Gasparutto, D.; Ollagnier-de-Choudens, S.; Fontecave, M.; Atta, M., DNA repair and free radicals, new insights into the mechanism of spore photoproduct lyase revealed by single amino acid substitution. *Journal of Biological Chemistry* **2008,** *283* (52), 36361-36368.

59. Yang, L.; Lin, G.; Nelson, R. S.; Jian, Y.; Telser, J.; Li, L., Mechanistic studies of the spore photoproduct lyase via a single cysteine mutation. *Biochemistry* **2012,** *51* (36), 7173-7188.

60. Debnath, J.; Siricilla, S.; Wan, B.; Crick, D. C.; Lenaerts, A. J.; Franzblau, S. G.; Kurosu, M., Discovery of Selective Menaquinone Biosynthesis Inhibitors against Mycobacterium tuberculosis. *Journal of Medicinal Chemistry* **2012,** *55* (8), 3739-3755.

61. Li, X.; Liu, N.; Zhang, H.; Knudson, S. E.; Li, H.-J.; Lai, C.-T.; Simmerling, C.; Slayden, R. A.; Tonge, P. J., CoA Adducts of 4-Oxo-4-phenylbut-2-enoates: Inhibitors of MenB from the M. tuberculosis Menaquinone Biosynthesis Pathway. *ACS Medicinal Chemistry Letters* **2011,** *2* (11), 818-823.

62. Choi, S.-r.; Larson, M. A.; Hinrichs, S. H.; Bartling, A. M.; Frandsen, J.; Narayanasamy, P., Discovery of bicyclic inhibitors against menaquinone biosynthesis. *Future Med. Chem.* **2016,** *8* (1), 11-16.

63. Matarlo, J. S.; Lu, Y.; Daryaee, F.; Daryaee, T.; Ruzsicska, B.; Walker, S. G.; Tonge, P. J., A Methyl 4-Oxo-4-phenylbut-2-enoate with in Vivo Activity against MRSA That Inhibits MenB in the Bacterial Menaquinone Biosynthesis Pathway. *ACS Infect. Dis.* **2016,** *2* (5), 329-340.

64. Matarlo, J. S.; Evans, C. E.; Sharma, I.; Lavaud, L. J.; Ngo, S. C.; Shek, R.; Rajashankar, K. R.; French, J. B.; Tan, D. S.; Tonge, P. J., Mechanism of MenE Inhibition by Acyl-Adenylate Analogues and Discovery of Novel Antibacterial Agents. *Biochemistry* **2015,** *54* (42), 6514-6524.

65. Lu, X.; Zhou, R.; Sharma, I.; Li, X.; Kumar, G.; Swaminathan, S.; Tonge, P. J.; Tan, D. S., Stable Analogues of OSB-AMP: Potent Inhibitors of MenE, the o-Succinylbenzoate-CoA Synthetase from Bacterial Menaquinone Biosynthesis. *ChemBioChem* **2012,** *13* (1), 129-136.

66. Li, X.; Liu, N.; Zhang, H.; Knudson, S. E.; Slayden, R. A.; Tonge, P. J., Synthesis and SAR studies of 1,4-benzoxazine MenB inhibitors: Novel antibacterial agents against Mycobacterium tuberculosis. *Bioorganic & Medicinal Chemistry Letters* **2010,** *20* (21), 6306-6309.

67. Dairi, T., An alternative menaquinone biosynthetic pathway operating in microorganisms: an attractive target for drug discovery to pathogenic Helicobacter and Chlamydia strains. *J. Antibiot.* **2009,** *62* (7), 347-352.

68. Tanaka, R.; Kunisada, T.; Kushida, N.; Yamada, K.; Ikeda, S.; Noike, M.; Ono, Y.; Itoh, N.; Takami, H.; Seto, H.; Dairi, T., Branched fatty acids inhibit the biosynthesis of menaquinone in Helicobacter pylori. *J. Antibiot.* **2011,** *64* (1), 151-153.

69. Evans, G. B.; Tyler, P. C.; Schramm, V. L., Immucillins in Infectious Diseases. *ACS infectious diseases* **2017**.

70. Wang, S.; Haapalainen, A. M.; Yan, F.; Du, Q.; Tyler, P. C.; Evans, G. B.; Rinaldo-Matthis, A.; Brown, R. L.; Norris, G. E.; Almo, S. C.; Schramm, V. L., A Picomolar Transition State Analogue Inhibitor of MTAN as a Specific Antibiotic for Helicobacter pylori. *Biochemistry* **2012,** *51* (35), 6892-6894.

71. Wang, S.; Cameron, S. A.; Clinch, K.; Evans, G. B.; Wu, Z.; Schramm, V. L.; Tyler, P. C., New Antibiotic Candidates against Helicobacter pylori. *Journal of the American Chemical Society* **2015,** *137* (45), 14275-14280.

72. Yamamoto, T.; Matsui, H.; Yamaji, K.; Takahashi, T.; Øverby, A.; Nakamura, M.; Matsumoto, A.; Nonaka, K.; Sunazuka, T.; Ōmura, S.; Nakano, H., Narrow-

spectrum inhibitors targeting an alternative menaquinone biosynthetic pathway of Helicobacter pylori. *Journal of Infection and Chemotherapy* **2016,** *22* (9), 587-592.

73. Matsui, H.; Takahashi, T.; Murayama, S. Y.; Kawaguchi, M.; Matsuo, K.; Nakamura, M., Protective efficacy of a hydroxy fatty acid against gastric Helicobacter infections. *Helicobacter* **2017,** *22* (6).

74. Ogasawara, Y.; Kondo, K.; Ikeda, A.; Harada, R.; Dairi, T., Identification of tirandamycins as specific inhibitors of the futalosine pathway. *The Journal of antibiotics* **2017,** *70* (6), 798.

75. Frantom, P. A.; Blanchard, J. S., 8.19 - Bisubstrate Analog Inhibitors. In *Comprehensive Natural Products II*, Liu, H.-W.; Mander, L., Eds. Elsevier: Oxford, 2010; pp 689-717.

76. Morrison, J. F.; Walsh, C. T., The behavior and significance of slow-binding enzyme inhibitors. *Advances in enzymology and related areas of molecular biology* **1988,** *61*, 201-301.

77. Zhang, X.-S.; Blaser, M. J., Natural transformation of an engineered Helicobacter pylori strain deficient in type II restriction endonucleases. *Journal of bacteriology* **2012**, JB. 00113-12.

78. Namanja-Magliano, H. A.; Evans, G. B.; Harijan, R. K.; Tyler, P. C.; Schramm, V. L., Transition State Analogue Inhibitors of 5'-Deoxyadenosine/5'-Methylthioadenosine Nucleosidase from Mycobacterium tuberculosis. *Biochemistry* **2017,** *56* (38), 5090-5098.

79. Ducati, R. G.; Namanja-Magliano, H. A.; Harijan, R. K.; Fajardo, J. E.; Fiser, A.; Daily, J. P.; Schramm, V. L., Genetic resistance to purine nucleoside phosphorylase inhibition in Plasmodium falciparum. *Proceedings of the National Academy of Sciences* **2018**, 201525670.

80. Chen, D.; Cunningham, S. A.; Cole, N. C.; Kohner, P. C.; Mandrekar, J. N.; Patel, R., Phenotypic and molecular antimicrobial susceptibility of Helicobacter pylori. *Antimicrobial agents and chemotherapy* **2017,** *61* (4), e02530-16.

81. Ducati, R. G.; Harijan, R. K.; Cameron, S. A.; Tyler, P. C.; Evans, G. B.; Schramm, V. L., Transition-State Analogues of Campylobacter jejuni 5′-Methylthioadenosine Nucleosidase. *ACS chemical biology* **2018,** *13* (11), 3173-3183.

82. Begley, T. P., Cofactor biosynthesis: an organic chemist's treasure trove. *Natural Product Reports* **2006,** *23* (1), 15-25.

83. Settembre, E.; Begley, T. P.; Ealick, S. E., Structural biology of enzymes of the thiamin biosynthesis pathway. *Curr. Opin. Struct. Biol.* **2003,** *13* (6), 739-47.

84. Begley, T. P.; Ealick, S. E., Mechanistic and structural studies on thiamine biosynthetic enzymes. *Oxidative Stress and Disease* **2004,** *11*, 15-28.

85. Spenser, I.; White, R., Biosynthesis of Vitamin B1 (thiamin): An instance of biochemical diversity. *Angew. Chem. Int. Ed. Engl.* **1997,** *36*, 1032-1046.

86. Fenwick, M. K.; Mehta, A. P.; Zhang, Y.; Abdelwahed, S. H.; Begley, T. P.; Ealick, S. E., Non-canonical active site architecture of the radical SAM thiamin pyrimidine synthase. *Nature communications* **2015,** *6*.

87. Banco, M. T.; Mishra, V.; Ostermann, A.; Schrader, T. E.; Evans, G. B.; Kovalevsky, A.; Ronning, D. R., Neutron structures of the Helicobacter pylori 5′-methylthioadenosine nucleosidase highlight proton sharing and protonation states. *Proceedings of the National Academy of Sciences* **2016,** *113* (48), 13756-13761.

88. Baciocchi, E.; Bietti, M.; Lanzalunga, O., Mechanistic aspects of β-bond-cleavage reactions of aromatic radical cations. *Accounts of chemical research* **2000,** *33* (4), 243-251.

89. Mehta, A. P.; Abdelwahed, S. H.; Fenwick, M. K.; Hazra, A. B.; Taga, M. E.; Zhang, Y.; Ealick, S. E.; Begley, T. P., Anaerobic 5-hydroxybenzimidazole formation from aminoimidazole ribotide: an unanticipated intersection of thiamin and vitamin B12 biosynthesis. *Journal of the American Chemical Society* **2015,** *137* (33), 10444-10447.

90. Gagnon, D. M.; Stich, T. A.; Mehta, A. P.; Abdelwahed, S. H.; Begley, T. P.; Britt, R. D., An Aminoimidazole Radical Intermediate in the Anaerobic Biosynthesis of the 5, 6-Dimethylbenzimidazole Ligand to Vitamin B12. *Journal of the American Chemical Society* **2018,** *140* (40), 12798-12807.

91. Zhang, Y.; Dougherty, M.; Downs, D. M.; Ealick, S. E., Crystal structure of an aminoimidazole riboside kinase from Salmonella enterica: implications for the evolution of the ribokinase superfamily. *Structure* **2004,** *12* (10), 1809-1821.

92. Vichier-Guerre, S.; Dugué, L.; Bonhomme, F.; Pochet, S., Expedient and generic synthesis of imidazole nucleosides by enzymatic transglycosylation. *Organic & biomolecular chemistry* **2016,** *14* (14), 3638-3653.